UiT
THE ARCTIC UNIVERSITY OF NORWAY

Faculty of Science and Technology

Department of Geosciences

Study of millennial scale paleoclimatic and paleoceanographic changes in conjunction with variations in the East Greenland Current during the late Quaternary

—

Linda Gabrielsen

Master thesis in Marine Geology and Geophysics (GEO-3900)
May 2017

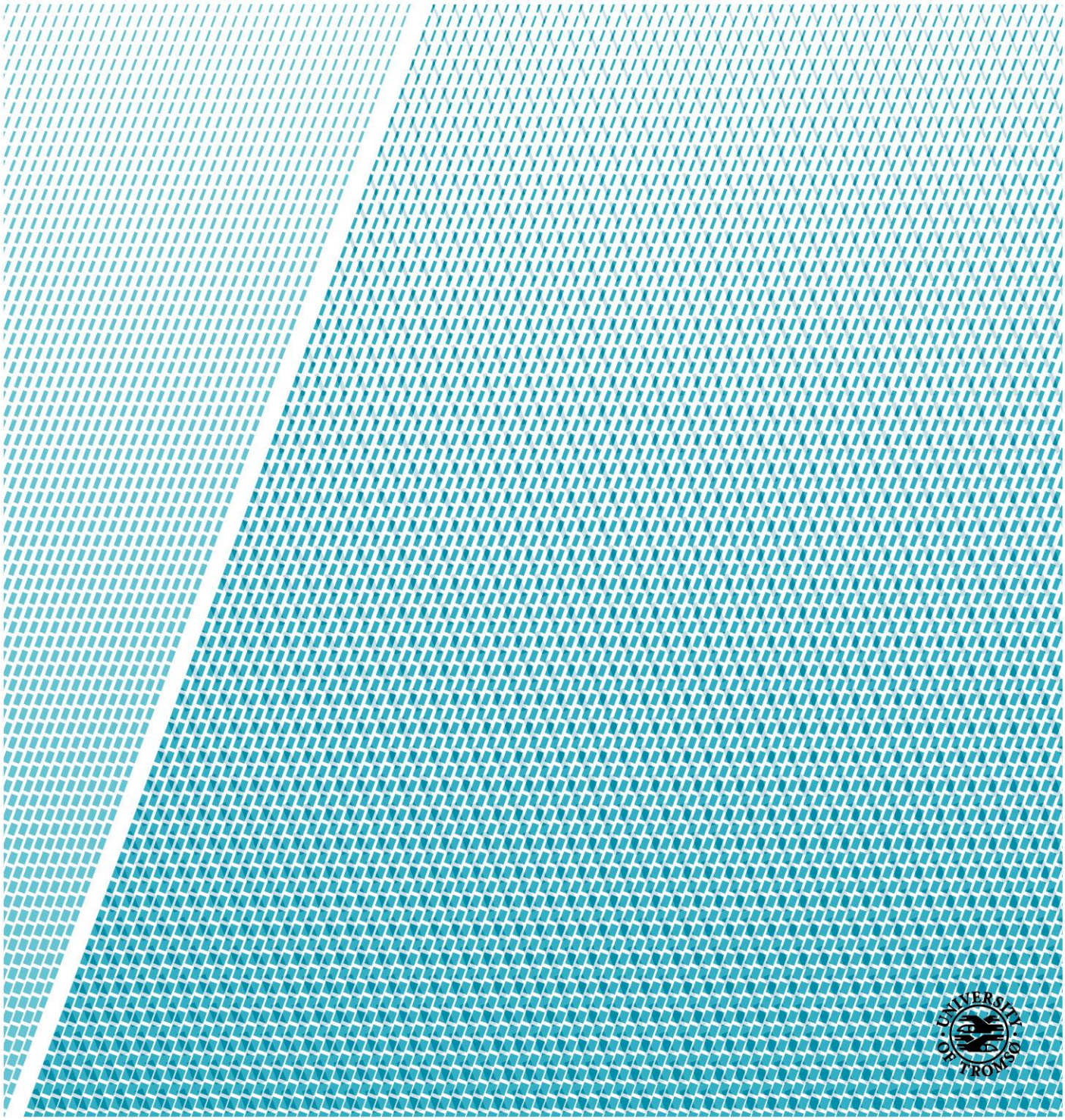

Abstract

Sediment core HH13-089GC (497 cm), collected from the continental slope off Scoresby Sund, East Greenland has been investigated in order to study paleoclimatic and paleoceanographic changes in the area in conjunction with variations in the East Greenland Current during the late Quaternary. The results are based on a multiproxy analysis of the sediment core, including faunal investigations of planktic- and benthic foraminifera, grain size analysis and IRD, stable oxygen- and carbon isotope analysis, and magnetic susceptibility. The grain size of sortable silt was also analysed for the reconstruction of bottom current dynamics.

An age model was established using AMS radiocarbon dates, in addition to ages for marine isotope stage boundaries from the global climate curve (Lisiecki and Raymo, 2005), interpreted by oxygen isotope stratigraphy. The stratigraphic interpretation and proxy results reviled the presence of marine isotope stages 1 – 5, and possibly the MIS 6/5 boundary. The isotope analysis was carried out on the planktic foraminifera *N. pachyderma*, and showed some excursions from the global curve, suggesting that certain climatic events where overridden by local/regional meltwater events.

Retreats and advances of the Greenland Ice Sheet during the last ~ 130 000 years have been indicated by several major pulses of increased supply of IRD. Maximum values were reached during MIS 2 (~ 28 800 – 14 300 yrs. BP), which also includes the Last Glacial Maximum. Some of the major pulses are believed to be related to Heinrich Events based on their characteristics, ages, and correlation with the NGRIP ice core record and other marine records from the North Atlantic. All peaks in the IRD record correlated with the Greenland Stadials recorded in the NGRIP ice core record.

The sortable silt record showed an interesting pattern, and was found to have a positive correlation with the climatic oscillations recorded in the NGRIP ice core record, and several magnetic susceptibility records from the North Atlantic. The sortable silt correlations indicated a relationship between large atmospheric climate variations and bottom current activity; where Greenland Interstadials correlated with increased current activity and high magnetic susceptibility, and Greenland Stadials correlated with reduced current activity and low magnetic susceptibility.

The planktic and benthic foraminiferal records provided important paleoceanographic information, such as variations in surface productivity and ventilation, events of surface freshening, influence of warmer surface/sub-surface waters, sea ice coverage, nutrient supply, and energy changes in the bottom environment.

Acknowledgements

After five years at the University of Tromsø, I am finally ready to submit my master thesis! It's been a lot of work, and I am so happy to have made it to the finish line. However, I would never have been able to do this without so many great people helping me along the way.

First and foremost, I would like to thank my supervisor Tine L. Rasmussen for great counselling and feedback. You have been very supportive and helpful throughout this entire process, and you have always made time for me and my questions. I have greatly appreciated it, thank you.

A big thank you to my co-supervisor Juho Junttila for showing me the procedure for grain size analysis, and helping me with the sortable silt analysis. Thank you to Simon P. Jessen for also helping me with the sortable silt analysis. I learned a lot from our email correspondence and our meetings in the lab.

A special thank you goes to the crew and everyone who participated in retrieving core HH13-089GC during the scientific cruise to Jan Mayen and East Greenland with the University's research vessel R/V Helmer Hansen between June 23rd to July 7th of 2013.

Thank you to Karina Monsen, Ingvild Hald and Trine Dahl at the UiT geology lab for being so helpful when I needed it. William J. Copeland, thank you for your help with the core.

My best friend, Priya. Thank you so much for being there for me. Our endless conversations about everything and nothing are always greatly needed and appreciated.

Mum and dad. Thank you for always believing in me, and for your love, advice, encouragement and support. I am forever grateful.

Finally, my love Morten. You are the most patient and loving man I know, and you have been my rock through this entire process. I would never have made it without you. You're the best!

Linda Gabrielsen

Tromsø 15.05.2017

Table of Contents

1 Introduction 1
1.1 Objectives 1
1.2 Background 1
1.2.1 Motivation 1
1.2.2 Previous marine studies 2
1.2.3 Glacial history of Greenland and the North Atlantic 3
2 Study area 9
2.1 Oceanography 10
2.1.1 The Norwegian Basin 11
2.1.2 The Greenland Basin 11
2.1.3 Formation of deep- and intermediate overflow-waters 13
3 Material and methods 15
3.1 Compressed High-Intensity Radiated Pulse (CHIRP) 15
3.2 Swath Bathymetry 16
3.3 Conductivity – temperature – depth profile (CTD) 16
3.4 Sediment coring 16
3.5 Multi sensor core logger (MSCL) 17
3.6 Laboratory work 17
3.6.1 X-ray imaging 18
3.6.2 Opening- and description of core 18
3.6.3 Colour images 19
3.6.4 Sediment sampling 19
3.6.5 Wet sieving 19
3.6.6 Foraminiferal analysis 20
3.6.7 Ice rafted detritus (IRD) 21
3.6.8 Sortable silt analysis 21
3.6.9 Radiocarbon dating 22
3.6.10 Stable Isotope analysis ($\delta^{18}O$ and $\delta^{13}C$) 25
3.7 Statistics and data processing 27
3.7.1 Handling of raw data for the sortable silt and grain size analysis 27
3.7.2 Calculating porosity, dry bulk density and flux 28
4 Foraminifera 29
4.1 Planktic foraminifera 29

4.1.1 Neogloboquadrina pachyderma (Ehrenberg, 1861) ... 30
4.1.2 Neogloboquadrina incompta (Cifelli, 1961) ... 30
4.1.3 Turborotalita quinqueloba (Natland, 1938) ... 31
4.1.4 Accessory planktic foraminifera ... 31
4.2 Benthic foraminifera ... 32
4.2.1 Oridorsalis umbonatus (Reuss, 1851) ... 32
4.2.2 Cassidulina neoteretis (Seidenkrantz, 1995) ... 33
4.2.3 Triloculina trihedra (Loeblich & Tappan, 1953) ... 33
4.2.4 Cassidulina reniforme (Nørvang, 1945) ... 33
4.2.5 Cibicides wuellerstorfi (Schwager, 1866) ... 33
4.2.6 Stainforthia loeblichi (Feyling-Hanssen, 1954) ... 34
4.2.7 Ioanella tumidula (Brady, 1884) ... 34
4.2.8 Astrononion gallowayi (Loeblich & Tappan, 1953) ... 34
4.2.9 Epistominella arctica (Green, 1959) ... 34
5 Results and interpretation ... 35
5.1 CTD desctription ... 35
5.1.1 Interpretation ... 36
5.2 Sedimentological description of HH13-809GC ... 36
5.2.1 Wet bulk density and water content ... 40
5.2.2 Magnetic susceptibility ... 41
5.2.3 Grain size distribution ... 42
5.3 Ice rafted detritus (IRD) analysis ... 44
5.3.1 Interpretation ... 44
5.4 Foraminiferal data ... 51
5.4.1 Planktic foraminifera ... 51
5.4.2 Benthic foraminifera ... 52
5.4.1 Planktic – benthic foraminiferal ratio ... 56
5.5 Stable isotope data (Planktic $\delta^{18}O$ and $\delta^{13}C$) ... 57
5.5.1 Interpretation ... 58
5.6 Sortable silt analysis ... 63
5.6.1 Potential ice-rafting – Test plot ... 63
5.6.2 Results of the sortable silt analysis ... 64
5.6.3 Interpretation ... 65
5.7 Chronology – AMS radiocarbon ages ... 66

6 Discussion 67
6.1 Age model 67
6.1.1 Sedimentation rates 68
6.1.2 Stable isotope stratigraphy and chronology 71
6.1.3 Flux data 72
6.2 Sortable silt (ΔSS) – Pattern matching with other records 73
6.2.1 Background – The NGRIP ice core isotope record 73
6.2.2 Interpretation and implications 74
6.3 Glacial history of the East Greenland margin 75
6.3.1 The MIS 6/5 transition (core interval 497 – 470 cm) 80
6.3.2 MIS 5: 130 ka – 75 ka yrs. BP (core interval 470 – 375 cm) 83
6.3.3 MIS 4: 70.5 ka – 57 ka yrs. BP (core interval 375 – 340 cm) 86
6.3.4 MIS 3: 57 ka – 28.8 ka yrs. BP (core interval 340 – 175 cm) 88
6.3.5 MIS 2: 28.8 ka – 14.3 ka yrs BP (core interval 175 – 60 cm) 91
6.3.6 MIS 1: 14.3 ka yrs. BP – present (core interval 60 – 0 cm) 94
6.4 Paleoceanographic implications 99
6.4.1 Foraminiferal record 99
6.4.2 Sortable silt record in relation to magnetic susceptibility and bottom current activity 107
7 Summary and conclusions 115
References 117
Appendix A: Benthic species list and distribution 137

List of Tables

Table 1 Coring location and other information about core HH13-089GC 15

Table 2 Study Chrip profile parameters (Ship speed, ping rate, frequency and pulse length 15

Table 3 Material for radiocarbon dating – sampling depth, material type and sample weight 23

Table 4 AMS radiocarbon dating results from core HH13-089GC. Material for all samples was *Neogloboquadrina pachyderma* 66

Table 5 Linear Sedimentation Rates **(a)** and **(b)** 68

Table 6 Example for age-model calculations 69

List of Figures

Figure 1 Map over Greenland with names of different localities and the approximate position of the NGRIP ice core in red (Figure from Funder et al., 1998, modified by author) 3

Figure 2 Showing the Mid- and Upper Pleistocene stratigraphy in East Greenland, as well as the chrono-stratigraphy, the marine isotope stages and the age in thousand years BP (ka) 7

Figure 3 Map showing modern circulation in the North Atlantic Ocean and the Greenland-Iceland-Norwegian Seas. The location of the investigated core HH13-089GC is seen in green. Core ENAM93-21 is also on the map, and this core will be part of the discussion in this thesis. Legend is seen in the upper left corner. NIIC = North Icelandic Irminger Current, the Denmark Strait in red, the Iceland-Faeroe Ridge in blue and the Faeroe-Shetland channel in yellow (Figure from Rasmussen et al., 1996c, modified by author) 10

Figure 4 3D model of the Geotek MSCL-XCT 18

Figure 5 CTD data collected over HH13-089GC core locations in June 2013. PW = Polar Water, AIW = Atlantic Intermediate Water and GSDW = Greenland Sea Deep Water 35

Figure 6 Gravity core HH13-089GC shown by photographs and X-ray images plotted against depth (cm), and sedimentary log 37

Figure 7 (a) Water content (%) and wet bulk density (g/cm^3) for core HH13-089GC plotted against depth (cm). **(b)** Magnetic susceptibility record for core HH13-089GC plotted against depth (cm) 40

Figure 8 Grain size distribution data from the sieving process for size fractions **(b)** < 63 μm, (c) 63 – 100 μm and **(d)** 100 – 500 μm plotted against depth (cm). The composition of the finest grain size fraction **(a)** is based on the LDPSA analysis and given by the grain size analysis program GRADISTAT v8. The total IRD distribution (total IRD/g dry weight sediment against depth) **(e)** is also shown 42

Figure 9 Planktic foraminiferal fauna data for core HH13-089GC calculated as percentages against depth (cm). All the planktic foraminifera are compared to the total planktic foraminiferal abundance. Stippled lines indicate barren intervals 46

Figure 10 Relative abundance plots (%) for all dominating benthic foraminifera against depth (cm) for core HH13-089GC. All the benthic foraminifera are compared to the total benthic foraminiferal abundance (far left). Stippled lines represent the barren intervals. Divisions indicate marine isotope stages, needed for the discussion 47

Figure 11 Relative abundance plots (%) for the most common accessory benthic foraminifera against depth (cm) for core HH13-089GC. All the benthic foraminifera are compared to the total benthic foraminiferal abundance (**far lef**t). Stippled lines represent the barren intervals. Divisions indicate marine isotope stages, needed for the discussion 48

Figure 12 The dominating benthic foraminifera plotted as No. in each sample vs. depth (cm) for core HH13-089GC. All plots are compared to a plot showing the total number of benthic foraminifera counted within each fraction (**far left**) 49

Figure 13 The most common accessory benthic foraminifera plotted as No. in each sample vs. depth (cm) for core HH13-089GC. All plots are compared to a plot showing the total number of benthic foraminifera counted within each fraction (**far left**). Bar plots were used for some plots to see a trend 50

Figure 14 Results showing **(a)** the total abundance of planktic foraminifera (No. Planktic forams/g dry weight sediment). **(b)** total abundance of benthic foraminifera (No. Benthic forams/g dry weight sediment). **(c)** Planktic – Benthic ratio vs. depth for core HH13-089GC 56

Figure 15 Stable oxygen- and carbon isotope results for core HH13-089GC. Stippled lines indicate possible locations for marine isotope stage boundaries. The yellow symbol indicates the location of the tephra, and the red question mark represents the uncertain $\delta^{18}O$ measurement 57

Figure 16 Potential ice-rafting **(a)** Scatter plot of wt% sand vs. the measured median grain size of sortable silt (SS) and the linear fit line. **(b)** Scatter plot of the medial SS data vs. ΔSS data. Most of the data points plot close to the regression line, and the ones that do not, are the ones that will be affected by the IRD correction. **(c)** Scatter plot of wt% sand vs. ΔSS showing no correlation 63

Figure 17 Sortable silt records. **(a)** Median size of SS (μm). **(b)** Wt% sand and the calculated potentially ice rafted sortable silt $SS_{(pot)}$ (The two records display the same pattern and are therefore presented together). **(c)** The final ice rafted corrected sortable silt signal, ΔSS (μm). The bold lines within each plot represents three-point-running-averages 64

Figure 18 Age – depth model and linear sedimentation rates for core HH13-089GC. Numbers in black indicate the results for the calibrated ages. The yellow number represents the results of the calibrated Vedde ash. Red numbers indicate the approximate results for identified stage boundaries and sub-stage peaks (ages from Lisiecki Website). Blue numbers in the top of the figure represents marine isotope stages (MIS) 70

Figure 19 Revised stable isotope records plotted against age (ka yrs. BP), and separated into marine isotope stages based on interpretation and age model 71

Figure 20 Results of the flux calculations vs. depth (cm). **(a)** Planktic foraminifera flux (No. Planktic foraminifera/cm^2/ka) **(b)** Benthic foraminifera flux (No. Benthic foraminifera/cm^2/ka) **(c)** Total foraminifera flux **(d)** IRD flux (g/cm^2/ka) **(e)** Flux for grain size fraction 63 – 100 μm (g/cm^2/ka) **(f)** Flux for grain size fraction 100 – 500 μm (g/cm^2/ka) 72

Figure 21 The NGRIP stable oxygen isotope record (**red**) compared to the GRIP record (**blue**). The GRIP record (**blue**) has been plotted on the NGRIP depth scale for the bottom plot. (Figure from NGRIP members, 2004) 73

Figure 22 Showing correlations between the **(a)** ΔSS record for core HH13-089GC (investigated in this thesis) plotted against age (ka yrs. BP) **(b)** $\delta^{18}O$ record for the Greenland Ice Core NGRIP plotted against age (yrs. before 2000 AD) (data from NGRIP members, 2004; Andersen et al., 2006). The black numbers seen above each peak, represents the interstadials within the Dansgaard-Oeschger cycles, or Greenland Interstadials (**GI**) as they are also called. The blue letters show the identified Heinrich Events within the Greenland ice cores, **YD** = Younger Dryas, **BA** = Bølling – Allerød (Bond et al., 1993). The bold line within the ΔSS record represents a three-point-running-average for the record 74

Figure 23 Simplified scheme of the East Greenland continental margin, showing the major climatic and oceanographic factors and processes which control sedimentation in the area. These factors will be of great importance in the interpretation and discussion of the results. The approximate location for the investigated core is seen in green. Some of the cores investigated in Nam et al. (1995), Stein et al. (1996) and Funder et al. (1998). (Figure from Stein et al., 1993)..... 76

Figure 24 Main results of the present investigation of core HH13-089C plotted against age (ka yrs. BP). **(a)** Stable oxygen isotope record, **(b)** Stable carbon isotope record, **(c)** Sortable silt record, **(d)** Total IRD/g dry weight sediment, **(e)** Relative abundance of *N. pachyderma*, **(f)** Relative abundance of *N. incompta*, **(g)** Relative abundance of *T. quinqueloba*, **(h)** Relative abundance of *O. umbonatus*, **(i)** relative abundance of *C. neoteretis*. Marine isotope stages are indicated on the record, in addition to Greenland Interstadials (**GI**), Heinrich Events (**H**), Younger Dryas (**YD**) and Bølling – Allerød (**BA**) 77

Figure 25 Main results of the present investigation of core HH13-089GC, and interpreted chronology (**far left**). **(a)** Magnetic susceptibility record, **(b)** Sortable silt record (ΔSS), **(c)** Total IRD/g dry weight sediment, **(d)** Stable oxygen isotope record, **(e)** Relative abundance of *N. pachyderma*, **(f)** Stable carbon isotope record, **(g)** Relative abundance of *O. umbonatus*, **(h)** Relative abundance of *C. neoteretis*, **(i)** NGRIP oxygen isotope record. All records are plotted against depth (cm), except for the NGRIP record, which is plotted against age (yrs. before 2000 AD). Other features on the figure are: Radiocarbon dates, marine isotope stages (horizontal stippled lines), the Vedde ash layer (**yellow**), Greenland Interstadials (**GI**), Greenland Stadials (**light blue**), Heinrich Events (**H**), Bølling – Allerød, Younger Dryas, The Last Glacial Maximum (**LGM**), the presence of P. bulloides (**X**) and intervals barren of foraminifera (**general stippled lines**)..... 78

Figure 26 Results of the local slope core PS1726 from the studies by Nam et al. (1995), Stein et al. (1996) and Funder et al. (1998). (Figure from Funder et al., 1998) 79
Figure 27 Results of the local slope core PS1730 from the studies by Nam et al. (1995), Stein et al. (1996) and Funder et al. (1998). (Figure from Funder et al., 1998) 79
Figure 28 The MIS 6/5 transition from the ΔSS record showing the rapid fluctuations (**red circles**) which could correlate with changing NADW (Galaasen et al., 2014), and the possible "step-like" deglaciation phase (**black**). Note that the ΔSS record is plotted against depth (cm) in order to see the features. The MIS 6/5 transition is set to ~ 130 000 yrs. BP..... 82
Figure 29 Modelled Eemian minimum ice sheet extent for Greenland (Letréguilly et al., 1991) Figure is from Funder et al. (2011), who noted that this reconstruction was based on certain erroneous assumptions. (Terminal moraines from the Saalian glaciation is also seen for south-western Greenland in blue, arrows indicating ice sheet flow during MIS 6)..... 83
Figure 30 Pattern matching between the magnetic susceptibility curves for core HH13-089GC (**left**) and PS1730 (**right**) (right figure is from Funder et al., 1998, modified by author). Both cores are from the East Greenland continental slope and similar water depths. Marine isotope stage definitions are similar, except for MIS 4, which has been placed lower in PS1730. Coloured arrows show correlating peaks 90
Figure 31 (a) Reconstructed LGM ice sheet margin, ice flow, dates for break-up of shelf bound ice (figure from Funder et al., 2011). **(b)** Three LGM ice extents: Huy model (**red**) (Simpson et al., 2009), Funder et al. (2011) extent (**green**), and the revised Huy3 model (**blue**) (figure from Lecavalier et al, 2014) 91
Figure 32 Showing the chronology of lateral ice extent in Greenland from the Huy3 model (16 ka BP – **pink**; 14 ka BP – **dark blue**; 12 ka BP – **light blue**; 10 ka BP – **yellow**; 9 ka BP – **orange**; 6 ka BP – **red**; 4 ka BP – **green**; present-day – **black**). (Figure from Lecavalier et al., 2014)... 94
Figure 33 (a) Depositional model for the Bølling – Allerød interstadials, where glacier ice filled the fjord system, gradually retreating towards the inner fjords. (note that the extent of glacier ice has been questioned). **(b)** Depositional model for the Younger Dryas cold event, where glaciers terminated near the mouths of the smaller fjords in the western fjord system, and substantial sea ice cover was formed. **(c)** Near present day. (Figure a and b from Marienfeld et al. (1992) and figure c from Stein et al. (1993) 96
Figure 34 Correlation between **(a)** Faeroe Margin core ENAM93-21 magnetic susceptibility record (Rasmussen et al., 1996a) **(b)** Sortable silt (ΔSS) record for core HH13-089GC and **(c)** NGIRP stable oxygen isotope record (NGRIP members, 2004; Andersen et al., 2006). There seems to be a correlation between the first 15 oscillations recorded in all three records. X symbol marks the end of certain correlations 109

Figure 35 Describes the hypothesis of Rasmussen and Thomsen (2004) on causes for D-O events. **(a)** Interstadial intervals with open ocean convection in the GIN-Seas and NADW formation. **(b)** Transitional cooling intervals with limited convection and NADW formation. **(c)** Stadial intervals where the NAC/North Atlantic Drift flowed beneath the fresh surface waters, warming the deep waters, and eventually breaking through to the surface, releasing large amounts of energy to the atmosphere. (Figure from Rasmussen and Thomsen, 2004)..... 112

1 Introduction

1.1 Objectives

The aim of this study is to investigate millennial and orbital scale paleoceanographic and paleoclimatic changes in conjunction with variations in the East Greenland Current during the late Quaternary.

This master thesis project was carried out at the Department of Geosciences at the University of Tromsø, The Arctic University of Norway, from April 2016 to May 2017. A deep marine sediment core from the area off Scoresby Sund, East Greenland, was investigated. The planktic- and benthic foraminiferal faunas, the IRD-content, and the magnetic susceptibility were used in the investigation of the core. Radiocarbon dates were used for constructing an age model, and stable oxygen- and carbon isotopes provided important, additional information about the stratigraphy and climatic events. The findings were also compared to a reconstruction of the bottom current dynamics from the same core, using the grain size of sortable silt.

1.2 Background

1.2.1 Motivation

Greenland is the largest island in the world, and holds the world's second largest ice sheet. This ice sheet is also the only terrestrial ice sheet remaining in the northern hemisphere today (Bennike and Björck, 2002). At present, the ice sheet covers an area of approximately 1.7 million km^2, has an average thickness of 1600 m and stretches 2200 km from north to south (Thomas et al., 2001). The ice-sheet volume was estimated by Bamber et al. (2001) to be 2.9 million km^3. Massive amounts of the world's current freshwater reserves are stored in terrestrial ice, and it is estimated that if melted, the volume of the Greenland Ice Sheet is equivalent to a 7 m rise in sea level (Lemke et al., 2007).

Fluctuations in the extent of the Greenland Ice Sheet and sea-ice, changes in oceanic circulation, variations in the amount of drifting icebergs and meltwater input, are factors which are all assumed to be controlled by climate. These factors influence the sediment transport, the biogenic productivity and other seafloor properties along the East Greenland continental margin. (Stein et al., 1993; Stein et al., 1996; Mienert et al., 1992). In order to understand natural climate change, it is important to study and establish paleoclimatic records that go far back in time (Husum and Hald, 2012). In the investigated area, such records can provide a fuller picture of the climatic changes in the Greenland Sea (Hopkins, 1991), and possibly contribute to our understanding of the mechanisms that lead to large climatic

shifts (Kelly et al., 2008), in order to evaluate how the ice sheet may respond to climatic changes in the future.

The Greenland-Iceland-Norwegian Sea (GIN-Sea) has been and still is an area of great geological interest. The eastern part of the GIN-Sea, especially areas along the Norwegian continental margin has been subject to extensive studies due to its accessibility and relatively ice free conditions (Mienert et al., 1992). Being the largest eastern outlet from the Greenland Ice Sheet margin (Funder et al., 1998), the Scoresby Sund fjord system releases large amounts of icebergs to the East Greenland Current (EGC). That, combined with seasonal sea-ice cover, makes studies in this area difficult (Mienert et al., 1992; Stein et al., 1996). Correlations between climate proxies from the North Atlantic, Europe and Greenland do exist (Fronval and Jansen, 1997), however paleoclimatic studies from the East Greenland continental margin are rare, and the use of sortable silt as an indication for bottom current strength has not been done for this area.

1.2.2 Previous marine studies

The largest marine geologic study in the area is the ESF-PONAM programme (European Science Foundation-Polar North Atlantic Margins) which took place between 1990 – 1992 (Funder et al., 1998). The programme wanted to reconstruct the environmental history of the East Greenland margin and correlate the marine and terrestrial records (Elverhøi and Dowdeswell, 1991, cited in Stein et al., 1996). Some examples of other paleoenvironmental studies from the area are; Marienfeld, 1992; Mienert et al., 1992; Stein et al., 1993; Williams et al., 1993; Jennings and Helgadottir, 1994; Nam et al., 1995; Stein et al., 1996; Funder et al., 1998; Nam and Stein, 1999; Jennings et al., 2002; Jennings et al., 2011.

1.2.3 Glacial history of Greenland and the North Atlantic

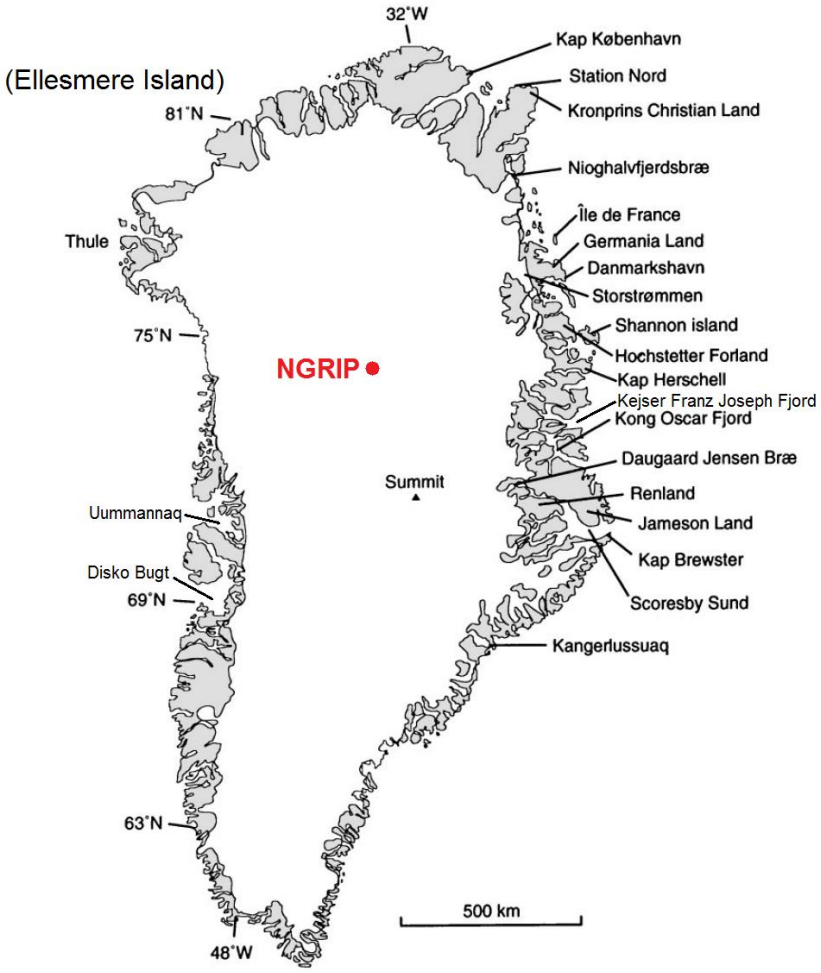

Figure 1: *Greenland with names of different localities and the approximate position of the NGRIP ice core in red. (Figure from Funder et al., 1998, modified by author).*

The timing of the first appearance of ice in the Northern Hemisphere has long been a subject of debates, but evidence now suggest that it may have been as early as the Mid-Eocene to Early Oligocene (Tripati et al., 2008). Full glacial conditions in East Greenland is believed to have been established around 7 million years ago (Ma) (Larsen et al., 1994; Solheim et al., 1998). The construction of the East Greenland continental margin has since the establishment of the Greenland Ice Sheet, been greatly influenced by changes in the ice extent.

1.2.3.1 The last glacial-interglacial cycle in the North Atlantic

The last glacial cycle in the North Atlantic spans between ~ 120 000 – 11 500 years before present (yrs. BP), and has been characterized by climatic instability (McManus et al., 1999). Following this glacial cycle is the present interglacial, the Holocene, which corresponds to marine isotope stage (MIS) 1. During the last glacial period, the air temperatures over Greenland fluctuated rapidly and drastically several times (5 – 10 ^{O}C). These high amplitude climatic oscillations are seen within the $\delta^{18}O$ records of Greenland Ice cores (e.g. GISP2, GRIP and NGRIP) (Dansgaard et al., 1993), and are often referred to as Dansgaard – Oeschger cycles (D-O cycles) (Broecker et al., 1992). Sea surface temperature changes during these climatic oscillations has been reflected in foraminiferal faunal shifts in the Atlantic Ocean (Bond et al., 1993; Oppo et al., 1998).

Dansgaard – Oeschger cycles

The Dansgaard – Oeschger cycles were first described by Dansgaard et al. (1982) and Johnsen et al. (1992). The cycles are represented in the Greenland ice core record as a series of abrupt temperature changes, as the $\delta^{18}O$ signal in polar glaciers is mainly determined by temperature (Dansgaard et al., 1993). A cycle starts with an abrupt and short lasting temperature increase. This peak represents a warm period known as an interstadial. Following the temperature peak is a gradually decreasing temperature trend, which ends with a very cold period, representing what is known as a stadial (Johnsen et al., 1992). Bond et al. (1993) described the abrupt temperature changes as a possible response to changes in the thermohaline circulation in the North Atlantic. Each D-O cycle lasted between 500 – 2500 years (Johnsen et al., 1992), and the most prominent, long lasting stadials have been found to correlate with the so-called Heinrich Events in the North Atlantic (Bond et al., 1993). A Dansgaard-Oeschger event can be described as a warming event during cold climatic conditions (Rasmussen and Thomsen, 2004).

Bond cycles

It was noted by Bond et al. (1993) that the Dansgaard – Oeschger cycles formed “saw tooth” shaped bundles, which typically lasted 6000 – 10 000 years (Bond cycles). These cycles show a gentle cooling trend, leading to a catastrophic release of icebergs to the North Atlantic, known as Heinrich Events (Heinrich, 1988; Bond et al., 1992), before they end abruptly with warmer temperatures. The origin of Heinrich Events is still discussed, though there seem to be an agreement of their description (Broecker et al., 1992).

Any drastic temperature changes within the air above Greenland, will influence and lead to shifts in sea surface temperatures, and the Dansgaard – Oeschger cycles should therefore be reflected in the marine record (Bond et al., 1993). Together with Heinrich Events, the Dansgaard – Oeschger cycles are the dominant features showing rapid climate change in the North Atlantic (Bond et al., 1999).

The Last Glacial Maximum and deglaciation

The Last Glacial Maximum (LGM), between 26 500 – 19 000 yrs. BP represents the peak of the most recent glacial period. During this time, global ice volumes reached a maximum and the global relative sea level was 120 – 130 m below present (Lambeck et al., 2002; Clark et al., 2009). Large areas in North America and Eurasia was covered in massive ice sheets, whereas the Greenland- and Antarctic Ice Sheets where larger than present (Lambeck et al., 2002; Lecavalier et al., 2014).

The ice sheets covering North America and Eurasia disappeared completely during the deglaciation which followed, but the ice sheets covering Antarctica and Greenland persisted (Lecavalier et al., 2014). The rising temperatures which followed the LGM, led to the rise of the global mean sea level (Funder and Hansen, 1996).

1.2.3.2 East Greenland through the last glacial-interglacial cycle

Marine isotope stage 5e; The Eemian

Marine isotope stage 5e is often termed the Langelandselv interglacial in Greenland studies (Figure 2), but will be referred to as the Eemian or MIS 5e, to avoid confusion when compared to studies outside the area. Marine sediments in the Scoresby Sund area, suggests that the melting of the Greenland Ice Sheet at the transition from the preceding Saalian glaciation (MIS 6) led to rapid sea level rise which influenced the area greatly (Funder et al., 1998). Geological evidence suggests that the Eemian interglacial was warmer than the present Holocene (Wastegård et al., 2001), and that the Greenland Ice Sheet responded greatly to this warming (e.g. Cuffey and Marshall, 2000; Huybrechts, 2002; Tarasov and Peltier, 2003; Greve, 2005).

Marine isotope stages 5; The Early Weichselian Period

The Weichselian period (MIS 5 – 2) represents the last glaciation, and is usually characterised by several climatic fluctuations, referred to as stadials (a period within a glacial stage, often accompanied by ice advance) and interstadials (a temporary warming period during a glacial stage, often accompanied by ice retreat).

Two major phases of glaciation and deglaciation in central East Greenland, have been recognized during the Early Weichselian period in studies from the area around Jameson Land and Scoresby Sund, East Greenland (Lyså and Landvik, 1994; Landvik et al., 1994; Funder at al., 1994; Elverhøi et al., 1998; Funder et al., 1998). The first phase; called the Aucellaelv stadial (115 000 – 105 000 years ago) in Greenland studies, corresponds to MIS 5d (Figure 2). MIS 5d is represented by a large ice-sheet advance (Funder et al., 1994; Funder et al., 1998; Elverhøi et al., 1998). The glaciation and deglaciation during this isotopic stage was quite rapid, and datings show that the process only took

about 10 000 years. Large beds of sub-glacial till from MIS 5d is part of the landscape in central East Greenland today, indicating that the glacier in the Jameson Land area (Figure 1) was warm-based (Funder et al., 1998).

The second phase is recognised as The Jyllandselv stadial in Greenland studies, and the advance of the Ice Sheet during this phase corresponds to MIS 5b (Figure 2) (Elverhøi et al., 1998; Funder et al., 1998). The processes linked to this phase is believed to have been similar to those during MIS 5d (Elverhøi et al., 1998).

Marine isotope stages 3 – 2; Middle to late Weichselian period

A third and last phase of glaciation-deglaciation is recognised during the middle to late Weichselian period. The phase is often referred to as the Flakkerhuk stadial, and corresponds to MIS 3 – 2 (~60 000 – 10 000 yrs. BP) (Figure 2) (Funder et al., 1994; Funder et al., 1998). This glaciation-deglaciation phase is believed to have lasted much longer than the previous two. Studies have suggested that it may have lasted for approximately 50 000 years (Funder et al., 1998; Elverhøi et al 1998).

The LGM occurs during MIS 2, and the Greenland Ice Sheet responded dramatically to the rapid drop in sea level which occurred during this time. It is believed to have stretched across the continental shelf, and all the way out to the shelf break in several areas (e.g Bennike et al., 2002; Roberts et al., 2009), however the exact extent of the ice sheet and its glaciers has been debated. Several studies (e.g. Dowdeswell et al., 1994; Funder and Hansen, 1996; Funder et al., 1998) have indicated that the Scoresby Sund basin was occupied by a thin low-gradient ice stream, which reached the Kap Brewster moraine ridge (Figure 1) just outside the fjord mouth during the LGM. Pieces of evidence such as the moraine ridge, low weathering limits, low marine limits at the coast and in the outer fjord, and evidence from a nearby ice core all pointed to this claim (Funder et al., 2011). Other, more recent studies however (e.g. Håkansson et al., 2007) have indicated that the Kap Brewster plateau was covered by a cold-based, local ice cap, and that the ice sheet reached far out to the outer East Greenland shelf during the LGM.

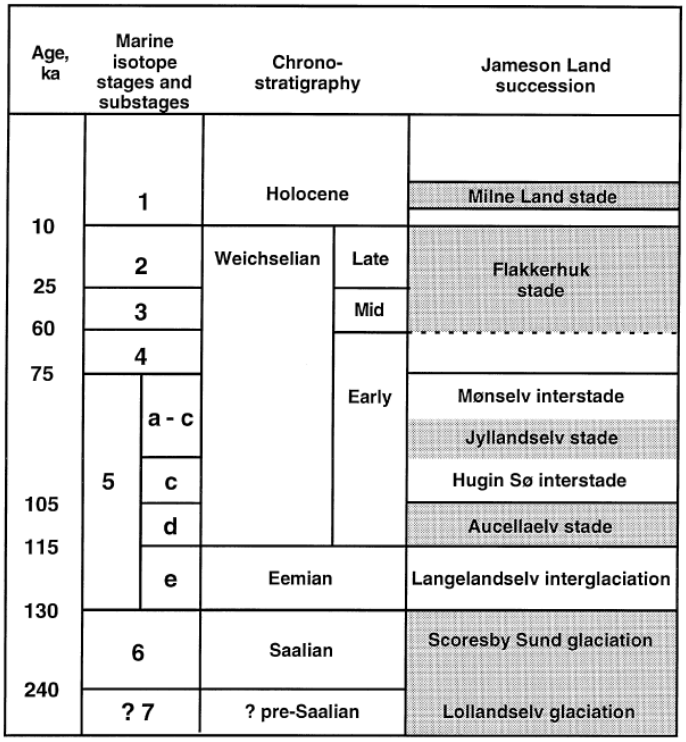

Figure 2: *Showing the Mid and Upper Pleistocene stratigraphy in East Greenland, as well as the chrono-stratigraphy, the marine isotope stages and the age in thousand years ago (ka) (Figure from Funder et al., 1998)*

1.2.3.3 East Greenland through the deglaciation and into the Holocene

The Greenland Ice Sheet reacted to the rise of the global mean sea level, which followed the LGM, by calving its marine-based ice (Funder and Hansen, 1996). The timing of the East Greenland deglaciation varies slightly from study to study due to the use of different proxies with different sensitivities. The beginning of the deglaciation in central East Greenland is indicated by several studies to be at approximately 19 000 yrs. BP (e.g. Stein et al., 1996; Evans et al., 2002). In the North-East however, the ice margin seems to have remained near the present coastline until approximately 10 000 yrs. BP (Landvik, 1994).

Dated material from Nioghalvfjerdsfjorden in North-East Greenland (Figure 1) provided minimum ages for the deglaciation in the area. The outer parts of the fjord were deglaciated prior to 9700 calibrated years before present (cal. yrs. BP), and the inner parts of the fjord were deglaciated prior to 7700 cal. yrs. BP (Bennike and Weidick, 2001; Bennike and Björck, 2002). A $\delta^{18}O$ isotope minimum for the areas around Kejser Franz Joseph Fjord farther south, indicates that the deglaciation in this area began after ca. 17 000 yrs. BP (15 300 ^{14}C yrs. BP) (Evans et al., 2002). Hall et al. (2008) and Kelly et al. (2008) suggested that the outer continental shelf off Scoresby Sund became ice-free some time before 12 400 yrs. BP.

The Younger Dryas (YD) cold period is recognized as a return to glacial climate at the end of the last deglaciation with a cooling of 10 – 20 ^{O}C, and that lasted more than 1000 years (Alley et al., 1993). The period is well documented in the Nordic Seas (e.g. Björck et al., 1998; Klitgaard-Kristensen et al., 1998; Jennings et al., 2006).

The glaciers in East Greenland continued to retreat into the Holocene due to calving and surface melting. Studies suggests that the present-day positions were reached sometime between 9 000 – 6 000 yrs. BP (Lecavalier et al., 2014).

1.2.3.4 South, West and North Greenland through the LGM and the deglaciation

During the LGM in Southern Greenland, the ice sheet reached the shelf break, and studies have suggested an initial retreat of the ice sheet between 14 000 – 12 000 cal. yrs. BP. The current position of the ice margin is believed to have persisted for around 10 500 years (e.g. Bennike et al., 2002; Bennike and Björck, 2002; Sparrenbom et al., 2006; Larsen et al., 2011; Woodroffe et al., 2014).

Studies from the areas around the Disko Bugt and Uummannaq in Western Greenland (Figure 1) have findings similar to those for Southern Greenland (e.g. Roberts et al., 2009; Ingólfsson et al., 1990; Bennike and Björck, 2002; Lloyd et al., 2005; Lane et al., 2013). The ice sheet in the North-Western parts of Greenland was connected to the ice sheet on Ellesmere Island, Canada during the LGM (England, 1999; Blake, 1999). The marine-based ice in this area was fed by ice streams until 11 200 yrs. BP, when they retreated, causing a collapse of the ice around 10 000 yrs. BP (Kelly and Bennike, 1992; Zreda et al., 1999).

The ice sheet in the far north of Greenland was also fed by ice streams (Funder et al., 2004) and previous evidence have suggested that the ice sheet retreated between 16 000 and 10 300 yrs. BP, before reaching a land-based position around 10 100 yrs. BP (Larsen et al., 2010).

2 Study area

The present day, continental shelf off Scoresby Sund, East Greenland stretches between ~ 50 – 100 km offshore. It is at its widest beyond the mouth of the Scoresby Sund fjord system (Dowdeswell et al., 1993, 1997). Scoresby Sund is the largest fjord system in the world. It is located between 70 – 72°N and extends almost 350 km from the inland glaciers to the outer East Greenland coast (Marienfeld, 1992; Dowdeswell et al., 1993). The fjord system inlet is located approximately 170 km to the west of the coring site for the deep marine slope core HH13-089GC investigated in this study (Figure 3). The Scoresby Sund fjord system is one of the greatest sources of icebergs to the EGC (Hopkins, 1991) which in turn plays an important role in North Atlantic oceanography, and hence the global oceanographic system. The fjord system is also of major importance when it comes to the transport of coarse grained material such as sand and gravel with sea ice and icebergs to the continental shelf and slope, and to the abyssal plain (Stein et al., 1996).

Late Quaternary glacial-interglacial processes had major impacts on the subpolar and polar ocean, the Greenland Sea being an example (CLIMAP project, 1981, as cited in Nam et al., 1995). The East Greenland continental margin is ideal for studying the impacts of these processes, since changes in the ocean's climatic conditions are often well documented in marine sediments (Nam et al., 1995).

2.1 Oceanography

The Greenland – Iceland – Norwegian Seas or GIN-Seas as they will be referred to in this study (Hopkins, 1991) are influenced by several water masses of different properties. The GIN-Seas are comprised of two major basins which are separated by the North Atlantic Mid-Ocean Ridge. To the east is the Norwegian Basin, which consists of several minor basins, and to the west is the Greenland Basin (Hopkins, 1991).

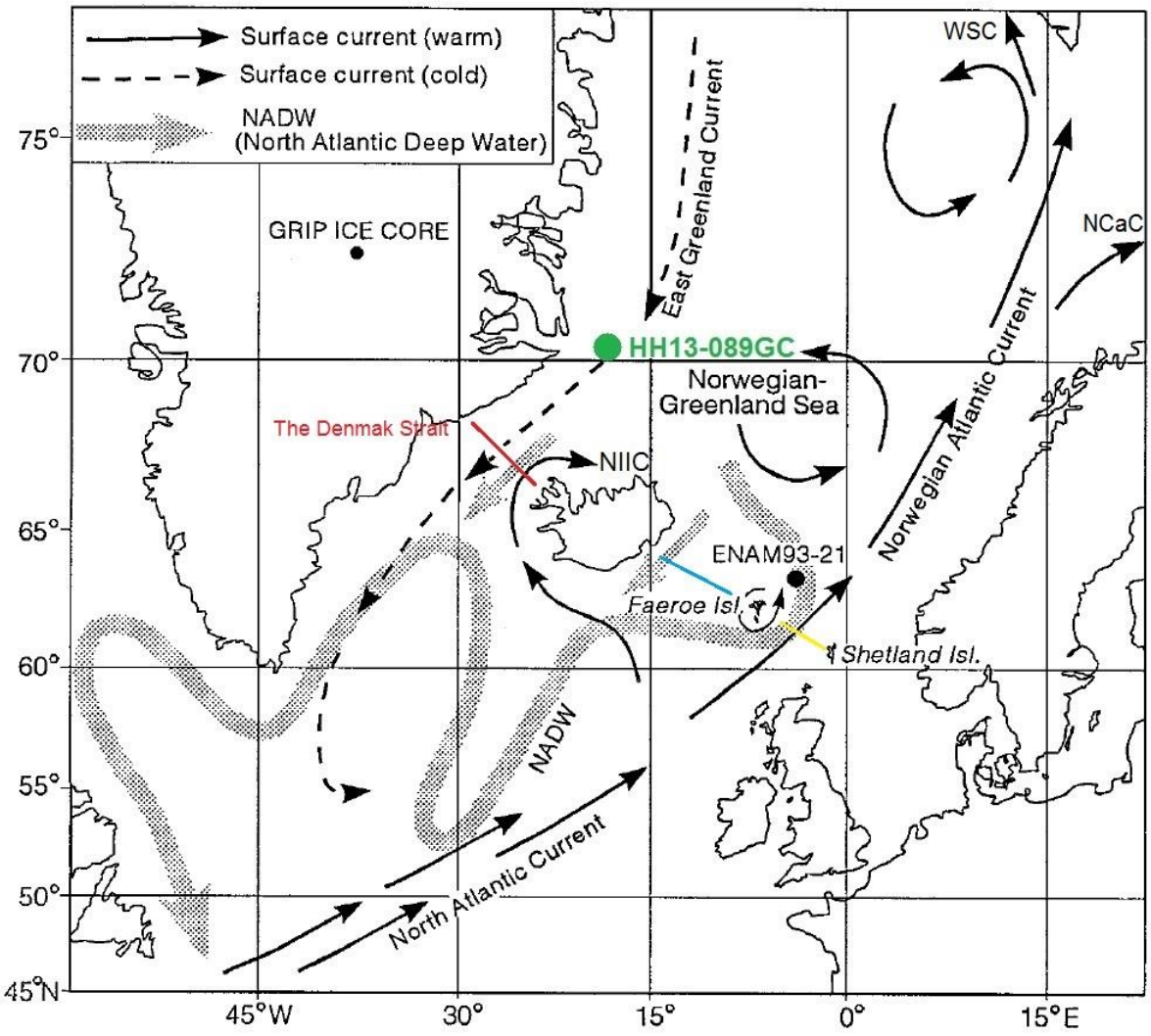

Figure 3: *Map showing modern circulation in the North Atlantic Ocean and the Greenland-Iceland-Norwegian Seas. The location of the investigated core HH13-089GC is seen in green. Core ENAM93-21 is also on the map, and this core will be part of the discussion in this thesis. Legend is seen in the upper left corner. NIIC = North Icelandic Irminger Current, WSC = West Spitsbergen Current, NCaC = North Cape Current, the Denmark Strait in red, the Iceland-Faeroe Ridge in blue, the Faeroe-Shetland channel in yellow (Figure from Rasmussen et al., 1996c, modified by author).*

2.1.1 The Norwegian Basin

The Eastern part of the GIN-Sea has predominantly ice-free conditions all year around, with some exceptions. Here, the North Atlantic Current (NAC) is drawn from the south, bringing warm (>2 ^{o}C), saline (>35 PSU) Atlantic Water (AW) northwards (Hopkins, 1991). There are three locations where inflow of AW from the NAC occurs; through the Denmark Strait, across the Iceland-Faroe Ridge and through the Faroe-Shetland channel (Figure 3). The warmest and saltiest waters arrive through the latter and continues northwards along the Norwegian continental slope (Blindheim and Østerhus, 2005; Hansen et al., 2008). A branch of the NAC flows north-westward towards Jan Mayen, where it brings warmer waters towards the Greenland Basin. Just off the coast of northern Norway, the NAC branches out into the adjacent regions through the West Spitsbergen Current (WSC) and the North Cape Current (NCaC) (Hopkins, 1991). This vast extension of the NAC towards the Arctic Ocean is a massive contributor to the unusually warm climate in these high latitude regions (Hansen and Østerhus, 2000; Rudels et al., 2005). Part of the warmer West Spitsbergen Current turns southward near the Fram Strait (Hansen and Østerhus, 2000; Rudels et al., 2005), and contribute recirculated Atlantic Water to the Return Atlantic Current (RAC), which is an important part of the East Greenland Current (EGC) (Quadfasel, 1987; Bourke et al., 1987).

2.1.2 The Greenland Basin

The present-day Greenland Sea, is dominated by the cold, southward flowing East Greenland Current. The current flows along the entire East Greenland continental margin between the Fram Strait in the north, and the Denmark Strait in the south. The Denmark Strait connects the Greenland Sea with the North Atlantic, and the Fram Strait, located at ~ 77^{O}N – 81^{O}N acts as a main gateway between the Greenland Sea and the Arctic Ocean (Quadfasel et al., 1987). In addition to the EGC, the western part of the GIN-Seas is affected by the northward flowing branch of the NAC going through the Denmark Strait as surface waters, and the recirculated Atlantic Water flowing south-west from the WSC (Hansen and Østerhus, 2000; Rudels et al., 2005). The NAC and the EGC can be described as the "parent" water masses of the GIN-Seas (Hopkins, 1991).

2.1.2.1 The East Greenland Current

The East Greenland Current is highly affected by the oceanography of the Arctic Ocean. The current carries large amounts of sea-ice and icebergs southwards from the Arctic region and Northeast Greenland. Blindheim and Østerhus (2005) described the ice carried by the EGC, as the largest and most concentrated meridional ice flow in the World Ocean. The onset of the EGC is believed to have been 8.3 million years ago (Wolf and Thiede, 1991).

Pack-ice formed in the Arctic Ocean off the coast of Siberia follows the Transpolar Drift westwards, and eventually southwards through the Fram Strait where it continues its journey via the EGC until melting occurs (Hopkins, 1991). Icebergs of non-marine origin which result from glaciers that terminate in the sea, are also moved by the EGC.

The properties and components of the EGC varies on its journey from the Arctic Ocean to the North Atlantic Ocean. Three main water masses are recognized within the East Greenland Current north of the Denmark Strait (Aagaard and Coachman, 1968a; Hansen and Østerhus, 2000; Rudels, 1989; Rudels et al., 2005) All three are similar to those found in the Arctic Ocean. Aagaard and Coachman (1968a) describes some of the properties of these water masses as found in their study. The water masses can also be recognised on the recent CTD-data for this study (Figure 5).

As the EGC begins its journey southwards from the Arctic Ocean, it transports and exports sea-ice and cold, low salinity Polar Water (PW). The Polar Water stretches down from the surface to a depth of approximately 150 m. The temperature is usually around the freezing point and 0^{o}C. The lowest summer temperatures are found at around 50 m, whereas the winter temperatures remain around freezing point all the way down to 75 m. The salinity of this water mass is increasing from ~ 30 ‰ at the surface to ~ 34 ‰ near the lower boundary. Since this water mass constitutes the upper layer of the East Greenland Current, it is believed to an extent, to be in control of the ice distribution. (Aagaard and Coachman, 1968b). The Atlantic Intermediate Water (AIW) extends from approximately 150 – 800 m water depth. The temperatures of this water mass exceed 0^{o}C throughout the year, with a temperature maximum between 200 – 400 m. The salinity increased gradually from the upper limit of the water mass down to 400 m. The salinity is at its highest below 400 m, where it usually attains an almost constant value of ~ 35 ‰. (Aagaard and Coachman, 1968a). Below 800 m water depth, The Greenland Sea Deep Water (GSDW) with an average temperature below 0^{o}C and a salinity between 34.87 – 34.95 ‰ is found (Aagaard and Coachman, 1968a; Hopkins, 1991).

2.1.3 Formation of deep- and intermediate overflow-waters

Between Iceland and Jan Mayen, two branches of the EGC flows eastward towards the Jan Mayen branch of the NAC from the Norwegian Basin. The two branches lead to the formation of two cyclonic gyres in the central zone of the GIN-Seas; The Island Sea gyre to the south and the Greenland Sea gyre to the north (e.g. Swift and Aagaard, 1981; Aagaard et al., 1987; Hopkins, 1991). These gyres are bound by the Polar Front (the boundary between Polar waters of low salinity and cold Arctic waters of higher salinity) and the Arctic Front (the boundary between the cold Arctic waters and warm Atlantic waters). Glacial-interglacial fluctuations influence the position of the fronts (e.g. Mokeddem and McManus, 2016). Heat loss to the atmosphere during winter in the Iceland- and Greenland Sea gyres cools the upper water masses, making them denser. Through open ocean convection, the cold, dense water masses begin to sink, forming thick layers of dense, cooled, oxygenated waters in the sub-surface (Swift and Aagaard, 1981; Aagaard et al., 1985; Rudels et al., 2005). The products of this winter convection are the upper Arctic Intermediate Water (AIW), formed in the shallower Iceland Sea gyre, and the Greenland Sea Deep Water (GSDW), formed in the Greenland Sea gyre (Swift and Aagaard, 1981). The convection is important in order to maintain the mild climate in northwest Europe (Broecker and Denton, 1989). The intermediate and deep overflow waters formed in the gyres move southward in the GIN-Seas, where they will eventually move into the North Atlantic Ocean via the Denmark Strait, the Iceland-Faeroe Ridge, or the Faeroe-Shetland Channel (Hansen and Østerhus, 2000; Rudels, 1989; Rudels et al., 2005). After entering the North Atlantic, these cold and dense, overflow waters mix with the Labrador Water, and become part of the North Atlantic Deep Water (NADW) (e.g. Swift, 1984; Hansen and Østerhus, 2000) which plays a major role in the global thermohaline circulation (e.g. Broecker, 1991).

3 Material and methods

This study is based on the investigations of the deep marine sediment core HH13 – 089GC which was collected on a scientific cruise to Jan Mayen and East Greenland with the University's research vessel R/V Helmer Hansen. The cruise took place between June 23rd to July 7th of 2013, and core HH13 – 089GC was collected on June 30th 2013. Table 1 provides further information about the coring location, coring depth and core length for core HH13 – 089GC.

Table 1. Coring location and other information about core HH13-089GC.

Station	Date	Time (UTC)	Location	Latitude (N) Longitude (E)	Water depth (m)	Recovery (cm)
HH13-089GC	30.06.13	17:47	East Greenland Scoresbysund 4	70.04.955' N 017.44.911 W	1616	497

3.1 Compressed High-Intensity Radiated Pulse (CHIRP)

Chirp sub-bottom profilers provide vertical resolution of the upper 30 m of unconsolidated sediments. The profilers are high-frequency-modulated marine sources in which the vertical resolution of the system is dependent on the bandwidth of the source, and the horizontal resolution is dependent on the characteristics of the source (Quinn et al., 1998).

The R/V Helmer Hanssen is equipped with a hull-mounted sub-bottom profiler (EdgeTech 3300) which was used for collecting a chirp profile. Chirp data was obtained to find suitable core sites in undisturbed sediments.

Table 2. Study Chirp profile parameters (Ship speed, ping rate, frequency and pulse length)

Ship speed (knots)	Ping rate (Hz)	Frequency (kHz)	Pulse length (ms^{-1})
7 – 10 (transit line 014)	0.2	1.5 – 9	40
0 – 0.2 (station line 015)			

3.2 Swath Bathymetry

Swath bathymetry was collected on board R/V Helmer Hanssen using a multibeam eco-sounder system. The system consists of a large set of echo-sounders set in a line, opposite to the direction of travel. The eco-sounders are pointing sideways and each is inclined at a different angle to the vertical (Denbigh, 1989). The multiple beams are sent out by the echo-sounders in a fan shape, reflected at the seafloor and recorded by the ship. The frequencies used are dependant of water depth, and the data collected provide the basis for creating a bathymetric map illustrating the seafloor morphology (https://woodshole.er.usgs.gov/operations/sfmapping/swath.htm) Collected February 2nd 2017.

The multibeam eco-sound system used on board R/V Helmer Hanssen is the Kongsberg EM 300 which can map the seafloor bathymetry down to 5000 m, using a frequency of 30 kHz and a swath width of 150 degrees.

3.3 Conductivity – temperature – depth profile (CTD)

A CTD device is an important oceanographic research tool used for continuous measurement of conductivity and temperature changes with depth. The electronic instruments of the CTD device can provide a profile of the chemical and physical properties through the entire water column above the sampling site. The conductivity can be calculated to salinity, which together with temperature provides information about water density. The measurement was done prior to coring on board the R/V Helmer Hanssen using the Seabird 911 plus CTD instrument. It is important to remember that the CTD measurements represents the water masses at this specific study area in present time.

3.4 Sediment coring

The coring was done on board the R/V Helmer Hanssen using a gravity corer. The corer consists of a core- cutter and catcher at the end of a six-meter-long steel pipe, with a weight on top. Inside of the steel pipe is a plastic liner which will eventually hold the sediment sample. The weight at the top allows the core cutter and steel pipe to penetrate the sea floor sediments, and the core catcher prevents the material from falling out during retrieval. Once retrieved and back on deck, the sediment sample lies protected inside the plastic liner which is then removed from the steel pipe, closed off, cleaned and cut into meter-sections. The sections are closed off at both ends with plastic caps and labelled with the core- name, depth, upward direction and section number. In the case of core HH13 – 089 GC, the corer managed to retrieve 4.97 m of sediments. The core was cut into five sections, four of which measured 1 m and one which measured 97 cm. The sections were kept in the University's cooler room at approximately + 4 ^{O}C until their opening in April 2016.

3.5 Multi sensor core logger (MSCL)

The multi sensor core logging was done at the laboratory at the Department of Geosciences, University of Tromsø (UiT), Norway, and the MSCL used was the GEOTEK Multi Sensor Core Logger (MSCL-S). This system can provide high resolution data concerning physical, elemental and mineralogical properties from sediment and rock cores (GEOTEK, 2014). The MSCL system can measure magnetic susceptibility, wet bulk density, p-wave velocity and p-wave amplitude, and temperature (https://uit.no/om/enhet/artikkel?p_document_id=390245&p_dimension_id=88137&men=28927 Collected February 1st 2017).

Magnetic susceptibility

Magnetic susceptibility (MS) is a measurement of the degree of magnetization of the sediments when exposed to a magnetic field. Positive magnetic susceptibility reflects a strengthen magnetic field due to the presence of paramagnetic, ferromagnetic, ferrimagnetic or antiferromagnetic material. Negative magnetic susceptibility on the other hand reflects a weakened magnetic field due to the presence of diamagnetic material (GEOTEK, 2014). The measurement of magnetic susceptibility of core HH13-089GC was done using the MSCL loop sensor.

3.6 Laboratory work

Most of the laboratory work was carried out by the author in the laboratory of the Department of Geosciences, UiT. The work started in the beginning of April 2016 and carried out until February 2017. The dating of samples was carried out by the ^{14}CHRONO Centre at Queen's University in Belfast, United Kingdom, and the stable isotope analysis was carried out by the Department of Earth Science and Bjerknes Centre for Climate Research at the University of Bergen, Norway. A description of all the laboratory work will now follow.

3.6.1 X-ray imaging

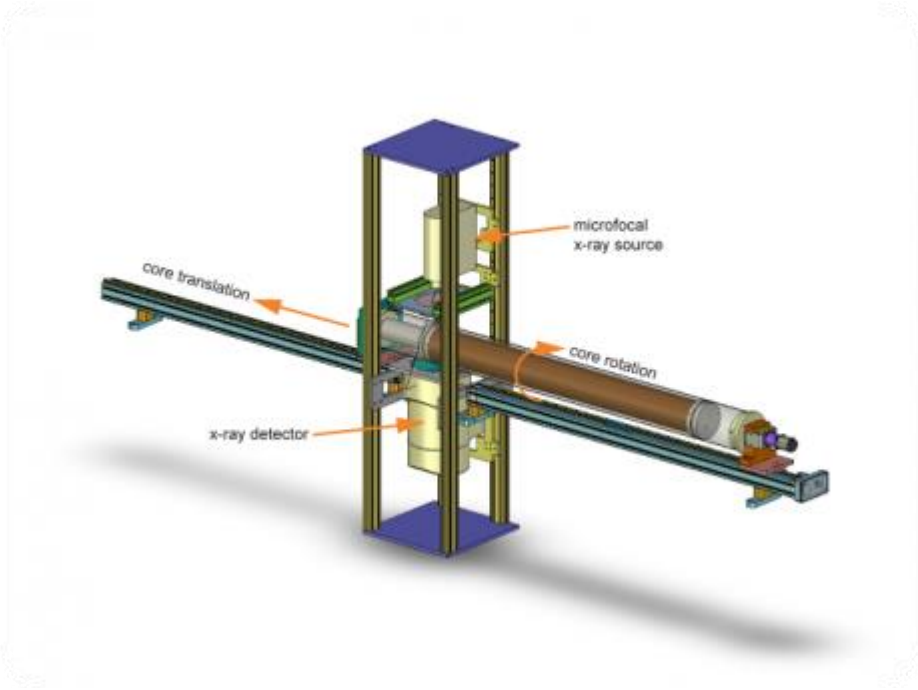

Figure 4: *3D model of the Geotek MSCL-XCT (Figure from http://www.geotek.co.uk/products/mscl-xct).*

X-ray photographs were taken of each whole section prior to opening at the department's laboratory using the Geotek MSCL-XCT x-ray imaging machine in April 2016. The intensity of an x-ray beam reduces as it passes through an object due to absorption and scattering of photons. This process is called X-ray beam attenuation. Differences in the sediment density will cause variations in this attenuation. The colour intensity of the X-ray images is proportional to attenuation. Changes in density therefore leads to different colour intensities on the images (Lofi and Weber, 2001). In the case of the X-ray images of this thesis, the coloration is inverse to regular X-ray images. Darker coloration reflects high density objects whereas lighter coloration reflects lower density materials. The images are useful tools to help recognizing objects and features in the core such as clasts, shells and sedimentary structures which can be difficult to identify on the sediment surface. The imaging process of one-meter-long, soft-sediment cores is fast, and usually done in less than five minutes.

3.6.2 Opening- and description of core

The core sections were opened on April 12th, 2016. The plastic liner surrounding the core material was cut using two circular saws, and the caps were cut using a knife. Once the liner and caps were cut, an osmotic knife was used to cut the sediments into two close to equal halves. One half of the core was chosen to be an archived half, where only non-destructive measurements could be made. The other half was chosen to be the working half where all sampling would be done. The archive half was properly marked, wrapped in cling-film and plastic before it was put in storage at 4 ^{o}C.

The surfaces of the working halves were gently cleaned before they could be investigated. Any visible features such as colour variations, lithological boundaries, sedimentary structures, clasts, shells etc. were described. Sediment colour was described using the *Munsell Soil Colour Chart* (Munsell, 1973). The lithological log presented in this paper (Figure 6) is based on these surface descriptions along with X-ray images, XRF colour-images and grain size data. The working half was kept wrapped in plastic in the cooling room at 4 ^{o}C in between work sessions.

3.6.3 Colour images

Colour images were taken on the archived core-halves. Prior to the procedure, they were taken out of the cooler in order to evaporate most of the surface water. This reduces reflections when the images are taken. The surfaces of the cores were gently smoothened using plastic cards, in order for the structures to be more visible. The colour images were taken using the Jai L-107CC 3 CCD RBG Line Scan Camera, which is installed on the Avaatech XRF core scanner at the geoscience laboratory at UiT, Tromsø.

3.6.4 Sediment sampling

The sampling interval was decided to be every five centimetres for the entire core. Each sample was approximately 1 cm in width, and was collected using a small spatula. The outer edge of each interval was not sampled due do possible disturbances from the coring process. Twenty samples were collected from each section, giving a total of 100 samples all together.

Each sample was put into labelled plastic bags of known weight. The bags with sample material were then weighed in order to record the sample wet weight. The wet weight varied between 34.07 g and 81.95 g. Following the weighing, the samples were placed in the freezer until freeze drying could commence.

The freeze dryer used was the *Christ Aplha 1 – 4 LSC plus* at the UiT Department of Geosciences' laboratory. The freeze drying process is one where the frozen water within the samples is vaporized directly without entering the liquid state. The process is more gentle when it comes to foraminiferal preservation. Following the freeze drying, all samples were weighed once again to record the dry weight and calculate water content.

3.6.5 Wet sieving

Each sample was wet sieved through four sieves of mesh-sizes 1 mm, 500 μm, 100 μm and 63 μm respectively. In between samples, the residues from each sieve was collected in thick, wetted filter papers using distilled water. The filter papers were labelled with core name, sample depth and size fraction. The sieves were cleaned thoroughly with water, put into ultrasonic bath for five minutes and

dried with compressed air to remove any remaining debris in between each sample. The filter papers were closed with a paper clip and placed in an oven for drying at 40 ^{o}C. The dried residues were weighed and put into small labelled glass jars with lids.

3.6.6 Foraminiferal analysis

For the counting of planktic and benthic foraminifera, the size fraction between 100 – 500 μm was used. The larger size fractions were also checked for larger forms. The entire residue or parts of the residue of known weight was spread as evenly as possible on a picking tray with 45 squares using a small spoon. Underneath the picking tray was a collecting tray. Planktic foraminifera was picked and identified from random squares until a total number of >300 specimens were counted. This number of specimens was suggested by Phleger (1960) for quantitative investigations. Foraminiferal fragments and severely damaged foraminifera were not counted. The planktic and benthic foraminifera were identified to species level, and the relative abundance (%) of each species, and the total foraminiferal abundance (No. foraminifera/g dry weight sediment) was calculated using the following formulas:

1) The relative abundance (%) of each species is calculated in the following way:

   *Relative abundance = (Number of specimens of species X * 100) / Total number of specimens*

2) Several steps were necessary in order to calculate the total abundance of foraminifera per g dry weight sediment.

   Number of foraminifera per square = Number of foraminifera counted / Squares counted

   *Number of foraminifera per tray = Number of foraminifera per square * 45*

   *Number of foraminifera per g tray residue = (Number of foraminifera per tray * Number of trays counted) / Weight of tray residue*

   *Number of foraminifera in >100 μm residue = Number of foraminifera per g tray residue * Weight of >100 μm residue*

   Total abundance = Number of foraminifera in >100 μm residue / Total dry weight sediment

Benthic foraminifera were generally rare, though some samples contained higher amounts. It was therefore decided along with my supervisor that only one tray of benthic foraminifera for each sample would be counted and identified. This was done to get a record of the total number of benthic

foraminifera/g in the sample. Most of the benthic foraminifera was identified to species level, while a few were identified to genus level only. The microscope used for the picking and identification of foraminifera was the *Leica M212*.

3.6.7 Ice rafted detritus (IRD)

Ice rafted detritus (IRD) is coarse grained material that has been transported and deposited by icebergs or sea-ice. IRD is therefore an important tool in the investigation and reconstruction of glacial activity and glacial outreach, factors that are mainly controlled by climate (Stein et al., 1996). Massive inputs of IRD often accompanies Heinrich Events.

The size fractions of >1 mm and 500 μm – 1mm were used for the counting of ice rafted detritus. The number of grains varied greatly throughout the 100 samples. All grains were counted, and the concentration of IRD was calculated as number of grains per gram dry weight sediment. The approximate percentage of dark mineral grains was also calculated. Most of the coarse IRD consisted of quartz.

3.6.8 Sortable silt analysis

Sortable silt analysis is a method which can be used as an indication for variations in paleocurrent strength. "Sortable" sediments refer to the grain size fraction that is physically sortable by the investigated bottom currents (Hass, 2002). The sortable silt fraction has been set to the range 10 – 63 μm. This is because sediment finer than 10μm has a tendency to have a cohesive behaviour where they clump together. In the sortable silt range, the particles usually behave in a non-cohesive manner (McCave et al., 1995a).

Sampling and method

The decision to perform a sortable silt (SS) analysis was made after sieving had been done for the original 100 samples. During the sieving process, the size fraction < 63μm was not preserved and could not be used for the SS analysis. In accordance with my supervisors, it was decided that one hundred new samples would be taken from the lower border/edge of the previous sampling sites for the SS analysis.

The samples were taken by scraping a small amount of sediment form the lower edge of the sampling scar with a small spatula. The samples were weighed in small labelled plastic bags before they were freeze dried. The empty plastic bags had been labelled and weighed before the sampling took place. Following the freeze drying, the samples were weighed again and their dry weight noted down.

For each of the one hundred samples, approximately > 2 g of dry sample was taken out and put into labelled PIDS tubes, and treated with ca. 40 mL of 20% hydrochloric acid (HCl) to remove calcareous residues (foraminifera etc.). The HCl was set to work for 24 hours in a laboratory fume hood before the samples were centrifuged for 4 minutes at 4000 rpm and washed with distilled water. The centrifuging and washing was repeated three times. Next, the samples were treated with 20% hydrogen peroxide (H_2O_2) to remove any organic material. The PIDS tubes were covered with aluminium foil and then put in a water bath (80^{o}C) for two hours. During the first fifteen minutes the bath needed constant monitoring in order not to lose any material if the reactions were strong. The reaction was very strong for all samples, and they had to be taken out of the bath in order to calm the reaction before they were put back. Some material was lost during the strongest reactions, but fortunately not a lot. The reaction was slightly less strong in the bottom section of the core. After two hours in the bath, the samples were again centrifuged and washed three times with distilled water. The clean samples were transferred into plastic cups and set to dry in a laboratory fume hood.

Once dry, approximately 0.5 g of dry sample was left behind in the plastic cups whereas the rest of the sample was put into labelled plastic bags for storing. 20 mL of tap water was added to the plastic cups, before they were placed on the shaker machine to mix for a minimum of 24 hours.

Two drops of Calgon solution was added to the suspended samples as a dispersing agent to prevent settling or clumping of the material before they were placed in an ultrasound bath for five minutes. The samples were sieved through a 2 mm sieve before they were analysed with the LS13320 Laser Diffraction Particle Size Analyzer (LDPSA).

3.6.9 Radiocarbon dating

Radiocarbon dating is a very useful method for dating material from the Late Quaternary (Bradley, 2014 p. 59). The method is based on measurements of the only unstable and therefore radioactive isotope of carbon, ^{14}C (Bowman, 1990).

Radiocarbon (^{14}C) is continuously formed in the upper atmosphere due to neutron “bombardment” of nitrogen atoms (^{14}N) from cosmic rays. This “bombardment” leads to the formation of ^{14}C, a carbon atom comprised of six protons and eight neutrons;

$$^{14}_{7}N + ^{1}_{0}n \rightarrow ^{14}_{6}C + ^{1}_{1}H$$

After being formed, ^{14}C combines with oxygen to form carbon dioxide which is indistinguishable from carbon dioxide containing^{12}C and ^{13}C. Through the formation of carbon dioxide, radiocarbon enters

into the carbon cycle and hence into the biosphere (Bowman, 1990). As mentioned earlier, ^{14}C is unstable, and will decay to nitrogen over time through the release of a β-particle.
The process of radiocarbon dating is based on the non-valid assumption that the production rate of ^{14}C in the atmosphere is more or less equal to the rate of decay, leading to a constant total weight of global ^{14}C (Bradley, 2014 p. 60). If the concentration of ^{14}C in the atmosphere is constant, then the ^{14}C level in all living organisms will also remain constant. When an organism dies however, the uptake of ^{14}C will cease, and since the isotope is unstable, the remaining ^{14}C atoms in the body will start to decay with a half-life of 5730 years. By comparing the number of ^{14}C atoms remaining in a dead sample with the constant atmospheric concentration, one can determine how much time has gone by since death (Bowman, 1990). There are different methods for radioactive dating. Accelerator Mass Spectrometry is the only method which will be described in this report. For more details about radiocarbon dating, see Bowman (1990).

3.6.9.1 Accelerator Mass Spectrometry (AMS)

Four depths were chosen for radiocarbon dating the core HH13-089GC. Table 3 shows the sampling depth, material type and material weight for the three samples. Based on correlation with the magnetic susceptibility data from core HH13-089GC with a nearby core from the same area (HH13-092GC) (Schröder, 2014, Geology Project at UiT) which was ^{14}C dated in 2014, it was believed that none of the four samples chosen would date older than approximately 30,000 years. The material needed was identified using a picking tray, and collected and weighed in small plastic vials of known weight. The four plastic vials were then labelled and packed thoroughly with bubble wrap before they were sent off to the ^{14}CHRONO Centre, Queen's University, Belfast, UK in a padded envelope to be dated.

The four radiocarbon dates were obtained by using an Accelerator Mass Spectrometer (AMS), and the procedure was done using the planktic foraminiferal species *Neogloboquadrina pachyderma* (*N. pachyderma*).

Table 3. Material for radiocarbon dating - Sampling depth, material type and sample weight.

Lab code	Sample ID	Sampling depth (cm)	Material type	Sample weight (mg)
UBA-33264	HH13-089GC	30 – 31	*N. pachyderma*	7.4
UBA-33265	HH13-089GC	85 – 86	*N. pachyderma*	11.7
UBA-33266	HH13-089GC	140 – 141	*N. pachyderma*	12.3
UBA-34237	HH13-089GC	245 – 246	*N. pachyderma*	12.9

The AMS-dating method measures the concentrations of individual ions of ^{12}C, ^{13}C and ^{14}C. The ions are sent through a magnetic field after being accelerated to extreme speeds in a tandem electrostatic accelerator. The magnetic field separates the different ions, and enables their concentrations to be measured. The method has many advantages to conventional ^{14}C-dating, the number one being sample sizes. Samples containing much less than 1mg of carbon have been dated, making this procedure great when it comes to dating material such as foraminiferal tests (Bradley, 2014 p. 62). The weight of the material dated in this thesis varied between 7.4 – 12.9 mg, which relates to 1200 – 1400 specimens of *N. pachyderma*.

3.6.9.2 Marine reservoir effect

There are several processes affecting the global concentration of ^{14}C, which means that it is in fact not constant. The ^{14}C concentration in living organisms will depend on several factors that need to be taken into account and calibrated for after radiocarbon dates have been obtained.

New ^{14}C can only enter the vast oceans at the sea surface-atmosphere boundary. At this boundary, the radiocarbon concentration will be equal to that of the atmosphere. As this water sinks, the introduction of "new" ^{14}C ceases, and the decay process begins. This process gives the water masses an apparent age. Organisms living within these water masses will take up the "old" ^{14}C and incorporate it into their shells etc. When these materials are used for radiocarbon dating they will thus appear older than they actually are (Bowman, 1990). This effect is called the marine reservoir effect (R), and is defined in Mangerud et al. (2006, p. 3228) as; "the ^{14}C-age-difference between a sample which acquired its carbon from the ocean water and a sample that contemporaneously obtained its carbon from the atmosphere". The average R of the surface ocean is 400 years, but varies in space and time (termed ΔR). The marine reservoir effect varies on a global scale and is an important calibration when dating deep marine materials.

The software program CALIB 7.0.4 and calibration curve Marine13 (Stuvier and Reimer, 1993; Reimer et al., 2013) was used to calibrate the radiocarbon dates obtained for this report (Table 4).

3.6.10 Stable Isotope analysis ($\delta^{18}O$ and $\delta^{13}C$)

> Marine sediments provide long continuous records of past climate changes…Stable isotopes provide the means to reconstruct a range of variables including surface and deep ocean circulation patterns, sea surface and bottom water temperature, sea surface salinity, iceberg activity and origin, upwelling intensity, productivity, nutrient utilization, surface-water dissolved carbon dioxide content and water-column oxygen content in addition to inferences on global ice volume, ice sheet failure, river discharge, aridity, vegetation composition, and continental erosion rates (Maslin et al., 2006 p. 227).

Oxygen isotopes

Oxygen is one of the most important elements on earth. It is a major constituent in water, a crucial liquid for every living processes on this planet (Urey, 1948). Oxygen exist in fixed amounts of different stable isotopes (^{16}O, ^{17}O and ^{18}O), the most important being ^{16}O and ^{18}O. Approximately 99.76 % of oxygen is in the "light" form of ^{16}O and only about 0.2 % in the "heavy" form of ^{18}O (Bradley, 2014 p. 141). As a result, water-molecules (H_2O) can exist as either "light" forms containing ^{16}O, or "heavy" forms containing ^{18}O. Water-molecules containing ^{18}O, has a lower vapor pressure than those containing ^{16}O. They therefore evaporate more slowly and condense more rapidly than water containing ^{16}O. This process is known as isotope fractionation and is related to the atomic mass of the isotopes, and most importantly to temperature (Bradley, 2014 p. 142).

Most foraminifera build their tests of calcium carbonate ($CaCO_3$) crystallized from sea water. This slow crystallization will lead to a slight concentration of ^{18}O in the $CaCO_3$ relative to the concentration in the water. This is a temperature dependent process, and the concentrating effect increases with lower temperatures (Bradley, 2014 p. 199). The ratio of the oxygen isotopes ($^{18}O/^{16}O$ defined as $\delta^{18}O$) in test building organisms such as foraminifera and coccoliths can be measured. The ratio makes it possible to determine the temperature (e.g. Kellogg et al 1978), water stratification and salinity (e.g. Duplessy et al., 1992) at which the organism lived (Urey, 1948).

Oxygen isotope stratigraphy

Oxygen isotope stratigraphy is a method which makes it possible to determine approximate ages of sediments based on oxygen isotopic ratio measurements. Over the years numerous studies from all over the world, have carried out oxygen isotope analysis ($\delta^{18}O$) of planktic and benthic foraminifera for instance. All studies on benthic foraminifera have found similarities in their results, and concluded that similar isotopic variations are recorded in all areas. These conclusions have been made after taking several factors into account such as vital effects (different foraminiferal species record different $\delta^{18}O$ values under similar temperature an salinity conditions), variations in sedimentation rates, and ice volume change (due to sea level changes). Isotopic changes in benthic foraminifera have been found

to mainly be a record of changes in terrestrial ice volumes, and hence climate over time (Bradley, 2014 p. 211). Foraminiferal tests have been found to be rich in ^{18}O during colder periods with high ice volume, and depleted in ^{18}O during warmer periods with low ice volume. The growth and decay of ice sheets is believed to be driven by orbital cycles. Several attempts of making a global oxygen isotope record has been conducted, the most recent being the LR04 benthic stack by Lisiecki and Raymo (2005). The result is a record showing more than 20 periods of major continental glaciation during the Quaternary period (Bradley, 2014 p. 199 – 214). The global signal makes it possible to correlate records from all over the world, and thereby develop an initial interpretation of the core stratigraphy and age, before any dating of core material has been made. The global isotopic signal can be recognized in numerous planktic records as well, however these records can be more affected by local temperature and salinity changes due to meltwater events for instance, thereby making them more difficult to interpret. The global isotope record has been divided into oxygen isotope stages where uneven numbers represent interglacial stages and even numbers represent glacial stages. Sub-stages are also given for interstadial- and stadial periods. Oxygen isotope stratigraphy in addition to radiocarbon dates will provide the basis for the construction of the age model later in this thesis.

Carbon isotopes

Carbon is vital for all life on earth and exists in the two stable forms ^{12}C and ^{13}C. ^{12}C accounts for approximately 99 % of the carbon present on Earth, whereas most of the rest is in the form of ^{13}C (Ruddiman, 2013, chapter 11). The stable carbon isotope ratio ($^{13}C/^{12}C$ defined as $\delta^{13}C$) in foraminiferal tests is a function of the dissolved inorganic carbon ratio in the seawater. Stable carbon isotope analysis can be used to reconstruct changes in paleoproductivity and ventilation of surface waters (Jansen, 1989). Carbon isotopes can help researchers understand the variations in the oceanic carbon cycle, and be a very useful tool in high latitude regions for chronology and correlation in addition to the oxygen isotope stratigraphy. (Jansen, 1989). The $\delta^{18}O$ or $\delta^{13}C$ ratios are measured as departures in parts per thousand (‰) from a laboratory standard (Ruddiman, 2013, chapter 11);

$$\delta(\text{Sample})\,‰ = \frac{\text{Ratio}_{(\text{sample})} - \text{Ratio}_{(\text{standard})}}{\text{Ratio}_{(\text{standard})}} \text{ X } 1000$$

Sampling

For this report, the foraminifera species *N. pachyderma*. was chosen for the stable isotope analysis of carbon and oxygen. The foraminifera needed to be of proper quality, which meant four clear chambers and no broken specimens. The foraminifera were picked once again using a picking tray and collected in small plastic vials. Approximately 15 – 25 specimens were picked from each sample. The plastic vials were labeled and packed closely in a small polystyrene box specifically made for sample transportation. Specimens from each of the 100 samples were to be sent off for the analysis, however

some samples contained too few specimens or specimens of poor quality. Therefore, only 96 samples were analyzed. The samples were analysed using the Finnigan MAT 253 mass spectrometer at the Bjerknes Centre for Climate Change, University of Bergen, Norway. A sheet containing information about sample depth, species, and number of specimens was sent along with the samples.

3.7 Statistics and data processing

Excel 2016 was used to plot all data related to foraminifera, IRD and sediment properties, and to carry out most of the calculations. Grapher 11 for Windows was used alongside Excel for plotting the graphs. Figures and figure adjustments were made using Grapher 11 and CorelDRAW for Windows. SedLog 3.1 was used to make the sedimentary log of the core, and GRADISTAT v 8.0 was used for grain size analysis of the sortable silt samples.

3.7.1 Handling of raw data for the sortable silt and grain size analysis

When investigating the fraction of sortable silt for the bottom current reconstruction, it was important to look at the possible influence of ice-rafting on the silt fraction. Any coarse-grained silt within the fraction that has potentially been ice-rafted, can result in coarser grain sizes than the current sorting process alone (Jessen and Rasmussen, 2015; Hass, 2002; Weltje and Prins, 2003) Since the core HH13-089GC is from an area that is highly influenced by icebergs and sea-ice, it seemed reasonable to expect that the sortable silt fraction consisted of both ice-rafted and current sorted material. The sortable silt mean size has been described to be the best parameter to overcome changes that are related to sediment supply, and is considered the standard (McCave et al., 1995a; Hass, 2002). Jessen and Rasmussen (2015) however have used the median size of sortable silt instead. Their reasons being that; “For any grain size distribution that is a mix of a current sorting signal and an ice-rafted signal, the median size will be less affected than the mean size.” Since the data from the present study is expected to possibly be influenced by ice-rafting, the median size of sortable silt has been used.

The median size was found by determining a “window” for the interval of sortable silt (10 – 63 μm) on each graph within the LDPSA computer program itself. By doing this, the program provides both the median and mean sizes of the “window” directly. As each sample was run three times, the average median size of these three runs are then calculated and used in the graph making.

Hass (2002) describes how it is possible to test if the silt fraction under investigation is primarily current sorted, or if parts of it is ice-rafted. This can be done by plotting the weight per cent sand (wt%) against median SS in this case. If there is a positive correlation between these parameters, it indicates that parts of the silt fraction has been ice-rafted (Hass, 2002). This is something that can be corrected for, although McCave and Hall (2006) found it not to be necessary, except if ice-rafting was very intense.

Sand is considered as IRD, and the wt% sand in the samples can therefore be used as a proxy for the degree of ice rafting (Jessen and Rasmussen, 2015). The mean of the complete grain size data for the three runs of all the samples was calculated and entered into the GRADISTAT v 8.0 grain size analysis program. The program runs the results and calculates several sample properties for all the samples, wt% sand being one of them.

3.7.2 Calculating porosity, dry bulk density and flux

Porosity and dry bulk density (g/cm^3) was calculated using the following formulas:

- Porosity = Water content / Volume
- Dry bulk density = Wet bulk density – (1.026 * (Porosity / 100))
  Where
  - Wet bulk density = Wet weight / Volume
  - Volume ($\pi r^2 h$) = 78.540 cm^3 (r = 5 cm; h = 1 cm)

Flux calculations:
Sediment Mass accumulation rates (MAR) needed to be calculated prior the flux calculations using the following formula:

- MAR (g/cm2/ka) = Dry bulk density * LSR

Fluxes of planktic and benthic specimens, grain size fractions 63 – 100 μm and 100 – 500 μm and IRD needed to be calculated after the age model was competed using the following formulas:

- No. Benthic foraminifera/cm2/ka = No. Benthic foraminifera/g * MAR
- No. Planktic foraminifera/cm2/ka = No. Planktic foraminifera/g * MAR
- Flux of 63 – 100 μm fraction (g/cm^2/ka) = % 63 – 100 μm * MAR
- Flux of 100 – 500 μm fraction (g/cm^2/ka) = % 100 – 500 μm * MAR
- Flux of IRD (g/cm^2/ka) = No. IRD grains/g * MAR

4 Foraminifera

Foraminifera are unicellular protozoans that live either in the upper water masses amongst the marine plankton, on the sea floor, or within the sea floor sediments (Armstrong and Brasier, 2005, p. 142). The cell of the foraminifera is enclosed in a test built from carbonate (CaCO3), which is secreted as calcite or aragonite. The species with such a test is called calcareous foraminifera (Corliss, 1985). Some benthic foraminifera are known as agglutinated species. These build their tests by collecting organic materials or sediment particles, which are "glued" together by the secretion of an organic substrate known as tectin (Corliss, 1985; Tappan and Loeblich, 1988). The tests are divided into one or several interconnected chambers (Armstrong and Brasier, 2005, p. 142), which can be added either episodically or by continuous growth (Jones, 2014). Foraminiferal tests can, under the right conditions, be preserved as microfossils in the marine sediment record, where they can be very abundant. (Armstrong and Brasier, 2005, p. 142).

Different foraminiferal species can have strong environmental preferences (Hald and Steinsund, 1992), and ecological factors such as; light, temperature, salinity, oxygen and nutrient availability, food supply, current strength, and water masses influence the distribution of the foraminiferal assemblage (Armstrong and Brasier, 2005, p. 152 – 155). Knowledge on foraminiferal ecology based on studies of modern assemblages have therefore provided the basis for making foraminifera an important and reliable proxy in paleoenvironmental and paleoceanographic reconstructions and research (Sejrup et al., 2004; Polyak et al., 2002). Foraminiferal microfossils are also used by the industry e.g. in oil exploration (Hemleben et al., 1989, p 3). Foraminiferal identification is based on morphological features such as aperture shape, chamber arrangement, test composition and wall structures (Tappan and Loeblich, 1988).

4.1 Planktic foraminifera

Most planktic foraminifera live in the upper parts of the oceanic water column. The majority of planktic species tend to live in the photic zone, but some are able to live below. Several species descend to deeper waters towards the end of their lives, or during their reproductive cycle (Hemleben et al., 1989, p 1). Densities of planktic foraminifera can be very high around the margins of oceanic gyres, which are linked to upwelling and mixing and provide high nutrient levels (Armstrong and Brasier, 2005, p. 159).

The only major ecological factors that control planktic foraminiferal assemblages and distribution are temperature and salinity. These characteristics make planktic foraminifera very useful when it comes

to estimating sea surface temperatures (SST) in recent fossil records for example (Armstrong and Brasier, 2005, ch. 15).

4.1.1 *Neogloboquadrina pachyderma* (Ehrenberg, 1861)

In high latitude samples, the planktic species *Neogloboquadrina pachyderma* dominates the assemblages (Darling et al., 2004) and can therefore be very useful in Quaternary climatic reconstructions. The species coils towards the left when building a test, and have specific environmental preferences. *Neogloboquadrina pachyderma* dominates in polar regions (Darling et al., 2004), and is linked to waters with low temperatures, low salinities and high nutrient levels (Bé and Hutson, 1977). The species is therefore a good indicator for these parameters. *Neogloboquadrina pachyderma* is known to be widespread throughout the entire Greenland – Norwegian Sea where it thrives between 25 – 250 m water depth (Simstich et al., 2003).

Neogloboquadrina pachyderma represents the surface and near-surface environment, as it in some regions can be considered a relatively deep dweller (Simstich et al., 2003). It has been found to reproduce and calcify in the deeper subsurface waters, and the isotopic composition of their tests mainly originates from these waters. Simstich et al. (2003) found the calcification depth of *N. pachyderma* to generally be between 70 – 130 m off East Greenland. It probably lives close to the transition between Atlantic Intermediate Water (AIW) and the surface Polar Water (PW) (e.g. Kohfeld et al., 1996).

4.1.2 *Neogloboquadrina incompta* (Cifelli, 1961)

Neogloboquadrina incompta has often been referred to as *Neogloboquadrina pachyderma* dextral by many researchers, and was considered to be a right coiling variant of *N. pachyderma*. Darling et al. (2006) presented genetic, biogeographic, ecological and fossil evidence that strongly implied that the two coiling variants of *N. pachyderma* should be considered different species. The name *Neogloboquadrina incompta* was suggested, as it was already recognized (Darling et al., 2006).

Neogloboquadrina incompta is a planktic species which prefers temperate areas but is also found in small quantities in the polar sedimentary record (Darling et al., 2006). It is a warm water indicator, and its maximum distribution in the North Atlantic is linked to the influx of temperate Atlantic Water (Bé and Tolderlund, 1971; Johannessen et al., 1994).

4.1.3 *Turborotalita quinqueloba* (Natland, 1938)

Turborotalita quinqueloba is can be among the most dominant planktic species in sediments (Bé and Hutson, 1977), and is therefore valuable in paleoceanographic interpretations (Bauch, 1994). It is most common in subarctic waters, but is also frequent in Arctic, Antarctic and transitional waters (Bé and Tolderlund, 1971). *Turborotalita quinqueloba* is often linked to warm, saline Atlantic Water in the Fram Strait area (Volkmann, 2000). It is also widespread in the entire Greenland and Norwegian Seas, and normally lives in the photic zone at ~ 35 – 75 m (Carstens et al., 1997; Simstich et al., 2003). The dominance of *T. quinqueloba* versus *N. pachyderma* in the sediment can be related to the presence of the Arctic front (Johannessen et al., 1994). *Turborotalita quinqueloba* is a symbiont bearing foraminifera, meaning that photosynthesizing organisms live on the tests (Hemleben et al., 1989).

4.1.4 Accessory planktic foraminifera

Globigerinita uvula (Ehrenberg, 1861)

Globigerinita uvula is a frequent faunal component of the temperate and polar ocean, and decreases in abundance towards lower latitudes (Schiebel and Hemleben, 2016).

Globigerinita glutinata (Egger, 1893)

Globigerinita glutinata is one of the most widely distributed planktic foraminifera, occuring all the way from the Antarctic, through tropical and subarctic waters. Here it is usually present in low numbers (Bé and Tolderlund, 1971). *Globigerinita glutinata* occurs over wide ranges of temperatures (3 – 30^{O} C) (Bé and Tolderlund, 1971) and salinities (34.4-36.4 %) (Bé and Hutson, 1977). Its peak abundance is between 24 – 27^{O} C (Bé and Tolderlund, 1971).

Globigerina bulloides (d'Orbigny, 1826)

Globigerina bulloides is a species that is typical in transitional to polar regions, especially in areas of upwelling. It is found throughout the water column above 400m, but mainly in and above the thermocline. It is not restricted to the photic zone, but occurs mostly above 400 m in cooler waters where non-spinose species are most dominant (Hemleben, 1989; Bé and Tolderlund 1971). *Globigerina bulloides* tolerates a wide range of SST (0 – 27^{O} C), with a peak abundance between 3 – 19^{O} C (Bé and Tolderlund, 1971). The species is generally associated with somewhat warmer, more saline, and lower nutrient levels than *N. pachyderma* (Bé and Hutson, 1977)

Jennings et al. (2004) described all the accessory planktic species mentioned to be associated with the warm and saline Atlantic water of the Irminger Current-branch extending north-eastwards through the Denmark Strait, along the west coast of Iceland.

4.2 Benthic foraminifera

Today's group of living benthic foraminifera, consists of thousands of taxa, and their distribution is determined by several environmental parameters. Benthic Foraminifera live on (epifaunal)- or within the sediment (infaunal) of the sea floor, and their abundance through time has made them very useful in paleoclimatic research (Sejrup et al., 2004).

The importance of different parameters which determine the distribution of benthic foraminifera has been debated. Depth and the hydrography of different water masses were thought to be the main controlling factors (Mackensen et al., 1985), but in Arctic regions it appears food availability and competition are the controlling factors (Wollenburg and Mackensen, 1998).

Benthic foraminiferal assemblages can be used to indicate parameters such as water depth, water temperature, proximity to glaciers and deep water circulation (Sejrup et al., 2004). Benthic foraminifera are also indicators of productivity in areas where productivity is high, such as zones of upwelling (Schnitker, 1994).

A short description of the dominating benthic species (>2 % of the identified total) and their ecological preferences will now follow. A complete list of all benthic foraminiferal species identified within the core, as well as their distribution within the core can be found in Appendix A.

4.2.1 *Oridorsalis umbonatus* (Reuss, 1851)

Oridorsalis umbonatus is a typical North Atlantic- (Bergsten, 1994) and Arctic deep-water species (Schröder et al., 1990). It is an epifaunal detrivore, that prefers salinities between 34.8 – 35‰, and is associated with deep waters down to ~ 3800 m (Murray, 1991). Schröder et al. (1990) describes *O. umbonatus* as a good deep water indicator.

Mackensen et al. (1985) described *O. umbonatus* as a species that prefers a relatively high oxygen content in the sediment, and that can tolerate relatively low food supply. *Oridorsalis umbonatus* is the most common deep-sea benthic foraminifera in the GIN-Sea and Arctic Ocean today, and several studies have found that *O. umbonatus* dominated in this area in periods with increased sea-ice cover (e.g. Streeter et al., 1982; Jansen et al., 1983; Mackensen et al., 1985). The species is believed to be more adaptable to reductions in surface productivity (Jansen et al., 1983).

4.2.2 *Cassidulina neoteretis* (Seidenkrantz, 1995)

Cassidulina neoteretis is a very frequent benthic foraminiferal species on the continental shelf and slopes of the North Atlantic (Mackensen and Hald, 1988). It is an infaunal detrivore, living within sandy or muddy sediments. It prefers marine salinities and cold to temperate waters. It is most commonly found at depths between 1000 – 1500 m (Seidenkrantz, 1995). Under modern conditions, the species is often tied with the Atlantic Intermediate Water in the Nordic Seas, and an indicator of modified Atlantic Water (Jennings and Helgadóttir, 1994; Jennings et al., 2004).

4.2.3 *Triloculina trihedra* (Loeblich & Tappan, 1953)

Triloculina trihedra is widely distributed in shallow waters with salinities greater than 32‰, and ranges into northern temperate waters (Huddart & Peacock, 1990). It is considered a part of the Arctic cold-water fauna (McCabe et al., 1986; Jones, 2011).

4.2.4 *Cassidulina reniforme* (Nørvang, 1945)

Cassidulina reniforme is common in Arctic, glaciomarine environments (Elverhøi and Bomstad, 1980; Hald and Vorren 1987; Hald and Korsun, 1997) where it lives in silty muds at depths greater than 100 m (Mudie et al., 1984). It is an infaunal detrivore, which prefers marine salinities and cold to temperate waters (Murray, 1991). Hansen and Knudsen (1995) found the species to be associated with muddy, sediment loaded waters in front of calving glaciers. Jennings et al. (2004) found that *C. reniforme* and *Elphidium excavatum* (Terquem, 1875) would dominate the fauna when the area was affected by cooler waters and variable salinity conditions.

4.2.5 *Cibicides wuellerstorfi* (Schwager, 1866)

Cibicides wuellerstorfi is a common species in the North Atlantic (Osterman et al., 1999). It is an epifaunal passive suspension feeder that is often attached to hard substrates. It prefers marine salinities and lives in many different environments such as lagoons and shelf-, to bathyal environments (Murray, 1991).

Mackensen et al. (1985) described *C. wuellerstorfi* as a species that; “prefer a relatively high primary productivity with high food supply, but can tolerate a relatively low oxygen content in the sediment.” Several studies have found that over time, *C. wuellerstorfi* dominated in relatively deep areas of the Norwegian-Greenland Sea during ice-free periods with high primary productivity (e.g. Streeter et al., 1982; Jansen et al., 1983; Mackensen et al., 1985).

4.2.6 *Stainforthia loeblichi* (Feyling-Hanssen, 1954)

Stainforthia loeblichi is a common Arctic benthic foraminiferal species (Cronin, 1999). Stainforthia species are known to be opportunistic, and they take advantage of pulses of high seasonal productivity (Polyak et al., 2002). The presence of *S. loeblichi* can therefore be an indication of high productivity at the sea surface.

4.2.7 *Ioanella tumidula* (Brady, 1884)

Ioanella tumidula is a species which is typical for the North Atlantic assemblages (Bergsten, 1994). It occurs in a variety of environments such as fine grained sediments in areas that are seasonally ice free, and in coarser sediments in areas that have permanent ice cover. Several studies (e.g. Green, 1960; Lagoe, 1979; Mackensen et al., 1985) found that *I. tumidula* thrives at different depths (~900 to >3000 m) with relation to ice coverage; The more permanent ice cover in the area, the shallower the depth (Wollenburg and Mackenson, 1998).

4.2.8 *Astrononion gallowayi* (Loeblich & Tappan, 1953)

Astrononion gallowayi is an epifaunal/infaunal detrivore, which prefers low temperatures and relatively high marine salinities (Murray, 1991). It is associated with shallow waters with increased current activities and coarse sediments (e.g. shallow, river-distal areas) (Polyak et al., 2002). *Astrononion gallowayi* found alongside *Cibicides lobatulus* (Walker & Jacob, 1798), is usually an indication of high energy environments (Polyak et al., 2002; Jennings et al., 2004).

4.2.9 *Epistominella arctica* (Green, 1959)

Epistominella arctica is a very small epifaunal/semi-infaunal detrivore living in muddy sediments. It prefers marine salinities and temperate to cold temperatures (Murray, 1991). It is a well-known species in the deep central Arctic Ocean (Lagoe, 1977), and occurs mostly at depths between ~1500 to 2000 m (Green, 1960). *Epistominella arctica* is considered an opportunistic species, which reproduce in large numbers during local blooms of phytoplankton. It can also be an indicator of increased productivity and higher food availability (Wollenburg and Kuhnt, 2000).

5 Results and interpretation

Chapter 5 will describe the results of the sampling site water properties, and the lithological-, sedimentological- and foraminiferal data from core HH13-089GC in separate subchapters. The results of the AMS-dating will also be presented. General interpretations of these results will be described at the end of each subchapter where interpretation is due. Correlation with other proxies and studies will be presented in the discussion.

The results will be described for the core in its entirety, unless stated otherwise. For all data, the results will be described in stratigraphical order from bottom to top, or oldest to youngest.

5.1 CTD desctription

The CTD data over the core location for HH13-089GC is described below (Figure 5). The description will move from the surface, downwards.

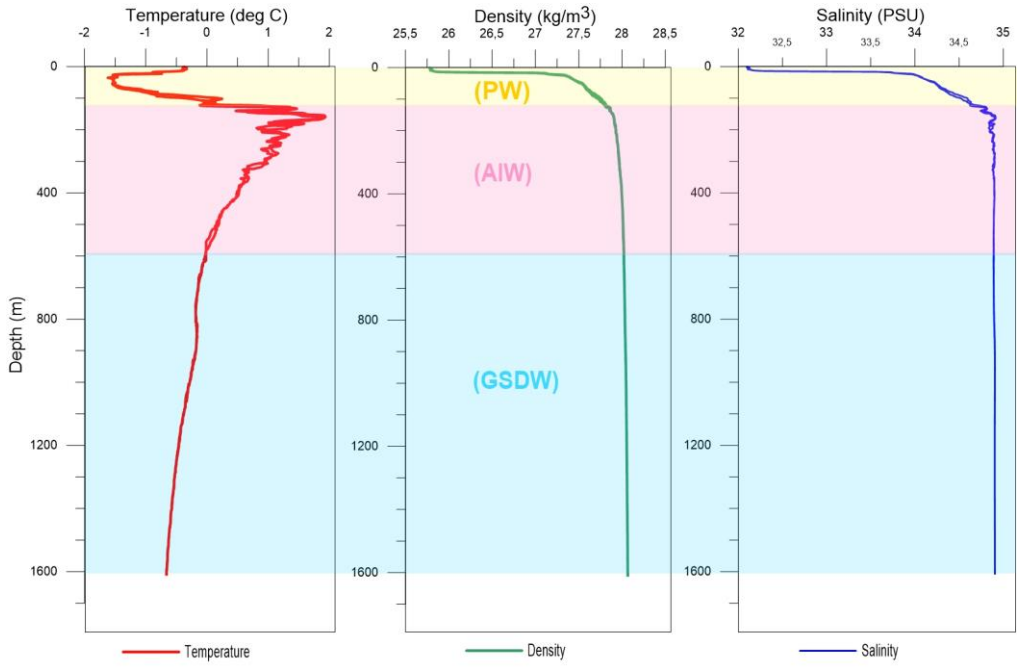

Figure 5: *CTD data collected over HH13-089GC core locations in June 2013. PW = Polar Water, AIW = Atlantic Intermediate Water and GSDW = Greenland Sea Deep Water*

The data display a rapid increase in both density and salinity in the uppermost water masses, before the values are stabilized. Within the upper ~150 m the density increases from ~ 25.7 kg/m^3 to ~ 27.9 kg/m^3. Below 150 m, there is a gradual increase to ~ 28.2 kg/m^3 where the value remains constant throughout the 1600 m water column. The salinity increases rapidly from a minimum of ~ 32‰ at the surface to 34.9‰ at 150 m. Below this boundary, the salinity is relatively constant at 34.9‰.

The temperature follows a slightly different trend. At the surface, the temperature is approximately -0.4°C, but instead of rapidly increasing, it shows a rapid decrease to -1.5°C within the upper 50 m. Between 50 – 160 m, the temperature increases drastically with some fluctuations to the maximum +1.9°C. Below 160 m, fluctuations between +0.5 and 2°C can be observed with an overall decreasing trend down to ~ 0°C at 600 m. A small average decrease is seen below this point and down to ~ 1600 m where temperature is -0.6°C. There is a small increase just below 800 m, before the decreasing trend continues.

5.1.1 Interpretation

The interval between ~ 0 – 100 m has been interpreted to represent the Polar Water (PW) fraction of the EGC due to the very low temperatures and relatively low salinities which is common for PW (Chapter 2.1.2). Meltwater presence in the uppermost parts is indicated by the very low densities and salinities. The interval which follows down to ~ 600 m has been interpreted to represent the Atlantic Intermediate Water (AIW) based on the high temperatures and high salinities (Chapter 2.1.2). The last interval has, based on the properties, been interpreted to represent the Greenland Sea Deep Water (GSDW) (Chapter 2.1.2).

5.2 Sedimentological description of HH13-809GC

The general lithological description of the core based on visual investigations and X-ray images, will be given separately for each section of the core. As mentioned earlier, the core was divided into 5 sections after retrieval, each of approximately 100 cm. The XRF colour images were taken for each of these sections, and by dividing the description in the same manner for this subchapter, it can easily be followed on the images in figure 6. The colour indications are given according to the Munsell Soil Color Chart.

The description of grain size distribution, wet bulk density, water content and magnetic susceptibility however, will be done for the core in its entirety in separate subchapters.

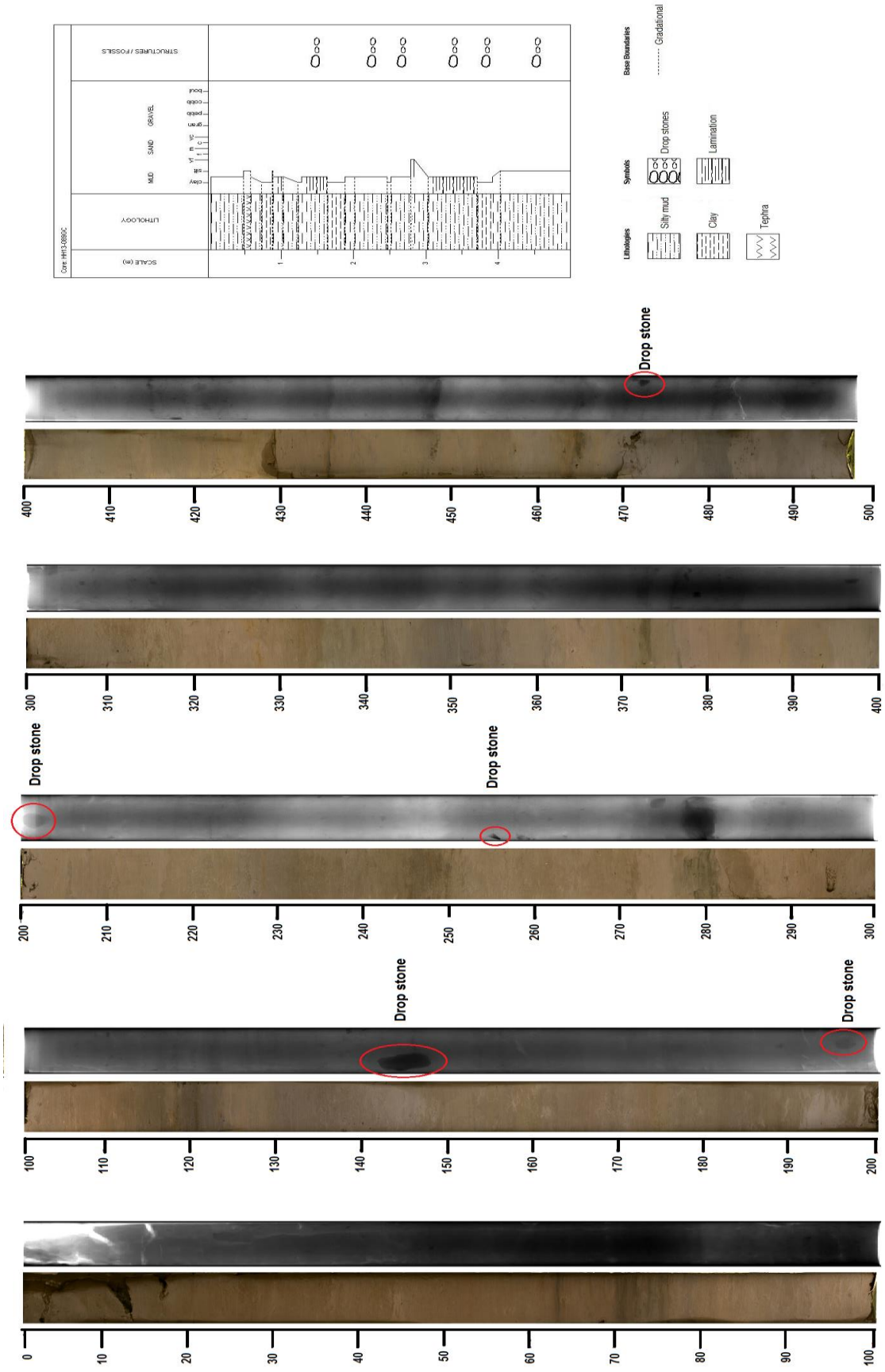

Figure 6: *Gravity core HH13-089CG shown by photographs, X-ray images plotted against depth (cm), and sedimentary log.*

Section 5 (497 – 400 cm)

The lowermost section of the core, section 5 consist of homogenous silty mud. The sediment appears to be slightly coarser than the other four sections. At ~ 483 – 479 cm a dark grey colour is seen (2.5 YR N4/0). From this point up to 470 cm, the sediment has a grey colour (10YR 6/1) before it changes to a light brownish grey (10YR 6/2), which continues up the rest of this section. Two brownish black lenses of clay are seen at 465 cm and 435 cm respectively.

At 471 cm, a black well rounded drop stone with low sphericity is found. This drop stone measures 3 cm at its widest (pebble sized). A black, well rounded drop stone of 2 cm (pebble sized) with high sphericity is found at 420 cm.

Section 4 (400 – 300 cm)

Most of section 4 consists of homogenous silty mud with a light brownish grey (10YR 6/2) colour. Between ~ 362 – 335 cm the colour is grey (2.5YR 5/0), before the light brownish grey is back, and continues towards the top of this section. Some slight lamination can be seen in this area, with some olive grey (5Y 4/2) and very dark grey (10YR 3/1) layers of clay at 389 cm, 377 cm, 372 cm, 370 cm and 368 cm respectively.

At 384.5 cm, a black drop stone measuring 2.5 cm (pebble sized) is found. The drop stone is sub-angular with relatively high sphericity. A drop stone consisting of quartz is found at 361 cm. It measures ~ 2 cm (pebble sized) and is sub-angular with low sphericity.

Section 3 (300 – 200 cm)

Section 3 consists of silty mud with interbedded layers of clay, and one layer of very fine grained sand. Most of the section is made up of homogenous silty mud and has a light brownish grey (10YR 6/2) colour. Between ~ 295 – 277 cm, the coarsest layer throughout the core is encountered. This layer has a dark greyish brown colour (10YR 4/2) and consists of fine grained sand with interbedded clay. Some dark layers of clay are also seen between 250 – 245 cm.

During the sampling procedure, two drop stones were found at 254 – 256 cm and 200.5 – 204.5 cm respectively. The drop stone at 254 cm measures ~ 2 cm (pebble sized), and is black and angular with low sphericity. The drop stone at 200.5 cm measures ~ 4 cm at the widest (pebble sized), and is black and sub-rounded with high sphericity.

Section 2 (200 – 100 cm)

Section 2 consists of silty mud, with interbedded layers of clay. The sediments in the bottom part of this section consist of slightly laminated silty mud with a light brownish grey colour (10YR 6/2). Between ~ 125 – 120 cm, some dark grey and brown layers of clay are seen (2.5YR 5/0 – 10YR 4/2), before the light brownish grey colour continues towards the top of this section. Some minor light yellowish brown (10YR 6/4) layers of clay are observed at 187 cm, 175 cm and 160 cm respectively.

At 142 – 147, a large black, sub-rounded drop stone with low sphericity is found, measuring 5 cm in length and ~ 4 cm in width at the widest (pebble sized).

Section 1 (100 – 0 cm)

The light brownish grey colour (10YR 6/2) from section 2 continues up to ~ 78 cm of section 1. Fine lamination is also seen in this bottom part of the section. Some thin dark layers of clay (10YR 3/1) occur between 78 – 70 cm, before the colour changes to a dark greyish brown colour (10YR 4/2), which continues towards the section top.

Section 1 seem to have a very high water content, and consists of silty mud, with interbedded layers of clay. There seem to be a slight change in coarseness between 85 – 86 cm and between 45 – 55 cm where the sediments consist of coarser silt. 45 cm is also the depth at which tephra is encountered during the counting of foraminifera and IRD.

5.2.1 Wet bulk density and water content

Figure 7(a) shows the wet bulk density (g/cm^3) for the sediments measured with the multi sensor core logger, and the water content in percentage. The wet bulk density (WBD) was measured at every centimetre of the core, and has therefore a higher resolution than the graph displaying water content. The water content was calculated by subtracting the sample dry weight from the sample wet weight for all 100 samples taken, and thereafter calculating the water percentage relative to the wet weight.

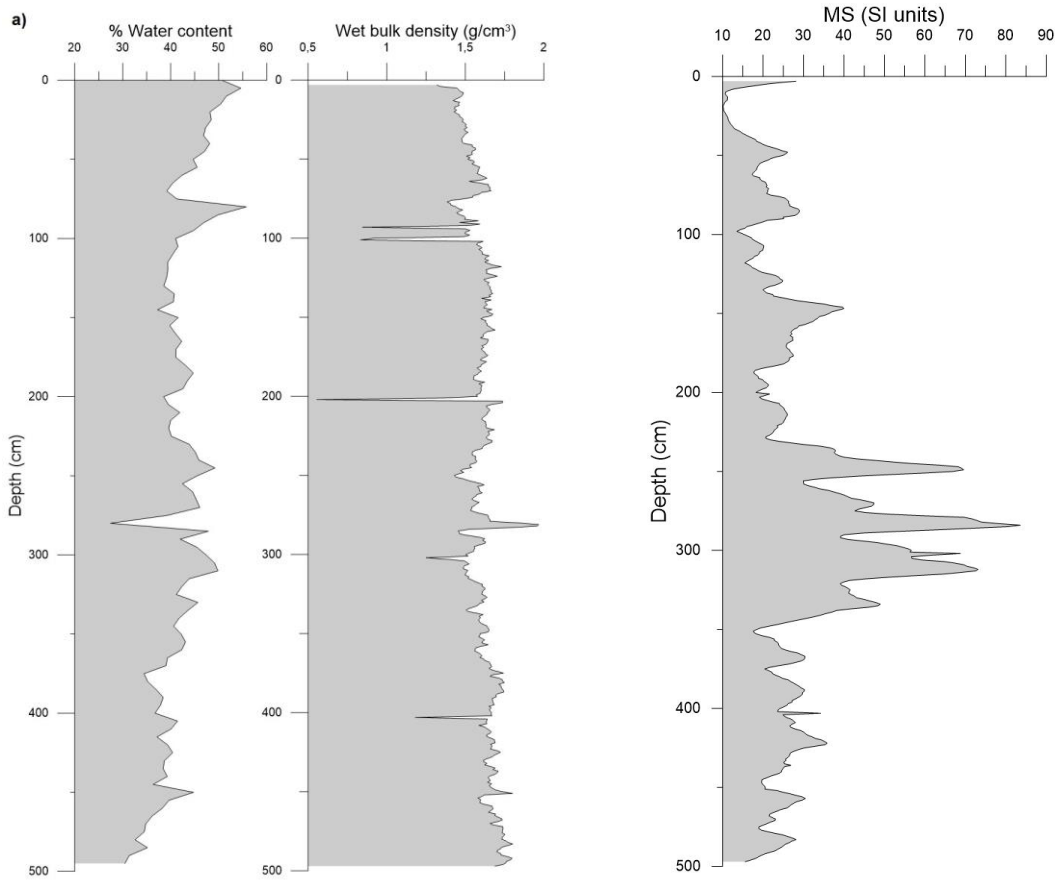

Figure 7: (a) *Water content (%) and wet bulk density (g/cm^3) for core HH13-089GC plotted against depth (cm).* ***(b)*** *Magnetic susceptibility (MS) record for core HH13-089GC plotted against depth (cm)*

The graphs display an inverse relationship between the two parameters; Wet bulk density decreases as water content increases. In the bottom parts of the core, the wet bulk density is relatively stable between 1.5 – 1.7 g/cm^3, with a general decrease towards 400 cm. At ~ 400 cm and 300 cm, the WBD drops to ~ 1.2 g/cm^3, but is relatively stable between these two drops. At ~ 280 cm, the WBD jumps to 1.9 g/cm3. At ~ 200 cm the largest drop in WBD is seen, before the values stabilizes just above 1.5 g/cm^3. At approximately 100 cm, the WBD decreases drastically to 0.9 g/cm^3. This rapid decrease occurs twice in a matter of a few cm before the wet bulk density stabilizes around 1.5 g/cm^3, with a decreasing trend towards the top of the core.

The water content generally follows the opposite pattern of the WBD, showing minor fluctuations around 40 – 45 %. There are some differences, but this is probably a result of the difference in resolution. The water content shows an overall increasing trend towards 50 % from the bottom of the core, to ~ 280 cm. Here, a drop down to 27 % is observed, the lowest of all the values. The water content then stabilizes just below 50 %, before the most significant increase occurs just above 100 cm, where it rises to 56 %.

5.2.1.1 Interpretation

The water content in core HH13-089GC is generally high, however lower readings could be an indication of increased consolidation of the sediments (Chauhan et al., 2014). Increased water content can therefore be an indication of increased pore volume.

5.2.2 Magnetic susceptibility

Figure 7(b) shows the magnetic susceptibility (MS) (~ 10 10^{-5} SI) of the core. MS was measured at every centimetre of the core, and therefore has the same resolution as the wet bulk density. The values show general fluctuation between 15 – 30 (10^{-5} SI) for the entire core with peaks at approximately every 20 cm. In the bottom ~ 150 cm of the core, MS values lie around the general fluctuation interval. There are seven major peaks in MS throughout the core. Six of these peaks are found between 340 – 230 cm, representing the highest MS values in the core. At 334 cm (48.9 10-5 SI), 312 cm (73.1 10^{-5} SI), 302 cm (68.8 10^{-5} SI), 284 cm (83.6 10^{-5} SI), 270 cm (47.4 10^{-5} SI), and 249 cm (69.5 10^{-5} SI) respectively. The remaining peak is seen at 147 cm with a value of 39.9 (10^{-5} SI). The lowest values of MS are observed in the upper ~ 50 m of the core.

The magnetic susceptibility curve peaks regularly, and it seems that for some of the largest peaks, the increase is abrupt, whereas the decreasing trend which follows is more gradual.

5.2.2.1 Interpretation

Changes in magnetic susceptibility (MS) within the record indicates changes in the input of ferromagnetic and/or paramagnetic minerals to the deep sea. So, a very high increase in magnetic susceptibility (i.e. between ~ 340 – 230 cm) indicates increased presence of ferromagnetic and/or paramagnetic minerals within the sediments (Grousset et al., 1993). Light minerals and high content of calcium carbonate has been found to give low MS (e.g. Rasmussen et al., 1996a). Magnetic susceptibility is often related to the grain size distribution, where coarser grain sizes give higher MS readings (e.g. Rasmussen et al., 1996a). IRD rich deposits with volcanic components for instance can give high magnetic susceptibility. The IRD- and MS records would then be peaking simultaneously. Magnetic susceptibility has been found to be an indication of Heinrich Events (e.g. Grousset et al., 1993; Robinson et al., 1995; Chi and Mienert, 1996; Rasmussen et al., 1996a; Moros et al., 1997), however this will be discussed later.

5.2.3 Grain size distribution

The distribution of the different grain size fractions (%) is shown in figure 8. The finest fraction (< 63 µm) was not retained in the sieving process, but remained in the samples that were used in the sortable silt analysis, taken from the same depths. These samples were analysed with the LDPSA laser, and the results were run in the GRADISTAT v 8.0 grain size analysis program. The composition (% silt and clay) of the finest fraction <63 µm was determined by the program and will be presented together with the grain size plots from the sieving process. The samples used in the sieving process were much larger, and these results will therefore be presented in this thesis for the fractions <63 µm, 63 – 100 µm and 100 – 500 µm.

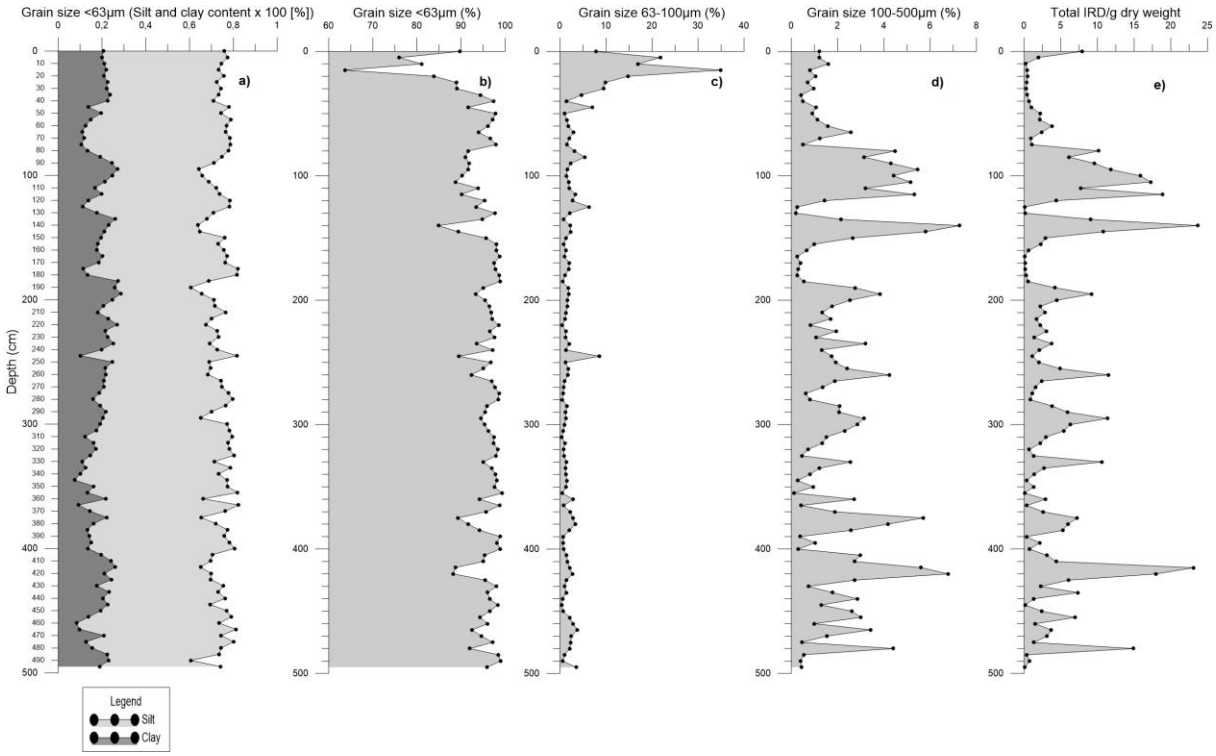

Figure 8: *Grain size distribution data from the sieving process for size fractions* ***(b)*** *<63 µm,* ***(c)*** *63 – 100 µm and* ***(d)*** *100 – 500 µm plotted against depth (cm). The composition of the finest grain size fraction* ***(a)*** *is based on the LDPSA analysis and given by the grain size analysis program GRADISTAT v8. The Total IRD distribution (total IRD/g dry weight sediment against depth)* ***(e)*** *is also shown.*

Grain size < 63 µm

The smallest size fraction makes up > 90 % of the sieved sediment samples throughout most of the core (Figure 8b). The same is true for the GRADISTAT data. The percentage shows minor fluctuations, and rarely drops below 90 %. The lowest values for the sieved samples are seen in the upper 30 cm of the core, the absolute lowest being 64 %. If compared to the GRADISTAT data, these low values could possibly be a result of difficulties with sieving, due to presence of sediment lumps in this part, which needs to be considered for the interpretation.

The GRADISTAT v8 software program showed that the finest fraction (< 63 µm) consisted of ~ 78.5 % silt (8.5 % very coarse, 14.4 % coarse, 19.8 % medium, 20.1% fine and 15.7 % very fine silt) and ~ 21.4 % clay on average (Figure 8a). It is important to remember that the samples used for the laser analysis only contained ~ 0.5 g sample.

Grain size 63 – 100 µm

The grain size fraction (63 – 100 µm) makes up < 5 % of the sediment throughout almost the entire core, and shows just about the opposite signal to that of the smallest grain size. Below 30 cm, the line shows four peaks above 5 %, all within the upper 250 cm. It reaches a maximum in the upper 30 cm, the absolute highest being 35 %. This particular maximum could, as mentioned for the previous fraction be a false result (Figure 8c).

Grain size 100 µm – 500 µm

The grain size fraction 100 – 500 µm, show a similar pattern as the IRD results (Figure 8d). In the bottom of the core, the fraction shows an increasing trend towards 420 cm. Between 420 – 350 cm, the trend is decreasing, followed by an interval with smaller fluctuations between 350 – 185 cm. The largest peak of 7.3 % is seen at 140 cm, before there is an overall decreasing trend throughout the rest of the core.

5.2.3.1 Interpretation

As seen in figure 8, the grain size fraction 100 – 500 µm follow a similar pattern to that of the IRD record. This suggests that most of this coarse grain size fraction is also ice rafted (e.g. Nam et al., 1995). The finest grain sizes dominate the record, as is typical for deep marine sediments that are not influenced greatly by sliding events for instance. Bottom currents can rework the marine sediments, and changes in the finest grain sizes can be an indication of changes in bottom current activity (Jessen and Rasmussen, 2015). The grain size of sortable silt is considered especially reliable for bottom current reconstructions (e.g. McCave et al., 1995a, 1995b; McCave and Hall, 2006), however, the record for that will be interpreted in a different chapter.

5.3 Ice rafted detritus (IRD) analysis

Figure 8 (e) shows the total IRD content in number/g dry weight sediment for the two fractions 500 μm – 1mm and IRD > 1 mm. The amount of IRD in the >1 mm fraction was significantly lower than that of the 500 μm – 1 mm fraction, but their trends were practically identical. The composition of the two fractions is also quite similar throughout the core. Out of the total counted number of IRD >1 mm, ~ 52 % was light coloured minerals such as quartz, feldspar and carbonate. For the 500 μm – 1mm fraction, the amount increased to ~ 66 %. The latter fraction contained quite a few agglutinated foraminiferal fragments in the upper parts of the core. They were unfortunately too fragmented to be identified. Some clay lumps containing tephra shards were found in both fractions at ca 45 – 51 cm. The tephra consisted of thin, transparent, probably rhyolitic flakes, with "rails".

Nine large peaks in concentration of IRD are seen within the record at 480 cm, 415 cm, 375 cm, 330 cm, 295 cm, 260 cm, 195 cm, 140 cm and 115 cm respectively. These nine peaks are also seen in the grain size fraction 100 μm – 500 μm. Smaller peaks are seen in between the larger ones, and all significant peaks seem to be relatively evenly spaced (~ 50 cm). In the bottom of the core, larger fluctuations are seen with an overall increasing trend towards ~ 360 cm. Between 360 – 150 cm, smaller fluctuations and the lowest values are seen. The largest peaks in IRD are seen within the upper 150 cm.

The most distinct increases in the concentration of IRD are observed within the intervals 470 – 415 cm and 160 – 140 cm. Above 140, the values remain high but with a decreasing trend towards 50 cm. Lower amounts of IRD are found in the lower 15 cm of the core and between 340 – 185 cm. The interval 185 – 160 cm and the upper 65 cm of the core have very low amounts of IRD, or no IRD at all.

5.3.1 Interpretation

Ice rafted detritus (IRD) is material which has been transported by and deposited from icebergs and sea ice. If transport by ice is believed to be the main mechanism for supply of terrigenous material to an area, IRD can be an important tool for reconstructing the activity of glaciers on land (e.g. Fronval et al., 1995; Nam et al., 1995; Stein et al., 1996). Since core HH13-089GC is located in an area that is highly affected by icebergs, IRD can possibly be a very important tool in this study as well.

IRD peaks is interpreted to indicate increased ice-rafting, which could be the result of a cooling climate causing glacier advances and increased calving (Jennings et al., 2002). In order for ice to transport IRD all the way out to the slope before melting, surface water temperatures need to be quite cold. Intervals with no, or very little IRD could thus reflect warmer ocean temperatures, which would cause the ice to melt before reaching the slope.

Figure 8 shows that IRD is present to a certain extent throughout most of the core, which is expected to represent a substantial time interval. This could indicate IRD deposition during both relatively warm conditions and relatively cold conditions (Funder et al., 1998). The IRD content of the core is highly fluctuating, and consist of many variations of higher amplitude. This can be an indication of large short term variations in glacier activity on Greenland (Nam, 1996). The larger peaks in IRD are evenly spaced, which could indicate some sort of relationship with larger climatic events such as the Heinrich Events (e.g. Bond et al., 1992; Broecker et al., 1992; Bond and Lotti, 1995). Further interpretation of such a relationship requires comparison with the age model, other proxies and studies, and is therefore left to the discussion.

The morphology of the tephra shards found within the coarse IRD- and finer fractions, it is very similar to the characteristics of the Vedde tephra (e.g. Mangerud et al., 1984). Mangerud et al. (1984) described thin, platy shards with lines occurring frequently along the particle to be the most common fragments in the Vedde Ash bed. The ash bed found in the present core has therefore been interpreted to be the Vedde Ash, which is most likely of Icelandic origin (Mangerud et al., 1984).

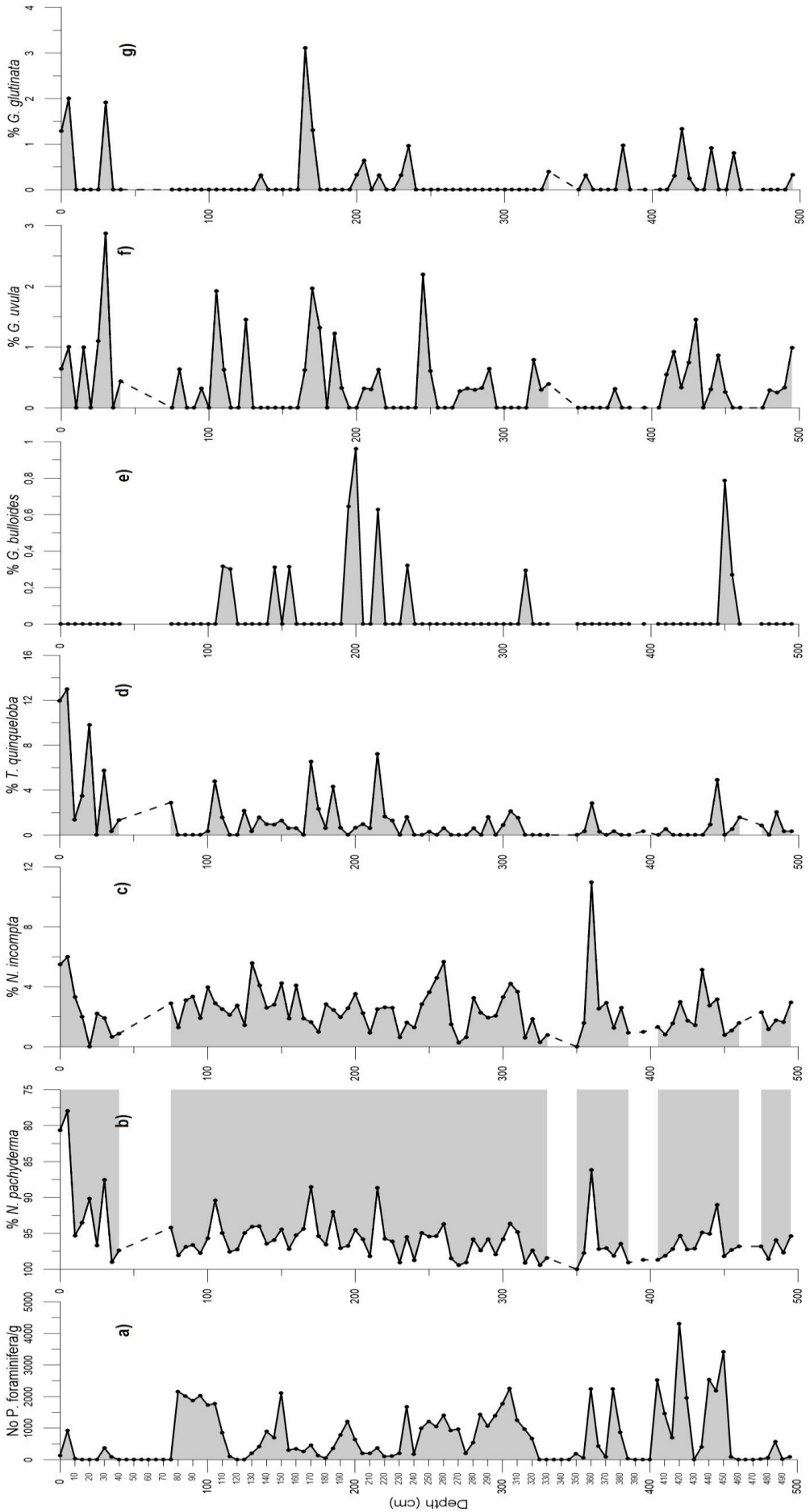

Figure 9: *Planktic foraminiferal fauna data for core HH13-089GC calculated as percentages against depth (cm). All the planktic foraminifera are compared to the total planktic foraminiferal abundance* ***(a).*** *Stippled lines indicate barren intervals.*

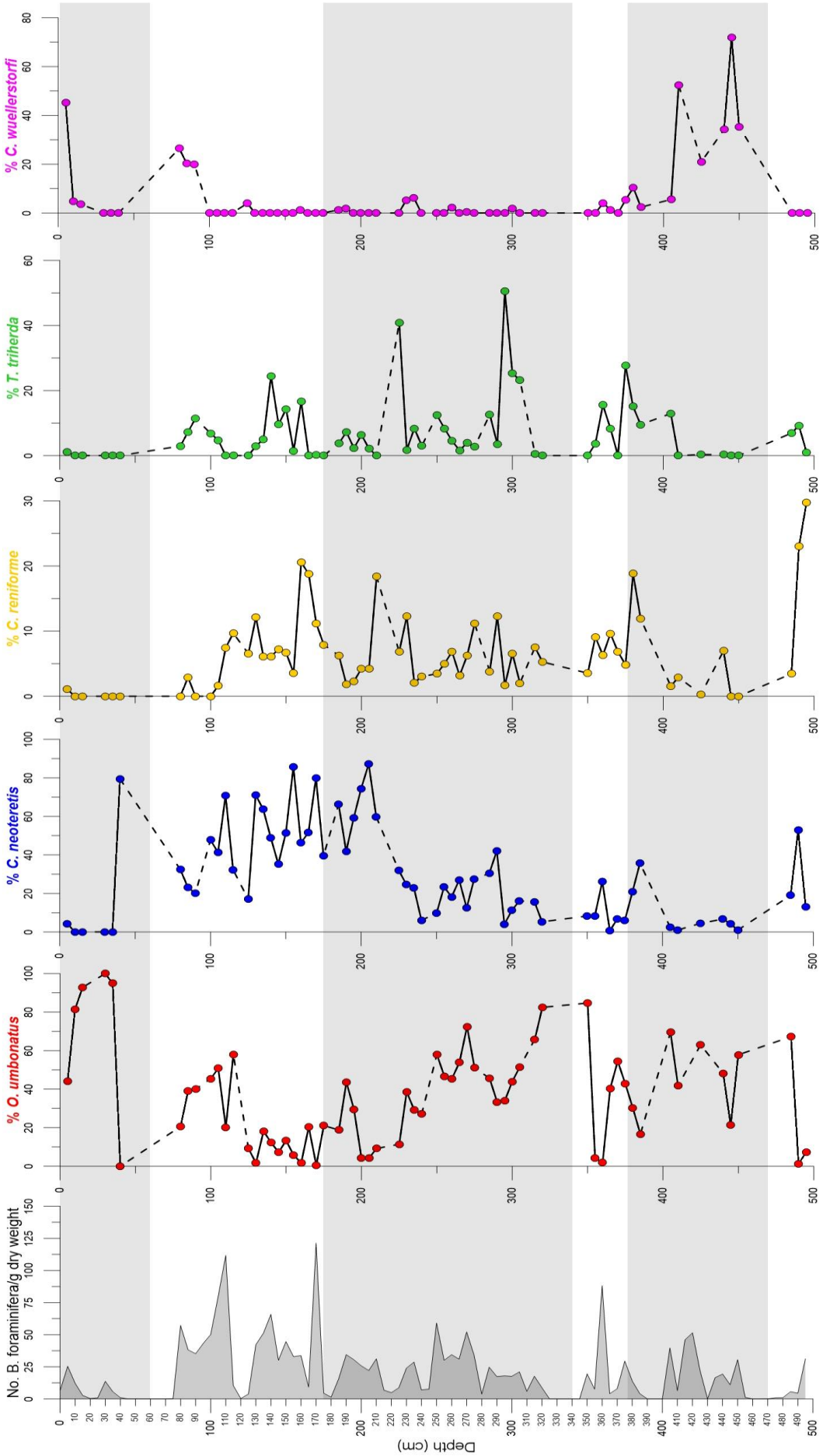

***Figure 10**: Relative abundance plots (%) for all dominating benthic foraminifera against depth (cm) for core HH13-089GC. All the benthic foraminifera are compared to the total benthic foraminiferal abundance (**far left**). Stippled lines represent the barren intervals. Divisions indicate marine isotope stages, needed for the discussion.*

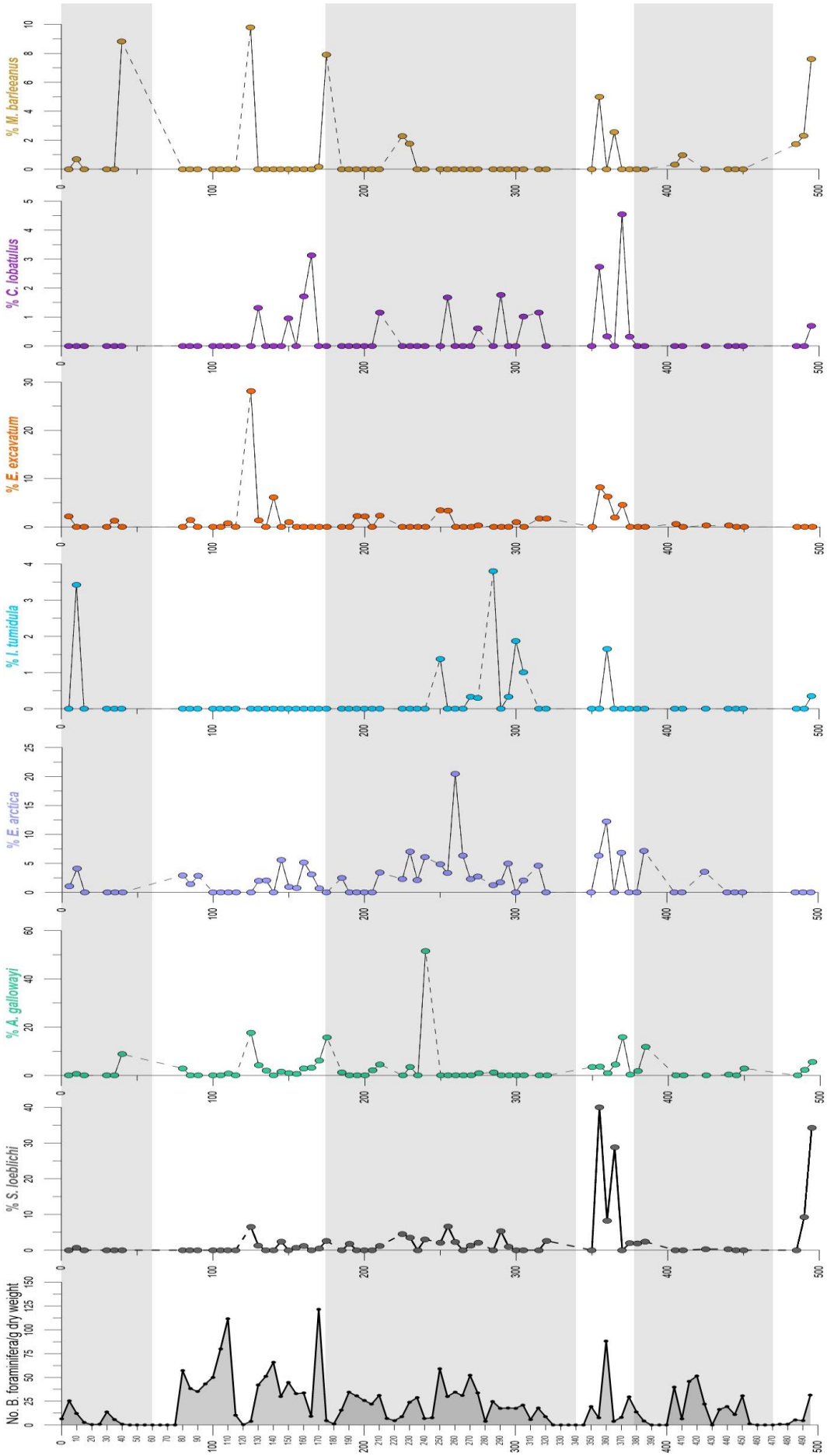

Figure 11: *Relative abundance plots (%) for the most common accessory benthic foraminifera against depth (cm) for core HH13-089GC. All the benthic foraminifera are compared to the total benthic foraminiferal abundance (**far left**). Stippled lines represent the barren intervals. Divisions indicate marine isotope stages, needed for the discussion.*

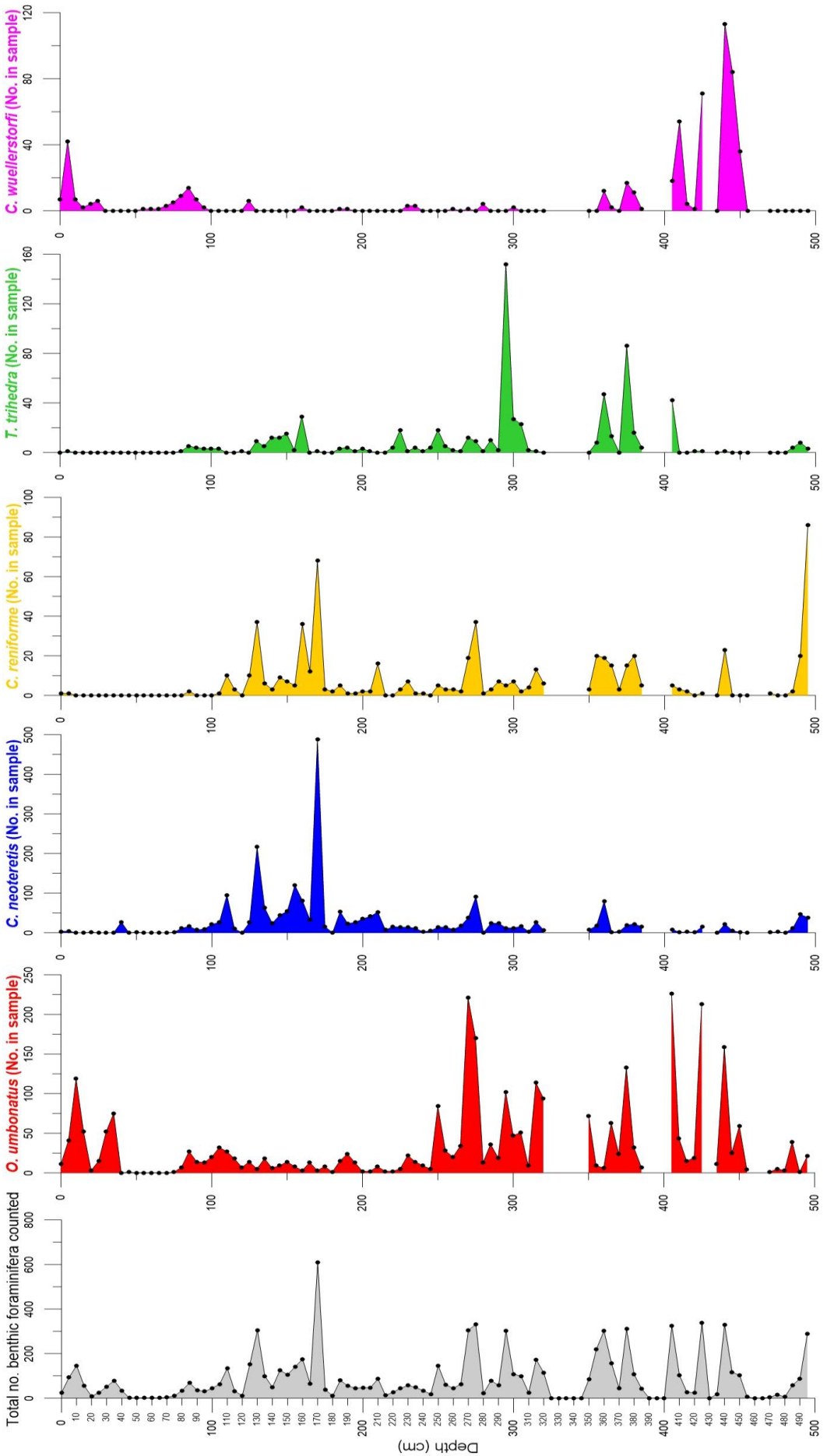

Figure 12: *The dominating benthic foraminifera plotted as No. in each sample vs. depth (cm) for core HH13-089GC. All plots are compared to a plot showing the total number of benthic foraminifera counted within each fraction* ***(far left)****.*

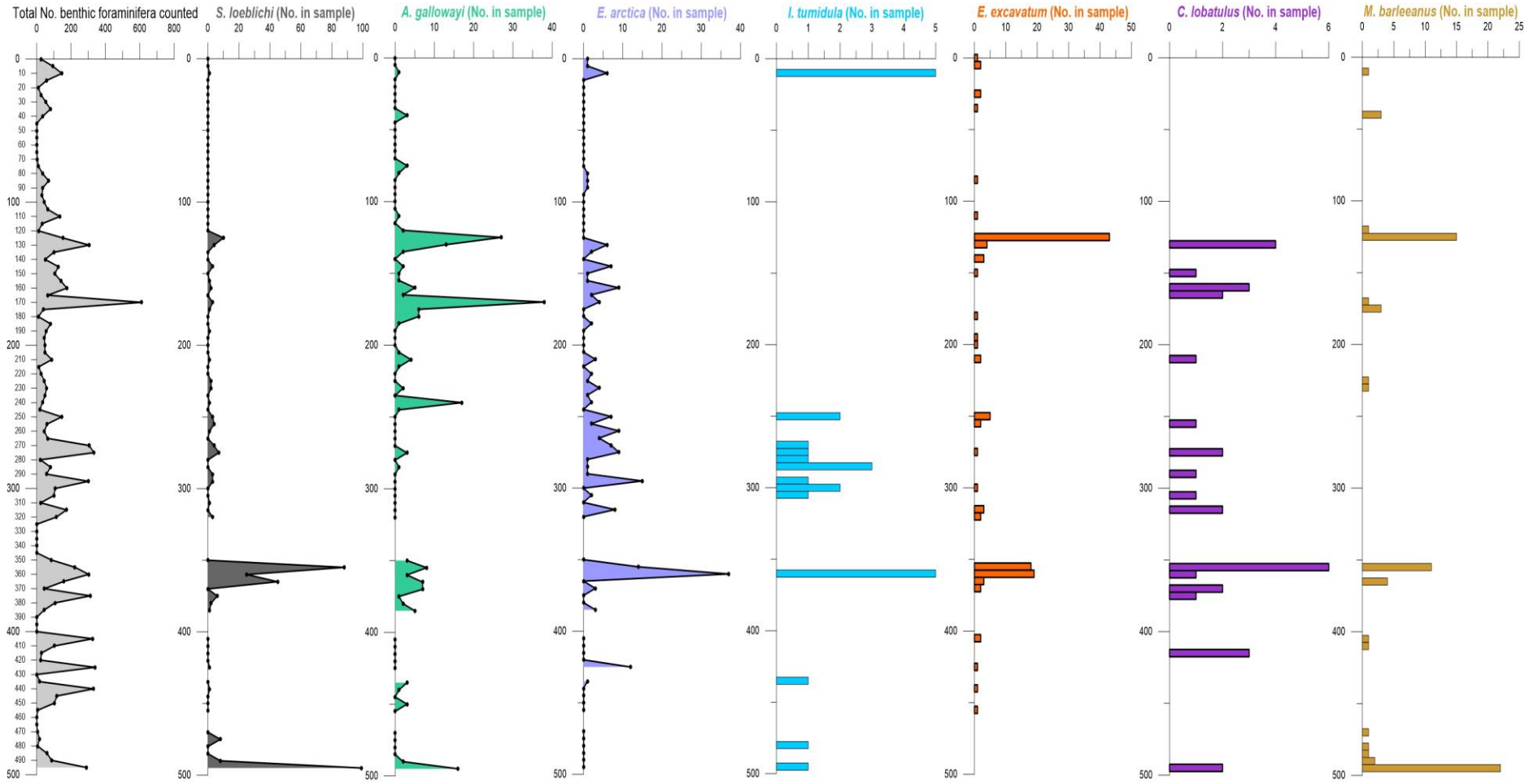

Figure 13: *The most common accessory benthic foraminifera plotted as No. in each sample vs. depth (cm) for core HH13-089GC. All plots are compared to a plot showing the total number of benthic foraminifera counted within each fraction (**far left**). Bar plots were used for some plots to see a trend.*

5.4 Foraminiferal data

The faunal assemblages of planktic and benthic foraminifera will be described for the core in its entirety in stratigraphical order from oldest to youngest.

5.4.1 Planktic foraminifera

The total abundance of planktic foraminifera (No. planktic foraminifera/g dry weight), is very high throughout most of the core as seen in figure 9(a) All samples contained some specimens of planktic foraminifera, though some contained less than 50 specimens and where considered barren (470 – 465 cm, 400 cm, 390 cm, 345 – 335 cm and 70 – 45 cm,). The data for the barren intervals will not be addressed. The faunal data for planktic foraminifera will be presented as percentages within a sample, from now on addressed as relative abundance, versus depth (Figure 9).

The planktic foraminiferal fauna is dominated by *Neogloboquadrina pachyderma*. This species accounts for > 90 % of the planktic fauna throughout most of the core, but show some distinct drops at 445 cm, 360 cm, 260 cm, 215 cm, 185 cm, 170 cm, 105 cm, 30 cm, 20 cm and 5 cm respectively (Figure 9b). Six of these drops reach below 90 %, and five of them are seen within the upper 250 cm.

The relative abundance of *N. pachyderma* generally fluctuate > 90 %. At 360, the second largest drop down to 86 % is seen, before it rises drastically at 350, where *N. pachyderma* accounts for 100 % of the identified specimens. Between 345 – 335, a barren interval is found, before the percentage is back to fluctuating between 90 – 97 %. Between 70 – 45 cm the largest barren interval is located. After this the relative abundance is decreasing towards the top of the core. The lowest relative abundance of *N. pachyderma* of 78 – 80 % is seen in the uppermost samples.

Neogloboquadrina incompta and *Turborotalita quinqueloba* have the second highest occurrences (Figure 9c and 9d), both showing a somewhat opposite signal to that of *N. pachyderma*. From the bottom of the core, up to ~ 240 cm, *N. incompta* has almost the exact opposite signal to *N. pachyderma*. The highest relative abundance of *N. incompta* at ~ 11 % is seen within this interval at 360 cm. *Turborotalita quinqueloba* only show minor occurrences in the lower parts of the core. From ~ 240 cm to the top of the core, *T. quinqueloba* is closest to the opposite signal of *N. pachyderma*, and peaks within the upper 5 cm of the core at 13 %.

Globigerinita glutinata, *Globigerinita uvula* and *Globigerina bulloides* are accessory planktic species, and occur only sporadically throughout the core. *Globigerinita uvula* appears in ~ 50 cm intervals throughout the core, each interval separated by ~ 25 cm long gaps. *Globigerinita glutinata* occurs in three parts of the core; between ~ 455 – 330 cm, between ~ 235 – 135 cm, and again within the upper

50 cm. It has its highest relative abundance of ~ 3 % at 165 cm. *Globigerina bulloides* only occurs sporadically between ~ 455 – 110 with a maximum of just below 1 % at 450 cm and 200 cm.

The curve showing the total abundance of planktic foraminifera (Figure 9a), show that the highest total abundances are seen below 400 cm, the highest being > 4300 foraminifera/g at 420 cm depth. Between ~ 250 – 120 cm, the values are quite low, whereas the upper 75 cm has the lowest total abundance of planktic foraminifera.

5.4.1.1 Interpretation

The almost monospecific planktic fauna of *N. pachyderma* is expected due to the location of the core. *Neogloboquadrina pachyderma* is an indicator of cold surface waters, such as the surface waters of the EGC. Larger drops in the relative abundance of this species could indicate the presence of warmer surface waters, especially if the drop is accompanied by an increase in the relative abundance of subpolar species such as *N. incompta* and/or *T. quinqueloba*, *G. glutinata*, *G. uvula* and *G. bulloides* (Haake and Pflaumann, 1989). This is often the case within the core.

The percentage of *T. quinqueloba* is generally low throughout the bottom half of the core, but begins to peak above 250 cm where *N. pachyderma* percentages are relatively low. The relative abundance of the accessory planktic species also increases above 250 cm, especially *G. bulloides*. This faunal composition could be related to the nearby presence of the Polar Front (Andersen et al., 2012).

The presence of *T. quinqueloba* in great numbers is related to warmer waters and high surface productivity. The increasing presence of *T. quinqueloba* versus *N. pachyderma* in the upper parts of the core can indicate proximity of the Arctic Front (Johannessen et al., 1994; John et al., 2004).

5.4.2 Benthic foraminifera

The content of benthic foraminifera within most samples was relatively low, and some samples and intervals contained no benthic foraminifera at all (465 – 460 cm, 430 cm, 400 – 390 cm, 345 – 325 cm and 70 – 45 cm). Even though there are generally fewer benthic foraminifera, their tests are often better preserved than the planktic. Due to this relatively low content of benthic foraminifera, the data will be presented both as the number of specimens found within a sample (no. per sample) (Figure 12 and 13), and as relative abundance (%) versus depth (Figure 10 and 11). The relative abundances for each benthic species is only shown for the samples, where counting exceeded 30 specimens. This was done to get a more accurate picture of the faunal composition, and samples where fewer than 30 specimens were counted were therefore considered barren. The faunal plots are all compared to the

total abundance of benthic foraminifera (No. benthic foraminifera/g dry weight) (Figure 10, 11, 12, and 13a).

The benthic foraminiferal fauna is dominated by the species *Oridorsalis umbonatus*, *Cassidulina neoteretis*, *Cibicides wuellerstorfi*, *Triloculina trhedra* and *Cassidulina reniforme*, respectively. Occurring as secondary and accessory species are *Astrononion gallowayi*, *Stainforthia loeblichi*, *Ioanella tumidula*, *Epistominella arctica*, *Melonis barleeanus* (Williamson, 1858), *Cibicides lobatulus* (Walker & Jacob, 1798) and *Elphidium excavatum* (Terquem, 1875). A complete list of the other species found in the samples can be seen in appendix A.

Oridorsalis umbonatus is a dominating species throughout almost the entire core. In the bottom parts of the core up to ~ 400 cm, the relative abundance of *O. umbonatus* is quite high, only interrupted by the first barren interval. Following 400 cm, the relative abundance is increasing towards a peak at 350 cm, before a gradual decrease is seen towards 250 cm. The interval between 250 – 35 cm, is the only interval where *O. umbonatu*s is not amongst the dominating species, and its relative abundance lies below 50 %. The upper 35 cm of the core is dominated by *O. umbonatus* and *C. wuellerstorfi*. The latter is either absent or present in small numbers throughout most of the core. It peaks between 450 – 400 cm, but is absent at the very bottom of the core.

Triloculina trihedra as a dominating species, and *E. arctica* as a secondary species follows a similar pattern to that of *O. umbonatus*, both having their highest occurrence around 300 cm. The secondary species *I. tumidula* is only present in small numbers within intervals where *O. umbonatus* has its highest occurrences. The plot showing the relative abundance of *O. umbonatus* follows the plot showing the total abundance of benthic foraminifera. The barren intervals can easily be seen on the latter plot.

In the interval where the relative abundance of *O. umbonatus* is below 50 %, *C. neoteretis* is the dominating species. *C. reniforme* and *A. gallowayi* also increase in relative abundance within this interval. *C. neoteretis* generally shows the opposite trend to that of *O. umbonatus*. This also seem to be the case for *C. reniforme* and *A. gallowayi*. *Cassidulina neoteretis* has its highest relative abundance near the very bottom of the core, and between 250 – 35 cm. *Cassidulina reniforme* also has some of its highest occurrences within this interval, but its highest peaks are found within the bottom samples of the core. The highest occurrences of *A. gallowayi* is found in the interval between ~200 – 100 cm.

The secondary species *S. loeblichi* is the dominating species in the very bottom samples of the core at 34 %, closely followed by *C. reniforme* at 30 %. The maximum relative abundance of *S. loeblichi* of 40 % is seen at 355 cm. The species also show minor occurrences between ~ 350 – 125 cm.

The benthic species *Pullenia bulloides* (d´Oribgny, 1846) occurs within the identified fraction of one sample only for the entire core (405 cm).

5.4.2.1 Interpretation

Oridorsalis umbonatus is as mentioned in chapter 4.2.1 one of the most common benthic foraminifera in the investigated area today. The very high relative abundance of this species throughout the core suggests that it has been a dominating species in the past as well. Today the species has also been found to be dominating in areas of increased sea ice cover (e.g. Streeter et al., 1982; Jansen et al., 1983; Mackensen et al., 1985). The low relative abundance between ~ 250 – 125 cm could indicate an interval of limited sea ice cover.

High relative abundances of *C. wuellerstorfi* is mainly an indicator for interglacial conditions (Haake and Pflaumann), as it is known to prefer ice-free periods with high primary productivity within the Norwegian – Greenland Sea (e.g. Streeter et al., 1982; Jansen et al., 1983; Mackensen et al., 1985). It's presence within the core could indicate occurrence of two much warmer intervals (~ 450 – 375 cm and above 100 cm) and probably two much colder intervals (~ 497 – 450 cm and 375 – 100 cm), the latter event being very long and slightly fluctuating. The species has also been found to be dominating during the penultimate interglacial MIS 5e (Streeter et al., 1982). When occurring together, the two species *O. umbonatus* and *C. wuellerstorfi* alternate; when the percentage of *O. umbonatus* is high, *C. wuellerstorfi* is lower and vice versa. As described in chapter 4.2.1 and 4.2.5, the they are both epifaunal, but have almost the exact opposite preferences, which could be an explanation of their alternation, when occurring simultaneously.

Cassudulina neoteretis follows almost the exact opposite signal to that of *O. umbonatus*. *Cassidulina reniforme* seems to also follow a somewhat opposite pattern, although not as clear. The two species are infaunal species that under modern conditions are common in areas influenced by chilled subsurface Atlantic Waters (Jennings and Helgadottir, 1994; Seidenkrantz, 1995; Hald and Korsun 1997; Steinsund, 1994; Jennings et al., 2002; Polyak et al., 2002). In the Arctic Ocean however, *C. neoteretis* and *C. reniforme* have been found to be amongst the dominant species during times of maximum glacial ice sheet extension, and during times of moderate productivity (e.g. Wollenburg et al., 2001). The lower relative abundance of these species have also been found to indicate influx of subsurface AW, stratified beneath a sea-ice rich EGC, when the planktic foraminiferal fauna was completely dominated by *N. pachyderma* in the same intervals (Andersen et al., 2012). The chilled AW could be from the Irminger Current (IC) or the return Atlantic Water (RAC) in the EGC (Jennings

and Helgadottir, 1994). Very high percentages of *C. reniforme* are often related to distal glacial marine conditions (e.g. Polyak and Solheim, 1994; Wollenburg et al., 2001).

Melonis barleeanus follows a similar pattern to that of *C. neoteretis*. The species is often found in areas with buried organic material, and can also be an indication of AW influence (e.g. Polyak et al. 2002). *Astrononion gallowayi* often increases together with *C. lobatulus*, which could indicate higher energy near the sea floor (Wollenburg and Mackensen, 1998), correlating well with coarser sediments in these intervals (Chapter 4.2.8). *Stainforthia loeblichi* is opportunistic and thrives during high productivity. Peaks in the relative abundance of this species could therefore be an indication of higher productivity at the sea surface (Chapter 4.2.6). It has been described to be a common species in Arctic foraminiferal faunas representing the late Saalian glaciation, MIS 6 (Knudsen, 1984). The presence of *E. excavatum* could indicate colder temperatures, low salinities and presence of sea ice. It usually prefers temperatures <1^{O}C (Miller et al., 1982). It is important to note that there are many subspecies of *E. excavatum*, however these were not distinguished in this thesis.

Pullenia bulloides is a species that is associated with chilled Atlantic water (Risebrobakken et al., 2010). It prefers temperatures between 2 – 4^{O} C, a salinity of ~ 35 ‰, and is considered to be a stratigraphic biomarker for MIS 5a and 5e within the Nordic Seas (Haake and Pflaumnn, 1989; Fronval and Jansen, 1997; Rasmussen et al., 1999; Rytter et al., 2002; Risebrobakken et al., 2010; Chauhan et al., 2014). The presence of the benthic foraminifera *P. bulloides* (d´Orbigny, 1846) within the core could therefore be an indication of either MIS 5a or 5e.

The presence of agglutinated foraminifera within the uppermost samples, could indicate that the core top represents the present/near-present.

Intervals that are barren of foraminifera could indicate the presence of perennial sea ice which made growth of planktic and benthic foraminifera difficult. It could also indicate dissolution, or a combination of both (Chauhan et al., 2014).

5.4.1 Planktic – benthic foraminiferal ratio

The ratio of planktic to benthic foraminifera (P:B ratio) is calculated by dividing the total abundance of planktic foraminifera with the total abundance of benthic foraminifera. The plot for this ratio is seen in figure 14. The ratio is much higher for the lower half of the core than the upper. In the lower half, the fluctuations are also stronger.

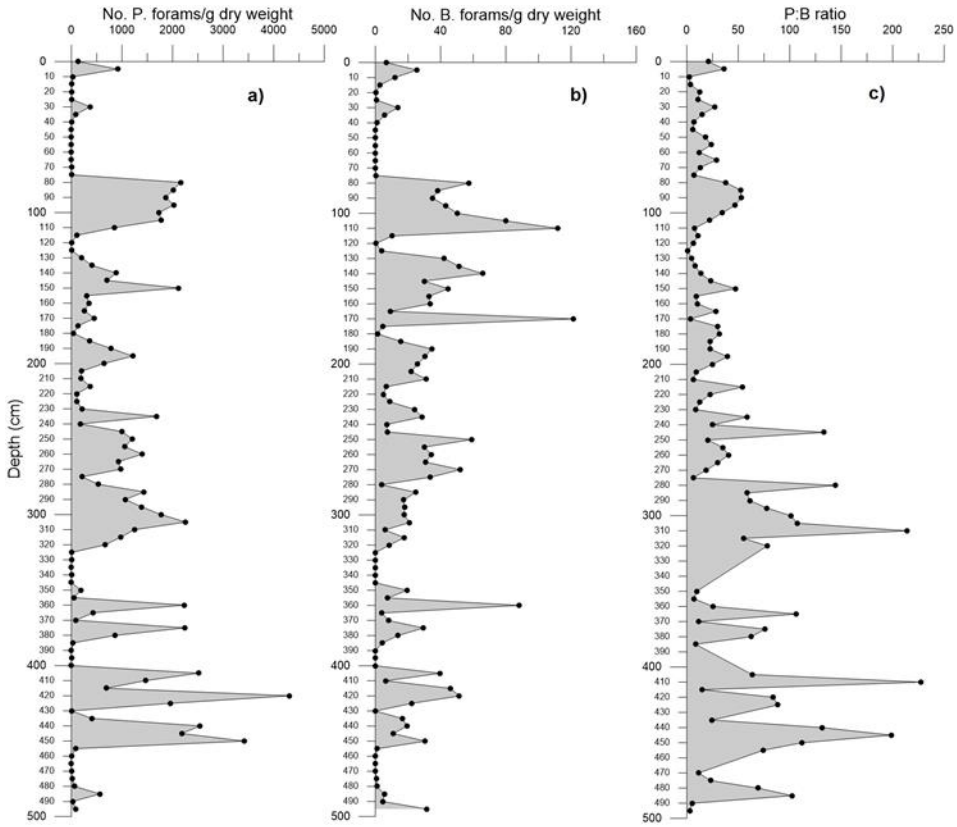

Figure 14: *Results showing* ***(a)*** *the total abundance of planktic foraminifera (No. Planktic forams/g dry weight sediment).* ***(b)*** *Total abundance of benthic foraminifera (No. Benthic forams/g dry weight sediment).* ***(c)*** *Planktic - Benthic ratio vs. depth for core HH13-089GC.*

5.4.1.1 Interpretation

Intervals with low P:B ratios could be an indication of preferential dissolution, where planktonic species are dissolved easier than benthic species (Rasmussen and Thomsen, 2014). Higher P:B ratios indicates increased preservation of planktic foraminifera.

5.5 Stable isotope data (Planktic $\delta^{18}O$ and $\delta^{13}C$)

The planktic stable oxygen and carbon isotope analysis was as mentioned preformed at the Bjerknes Centre for Climate Change, University of Bergen, Norway. Four samples contained too few foraminiferal tests for measurements to be made (45 cm, 60 – 65 cm and 335 cm). The sample taken at 455 cm showed an unusually low $\delta^{18}O$ value of 1.78 ‰, and was supposed to be measured again. The result of this new measurement has unfortunately not yet arrived. The uncertainty of this value, must be considered when interpreting and discussing the results.

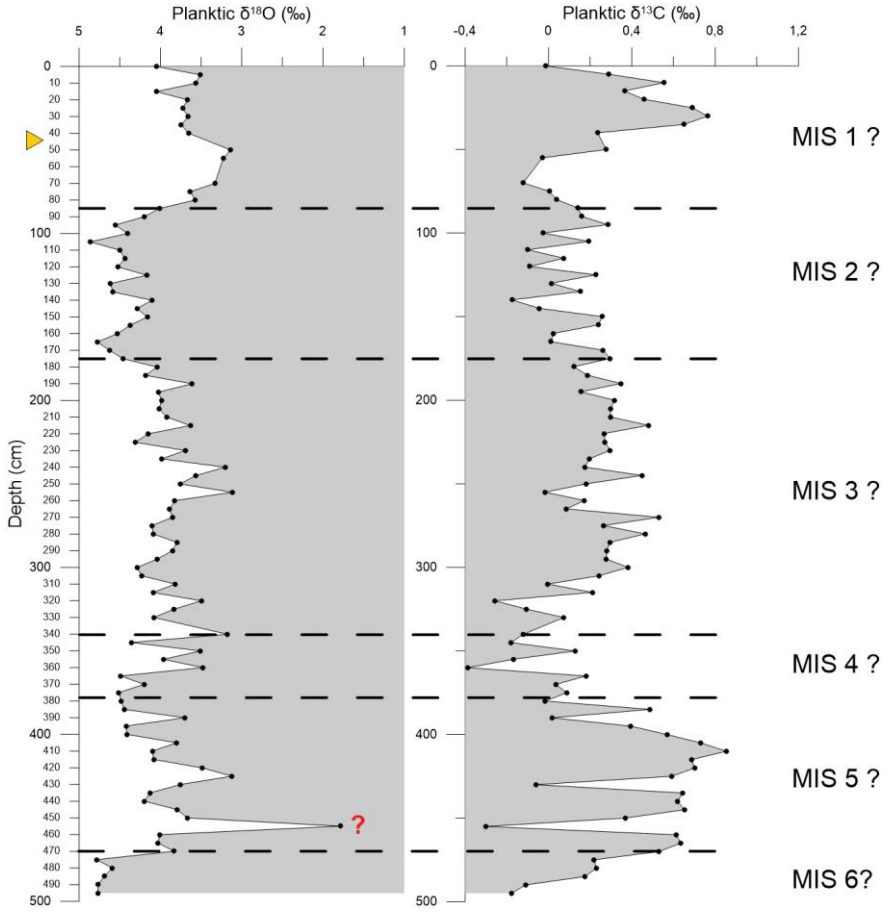

Figure 15: *Stable oxygen- and carbon isotope results for core HH13-089GC. Stippled lines indicate possible locations for marine isotope stage boundaries. The yellow symbol indicates the location of the tephra, and the red question mark represents the uncertain $\delta^{18}O$ measurement.*

The planktic stable oxygen isotope values fluctuates between 3.12 – 4.86 ‰ throughout the core, and show five, maybe six major changes (~ 470 cm, 385 cm, 355 cm, 178 cm and 85 cm) (Figure 15). These major changes will be helpful when determining the possible locations for the boundaries between different marine isotope stages (MIS) in the interpretation, and the complete plot for the

planktic stable isotopes will be useful for increased stratigraphical control in relation to the interpretation.

The bottom parts of the core have high $\delta^{18}O$ values, decreasing quite drastically towards the unconfirmed, unusually low value at 455 cm. Between ~ 455 – 400 cm, the $\delta^{18}O$ values are generally lower, but alternate between low (455 – 445 cm, 430 – 420 and 405 cm) and high (440 – 435 cm and 415 – 410 cm) values with a slightly increasing trend. A smaller interval with $\delta^{18}O$ values above 4‰ is seen between 405 – 365 cm. The interval which follows (~ 365 – 190 cm) is a more chaotic interval when it comes to $\delta^{18}O$, showing many minor and some major fluctuations. Most values within this interval however, are low and lie below 4 ‰. Between ~ 190 – 85 cm, a shift in the $\delta^{18}O$ values is observed. The values are higher and lie above 4 ‰, the highest being 4.86 ‰ at 105 cm. A new shift occurs at 85 cm, and all samples above this point, apart from two (4.05 ‰ at 15 cm and 1 – 0 cm) have lower values below 4 ‰.

The $\delta^{13}C$ values within the bottom parts of the core show an overall increasing trend towards 400 cm, showing two larger drops at 455 cm and 430 cm. After 400 cm, the values are low up to ~ 310 cm where they increase. In the interval between ~ 310 – 150 cm, the $\delta^{13}C$ values are positive, showing minor fluctuations. Between ~ 150 – 50 cm the $\delta^{13}C$ values are quite low, fluctuating below 0.2 ‰. After this there is a drastic increase to ~ 0.8 ‰ at 30 cm, before the values show a general decrease throughout the rest of the core. When comparing the two isotope records, the $\delta^{13}C$ signal is generally the opposite to the $\delta^{18}O$ signal (note that the x axis for $\delta^{18}O$ is flipped, making the two records appear similar in the figure).

5.5.1 Interpretation

High $\delta^{18}O$ values over time are generally described to represent a period with colder climatic conditions (i.e. during glacials), whereas low values generally represent warmer conditions (i.e. during interglacials). As this record is based on planktic foraminifera, smaller fluctuations in the $\delta^{18}O$ record represents depletion or enrichment of ^{18}O within the surface or near surface waters. Small ^{18}O depletions (yielding small drops in the $\delta^{18}O$ record) could be the result of increased influence of cold and fresh meltwater. Larger drops in the record can also indicate this, especially if they occur together with higher IRD concentrations (e.g. Voelker et al., 1998; Spielhagen et al., 2004; Risebrobakken et al., 2006; Chauhan et al., 2014). Shifts in the oxygen isotope record can sometimes also indicate salinity changes (Stein et al., 1996).

It is sometimes possible to distinguish larger climatic events such as Dansgaard – Oeschger cycles and Heinrich Events (Chapter 1.2.3.1) within the oxygen isotope records. Such indications however, need to be seen in relation to other proxy data, and interpreted thereafter. Since the $\delta^{18}O$ records for the

present study represent the surface environment in an area that is highly influenced by icebergs and meltwater, it is possible that certain evidence for larger climatic events are overridden by local signals. I will come back to this in the discussion.

Changes in the $\delta^{13}C$ records can be a possible indicator of paleo-productivity in the upper layers of the oceans, and the fluctuation of ^{12}C in surface waters (Shackleton and Pisias, 1985). Lower $\delta^{13}C$ values could be an indication of decreased surface productivity, whereas higher values could indicate increased productivity and high oxygen content within the surface waters. Very low $\delta^{13}C$ values could indicate reduced ventilation of the surface water (Sarnthein et al., 1995; Voelker et al., 1998). Changes in productivity can also be related to changes in sea ice cover, as the marine primary producers require light for their photosynthesis.

5.5.1.1 Initial interpretation of marine isotope stages

The results of the $\delta^{18}O$ analysis indicates the presence of marine isotope stages (MIS) 1 – 5. It is also possible that the very bottom of the core represents the termination of MIS 6, however this claim will be discussed further in the discussion. The oxygen isotope curve generally resembles the global isotope record (Shackleton and Opdyke, 1973; Martinson et al., 1987; Lisiecki and Raymo, 2005). The initial interpretation of the isotope stages is related to large scale changes in the stable isotope records, especially the stable oxygen isotope record. The identification of the stage boundaries was not straightforward, and it is therefore necessary to consider other proxy records, as well as the age model, for the fine-tuning of the MIS boundaries. This will be done in the discussion. Fronval and Jansen (1997) mentioned that some isotopic events can be difficult to identify in the Greenland Sea based on the planktic oxygen isotope record.

Clear shifts in this record are seen at ~ 470 cm, 385 cm, 355 cm, 178 cm and 85 cm respectively. The boundaries for different isotope stages are believed to be located near these points in the core, and are seen in figure 15.

Marine isotope stage 6 (MIS 6)

It is possible that the upper part of MIS 6 is present within the very bottom of the core (below ~ 470 cm). The high $\delta^{18}O$ values indicate colder climatic conditions, whereas a shift is seen at ~ 470 cm indicating transition from glacial- to interglacial conditions. Due to the uncertainty of the lowest $\delta^{18}O$ value at 455 cm, it is also possible that the core only reaches the MIS 6/5 boundary. However, even if the uncertain measurement had values similar to the measurement above (450 cm), there would still be a significant drop around ~ 470 cm. Based on this, the MIS 6/5 boundary has for now been placed at 470 cm.

Marine isotope stage 5 (MIS 5)

The interval between 470 – 385 has low $\delta^{18}O$ values, indicating a warmer climate and increased influence of freshwater at the surface, which could be the result of increasing water temperatures causing iceberg calving (Rasmussen and Thomsen, 2008). The values decrease towards ~ 385 cm, and at this point, a slightly longer interval of higher $\delta^{18}O$ values is seen, indicating a new climatic shift. The interval also shows very high $\delta^{13}C$ values which could also be an indication of MIS 5 (e.g. Streeter et al., 1982; Nam et al., 1995; Stein et al., 1996)

The initial thought when looking at the low value at 455 cm, is that it probably represents the unusually warm Eemian interglacial (MIS 5e). However, the value is uncertain, and comparison with other proxy records and studies is therefore required to confirm or disprove this thought. The approximate location of the MIS 5/4 boundary within the record has been interpreted to be at ~ 385 cm.

Marine isotope stage 4 (MIS 4)

The MIS 4 is determined by a characteristic shift in the $\delta^{18}O$ and $\delta^{13}C$ records to higher (indicating colder climate) and lower values (indicating reduced surface productivity) respectively. A minimum in in planktic $\delta^{13}C$ during MIS 4 is well-known in the northwest Atlantic (Haake and Pflaumann, 1989; Labeyrie and Duplessy, 1985). The initial interpretation of the isotope data places MIS 4 between 385 – 355 cm.

Marine isotope stage 3 (MIS 3)

Between ~ 355 – 178 cm, the $\delta^{18}O$ record shows generally lower values, which fluctuates between 3 – 4 ‰, indicating slightly warmer climatic conditions and increased meltwater. The $\delta^{13}C$ values are very low in the beginning of the interval. This is a trait that has been recognised for MIS 3 in the area (Nam et al., 1995; Stein et al., 1996), and can be an indication of reduced ventilation of the surface water (Sarnthein et al., 1995; Voelker et al., 1998). MIS 3 has been placed between 355 – 178 cm for now.

Marine isotope stage 2 (MIS 2)

A new shift in the record is seen at ~178 cm, from generally low $\delta^{18}O$ values to quite high values. The $\delta^{13}C$ values are lower. This trend continues up to 85 cm, where the last drastic shift within the records is seen.

Marine isotope stage 1 (MIS 1)

MIS 1 has been interpreted to represent the upper ~ 85 cm of the core, following the last major shift from high to low $\delta^{18}O$ values. This shift in the oxygen isotope record is interpreted to reflect warming during the deglaciation phase, prior to the Holocene (Jennings et al., 2002). The $\delta^{13}C$ values are generally high within this interval.

Note that these are the initial placements of the marine isotope stage boundaries, based on the interpretation of the stable isotope data only, and they are therefore placed right at the visible transitions from low to high-, or high to low values. Correlation with other proxies and studies may lead to the movement of some of the boundaries, and possibly increase the reliability of the interpretation.

5.6 Sortable silt analysis

Before the results of the sortable silt analysis is presented, It is necessary to describe the handling of the raw data, and why it was done in this way.

5.6.1 Potential ice-rafting – Test plot

The method by Hass (2002), described in chapter 3.7.1 was used to investigate if parts of the silt fraction had been ice rafted (Figure 16a).

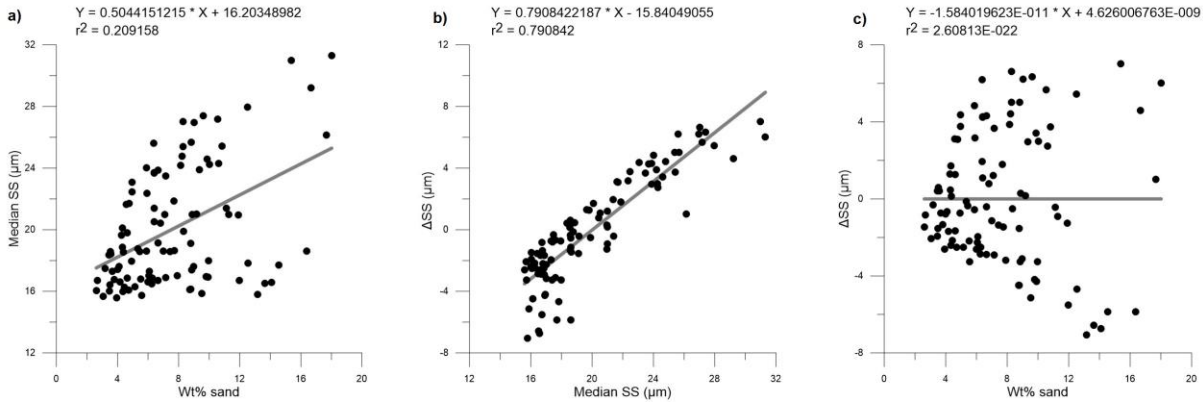

Figure 16: *Potential ice-rafting* ***(a)*** *Scatter plot of wt% sand vs. the measured median grain size of sortable silt (SS) and the linear fit line.* ***(b)*** *Scatter plot of the median SS data vs. ΔSS data. Most of the data points plot close to the regression line, and the ones that do not, are the ones that will be affected by the IRD correction.* ***(c)*** *Scatter plot of wt% sand vs. ΔSS showing no correlation.*

Some of the data points in figure 16(a) plot close to the fit line (y), and the correlation seems to be positive with an r^2 of 0.21. So, as the sand content increases, so does the coarseness of the silt fraction. A slight correlation is seen, but it does not seem that ice rafting was very intense. Even though McCave and Hall (2006) found it not to be necessary to IRD-correct data unless ice rafting was very intense, it was decided to make the correction in this investigation to learn about the complete process of a sortable silt analysis, and to make sure that data clearly affected by IRD was filtered out. Major features of the record can also be enhanced by doing the correction (McCave and Hall, 2006). The ice rafted corrected median sortable silt (ΔSS) was calculated following the methods of Hass (2002);

$$y = 0.5044151215 * x + 16.20348982$$

Where:

- $y = SS_{(pot)}$ (The sediment which is potentially influenced by ice-rafting)
- x = sand content in wt%

The fit line equation above from figure 16(a), was used to find the sediment which had primarily been influenced by ice-rafting, $SS_{(pot)}$, by inserting the wt% sand values into x. The ice rafting corrected median grain size of sortable silt, ΔSS was then calculated using the following equation;

$$\Delta SS = \text{Median SS} - SS_{(pot)}$$

The correction is supposed to filter out the grain size maxima which coincide with the highest sand contents (Figure 17), and reduce the average amplitude of the variations (Jessen and Rasmussen, 2015). In the scatter plot of median SS vs. ΔSS (Figure 16b), most of the samples plot close to the fit line. This indicates that the IRD correction is insignificant for most of the data points.

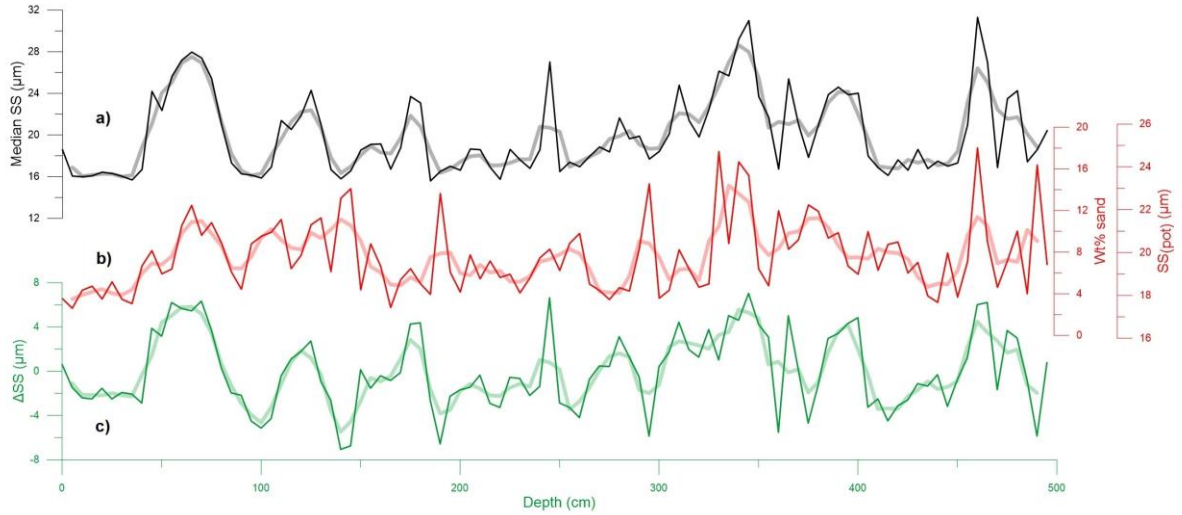

Figure 17: *Sortable silt records.* ***(a)*** *Median size of SS (µm).* ***(b)*** *Wt% sand and the calculated potentially ice rafted sortable silt $SS_{(pot)}$ (The two records display the same pattern and are therefore presented together).* ***(c)*** *The final ice rafted corrected sortable silt signal, ΔSS (µm). The bold lines within each plot represents three-point-running-averages.*

The IRD-corrected record (ΔSS) does seem to enhance certain features, and is believed to provide a more accurate image of the bottom current strength since IRD affected data has been filtered away (Figure 17c) (Jessen and Rasmussen, 2015). This record (ΔSS) was therefore used for the interpretations.

5.6.2 Results of the sortable silt analysis

The raw median SS record and the IRD corrected ΔSS record show similar patterns (Figure 17a and 17c), though certain features have changed and seem to have been enhanced for the ΔSS record. Distinct low points on the plot are more defined, and intervals where peaks in median SS correlate with peaks in the wt% sand record seem to have been smoothened out in the ΔSS record.

The raw median SS- and ΔSS records seem to possibly be following a cyclic pattern with approximately nine major peaks, which holds minor peaks as well. The first major peak is seen between ~ 460 – 480 cm. After this the values drop, and a larger interval of decreasing values is seen. Additional peaks are seen at ~ 410 – 385 cm, 365 cm, 360 – 300 cm, 280 cm, 245 cm, 180 – 150 cm, 130 – 110 cm and 75 – 45 cm. The clearest minima in the ΔSS record are seen at ~ 490 cm, 415 cm, 375 cm, 360 cm, 295 cm, 260 cm, 190 cm, 145 cm and 100 cm. The values are also quite low for the upper 40 cm of the core.

5.6.3 Interpretation

Changes in the ΔSS records have been found to be an indicator for bottom current variations, where high ΔSS values represent increased current activity, whereas low values represent decreased current activity. Changes in the sortable silt record can also be related to vertical current migration (e.g. Bianchi et al., 2001; Thornalley et al., 2013; Ezat et al., 2014). This is especially important to remember when interpreting the lower ΔSS values. The cyclic pattern which seems to be present is certainly an interesting feature, but any further interpretation of this requires comparison with other studies, and is therefore placed within the discussion.

5.7 Chronology – AMS radiocarbon ages

The basic chronology of this study is based on four AMS radiocarbon dates obtained from core HH13-089GC. The ^{14}C dates were calibrated to calendar years by using the software program CALIB 7.0.4 and calibration curve Marine13 (Stuvier and Reimer, 1993; Reimer et al., 2013). AMS radiocarbon dating results is shown in table 4 below. The software program automatically corrects for the global ocean reservoir age of 405 years (Hughen et al., 2004), and the regional correction $\Delta R = 140 \pm 20$ was used in addition for all samples, since the marine reservoir effect for East Greenland is ~ 550 years (Hjort, 1973).

Table 4: *AMS radiocarbon dating results from core HH13-089GC. Material for all samples was Neogloboquadrina pachyderma.*

Lab code	Sample ID	Sampling depth (cm)	^{14}C age	Calib 7.0.4 1 σ range (Cal. yrs. BP)	Calib 7.0.4 1σ mean (Cal. yrs. BP)
UBA-33264	HH13-089GC	30	7123 ± 37	7432 – 7516	7474 ± 42
UBA-33265	HH13-089GC	85	15 265 ± 81	17 798 – 18 032	17 915 ± 117
UBA-33266	HH13-089GC	140	21 194 ± 126	24 623 – 25 082	24 853 ± 230
UBA-34237	HH13-089GC	245	33 301 ± 328	36 262 – 37 243	36 753 ± 491

6 Discussion

Within this chapter, the basic interpretation of the results from HH13-089GC will be expanded and discussed in relation to age, and other studies both local and regional. The chapter will be divided into four parts:

1) The age model will be presented, along with the revised stable isotope stratigraphy.
2) The sortable silt (ΔSS) record will be compared to the Greenland ice core NGRIP.
3) The glacial history of the East Greenland continental margin will be presented; The results regarding the lithology, magnetic susceptibility, grain sizes, IRD, stable isotopes and sortable silt will be interpreted, discussed and compared to other studies.
4) Paleoceanography, where the results of the foraminiferal investigations will be discussed and linked to the glacial history and correlations in part three. The results of the sortable silt analysis will also be discussed further in this part.

6.1 Age model

To construct an age model, the four calibrated dates from core HH13-089GC were used (Table 4), as well as the occurrence of an ash layer found at ~ 45 cm, which correlates to the mid-Younger Dryas, Vedde ash dated to 10 310 ± 50 ^{14}C yrs. BP (Birks et al., 1996) and to 10 330 ± 65 ^{14}C yrs. BP (Wastergård et al., 1998). This ash layer has also been identified in the nearby East Greenland cores PS1725, PS1726 and PS1730 (e.g. Nam et al., 1995; Stein et al., 1996) where the age used was 10 600 ± 60 ^{14}C yrs. BP (Mangerud et al., 1984). The more recent age for the Vedde ash of ~ 10 300, is described to be a conventional ^{14}C age, and was therefore calibrated to calendar years, using the Calib 7.0.4 software program (Table 5a*). In addition to these dates, the initial interpretation of the δ^{18}O records and certain findings within the foraminiferal record, provided the basis for determining approximate depths of some MIS boundaries and MIS peaks. The ages of these boundaries and peaks are from the LR04 benthic stack model (Lisiecki and Raymo 2005) (Table 5b). Before an age model could be constructed, the linear sedimentation rates needed to be estimated.

6.1.1 Sedimentation rates

Linear Sedimentation Rates (LSR) can be estimated by assuming constant sedimentation between the radiocarbon dated levels. The interval between two calibrated radiocarbon ages, and the interval between the depths that these ages represent are calculated. Next, the depth interval is divided by the age interval and multiplied by 1000 to get the LSR in cm per thousand years (cm/ka) (Table 5).

Table 5: *Linear Sedimentation Rates (a) and (b)*

(a) **Depth (cm)**	**^{14}C age**	**Mean cal. age (cal. yrs. BP)**	**LSR (cm/ka)**	**Yrs/cm**
0	(550)	(0)		
			4.01	249.1333
30	7123 ± 37	7474 ± 42		
			3.17	315.0666
45	*~ 10 300	~ 12 200		
			6.99	142.8750
85	15 265 ± 81	17 915 ± 117		
			7.93	126.1454
140	21 194 ± 126	24 853 ± 230		
			8.82	113.3333
245	33 301 ± 328	36 753 ± 491		
**Conventional radiocarbon age for the Vedde ash layer from Birks et al. (1996) and Wastegård et al. (1998).*				
(b) **Identified feature**	**Depth (cm)**	**Age (yrs. BP)**	**LSR (cm/ka)**	**Yrs/cm**
			4.69	213.1263
MIS 3/4	340	57 000		
			2.60	384.6153
MIS 5a (peak)	504	82 000		
			1.43	700
MIS 5c (peak)	425	96 000		
			1.11	900
MIS 5e (peak)	455	123 000		
			2.14	466.6666
MIS 5/6	470	130 000		

To find approximate ages for the undated samples of the core, the intervals between two calibrated radiocarbon ages and the interval of the depths they represent was used once again. In this case however, the age intervals were divided by the depth intervals to find years per cm (yrs/cm). This value was then used in a calculation to determine the unknown ages. A simple example of the calculation of such an unknown age is seen here:

Table 6: *Example for age-model calculations.*

	Depth (cm)	Age (yrs. BP)	yrs/cm (interval 0 – 30 cm)
A	15 cm	Unknown?	249.13333
B	30 cm	7474	

Calculating unknown age:

- Initial age of depth B – (yrs/cm * (depth B – depth A)) = Unknown age of depth A (yrs. BP)
  - 7474 – (249.13333 * (30 – 15)) = 3737 yrs. BP

Similar calculations were made for all unknown ages using the different values of yrs/cm for the different known intervals. The result of these calculations is a continuous age model of the core (Figure 18). The same ages were also found with linear interpolation.

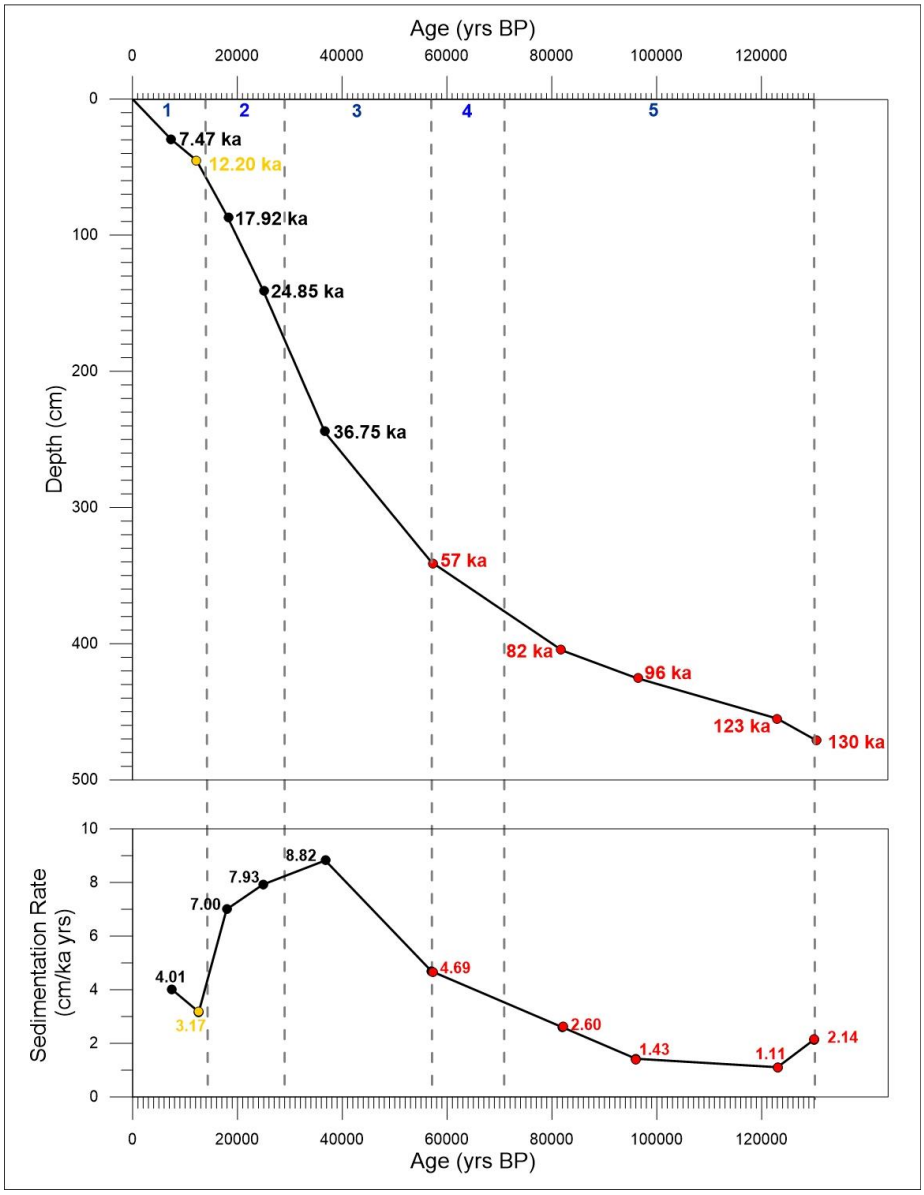

Figure 18: *Age – depth model and linear sedimentation rates for the core HH13-089GC. Numbers in black indicate the results for the calibrated ages. The yellow number represents the results of the calibrated Vedde ash. Red numbers indicate the approximate results for identified stage boundaries and sub-stage peaks (ages from Lisiecki Website). Blue numbers in the top of the figure represents marine isotope stages (MIS).*

The average sedimentation rate within the dated section of the core (Table 5a) is 6.18 cm/ka. The sedimentation rate is relatively high, but show a decrease towards the top of the core. It is particularly high between 36 753 – 12 200 cal. yrs. BP.

The sedimentation rates that were based on the initial interpretation of the $\delta^{18}O$ records (Table 5b) are much lower than those within the dated part of the core, with an average of 2.39 cm/ka. The largest difference seems to be at the MIS 4/3 boundary at 57 000 yrs. BP.

The age model has made it possible to plot the magnetic susceptibility results, the $\delta^{18}O$- and $\delta^{13}C$ records, the distribution of IRD, the relative abundance of planktic and benthic foraminifera, and the ΔSS records against calibrated years before present (cal. yrs. BP) (Figure 24).

6.1.2 Stable isotope stratigraphy and chronology

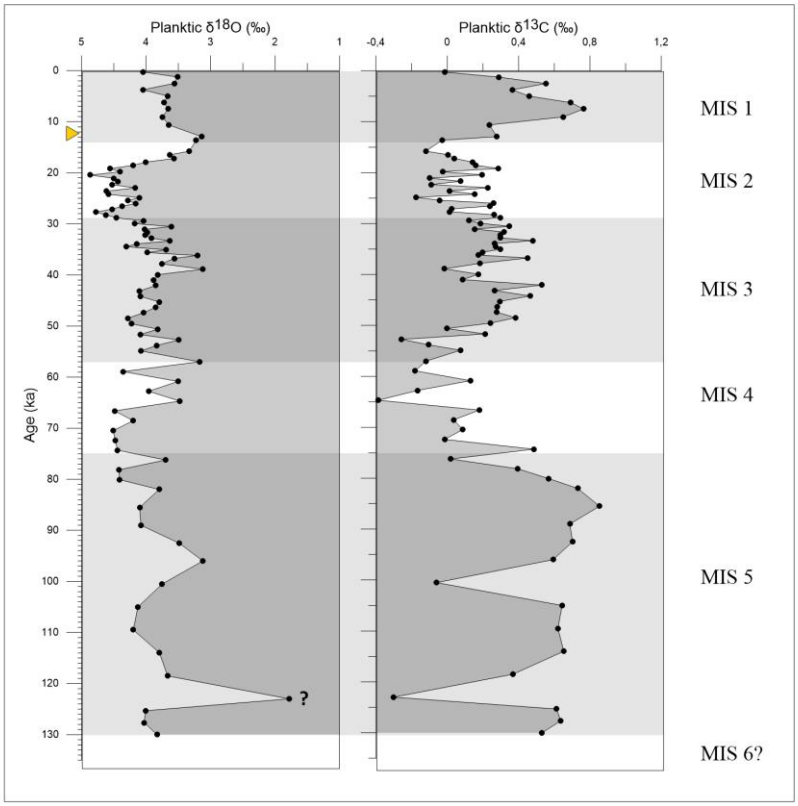

Figure 19: *Revised stable isotope records plotted against age (ka yrs. BP), and separated into marine isotope stages based on interpretation and age model.*

The possible positions of the marine isotope stage boundaries within the core, was interpreted based on shifts in the isotope record only (Chapter 3.6.10). The ages for the stage boundaries 6/5 (130 ka yrs. BP) and 4/3 (57 ka yrs. BP) as well as the possible peaks of MIS 5a (82 ka yrs. BP), MIS 5c (96 ka yrs. BP) and MIS 5e (123 ka yrs. BP) are based on the LR04 benthic stack results from Lisiecki and Raymo (2005), and the specific dates are from Lisiecki's personal website (http://www.lorraine-lisiecki.com/LR04_MISboundaries.txt) referred to as Lisiecki Website hereafter. The placement of these boundaries and features within the record was based on the initial interpretation of the isotope records and presence of the foraminiferal stratigraphic biomarker *P. bulloides* (Chapter 5.4.2), and are therefore only estimates. The core does extend back in time, maybe a couple thousand years below 130 ka yrs. BP, though exactly how far back is unknown. Stage boundaries 5/4, 3/2 and 2/1 were initially interpreted from the stable isotope records only, however the age model suggests that some of

these initial placements needs to be adjusted slightly. The approximate ages found for these stage boundaries was 70 462 yrs. BP, 28 820 yrs. BP and 14 343 yrs. BP respectively. Lisiecki Website defined these boundaries at 71 ka–, 29 ka– and 14 ka years BP, which is similar to the results of the age model (Figure 18). The MIS intervals identified will be used later in the discussion.

6.1.3 Flux data

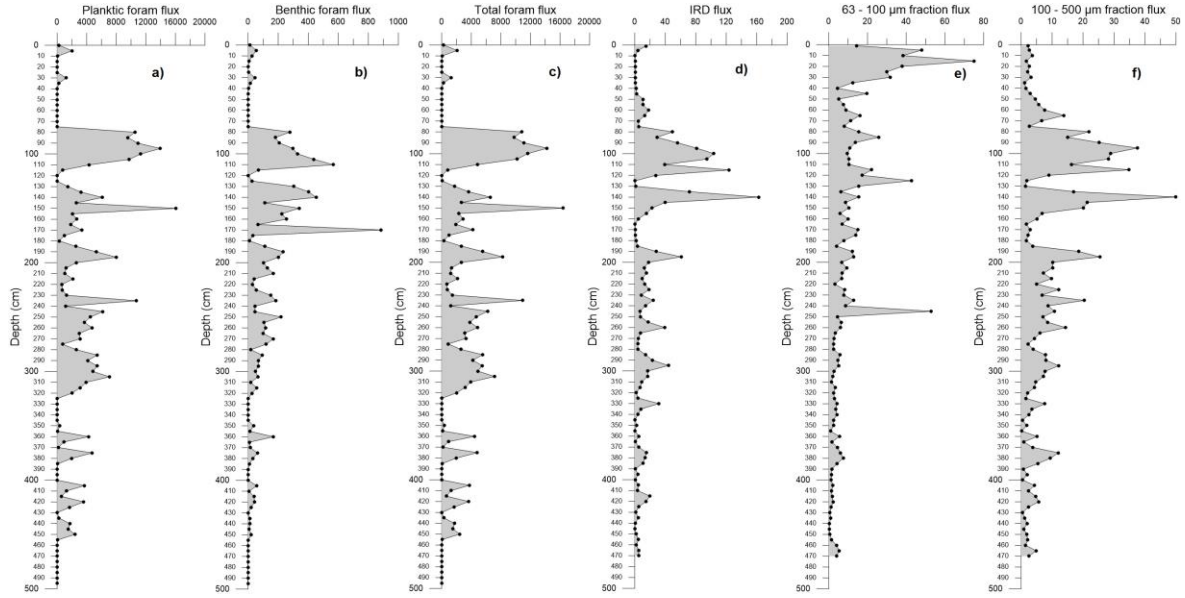

Figure 20*: Results of the flux calculations vs. depth (cm).* ***(a)*** *Planktic foraminifera flux (No. Planktic foraminifera/cm^2/ka)* ***(b)*** *Benthic foraminifera flux (No. Benthic foraminifera/cm^2/ka)* ***(c)*** *Total foraminifera flux* ***(d)*** *IRD flux (g/cm^2/ka)* ***(e)*** *Flux for grain size fraction 63 – 100 µm (g/cm^2/ka)* ***(f)*** *Flux for grain size fraction 100 – 500 µm (g/cm^2/ka).*

6.2 Sortable silt (ΔSS) – Pattern matching with other records

The results of the sortable silt analysis showed an interesting and clear cyclic pattern. The pattern reminded of the oscillations in the $\delta^{18}O$ records for the Greenland ice cores (e.g. North Greenland Ice Project – NGRIP ice core, Greenland Ice Project – GRIP ice core and Greenland Ice Sheet Project 2 – GISP2 ice core). In the study by Jessen and Rasmussen (2015), the sortable silt record (ΔSS) was found to correlate with several of the events recorded in the NGRIP ice core. Based on this knowledge, it was decided to compare the ΔSS record from core HH13-089GC with the $\delta^{18}O$ record for the Greenland ice core NGRIP (NGRIP members, 2004; Andersen et al., 2006), to see how the results of the present study relates to the climatic changes recorded in this ice core.

6.2.1 Background – The NGRIP ice core isotope record

The stable isotope record from the NGRIP ice core is measured in 5 cm resolution. Down to a depth of 2900 m (105 000 yrs. before 2000 AD), the record shows the same general climatic features as observed in other Greenland ice cores (Figure 21), however it extends slightly farther back in time than these. Climatic features observed in this ice core includes the Younger Dryas cold event, the Bølling–Allerød interstadials and the 24 abrupt, climatic Dansgaard – Oeschger events (Chapter 1.2.3.1) during the last glacial period (NGRIP members, 2004). Moving from past to present, the oscillations show rapid temperature increases followed by a more gradual decrease towards an ultimate minimum, some of which have been found to be related to Heinrich Events (Bond et al., 1993).

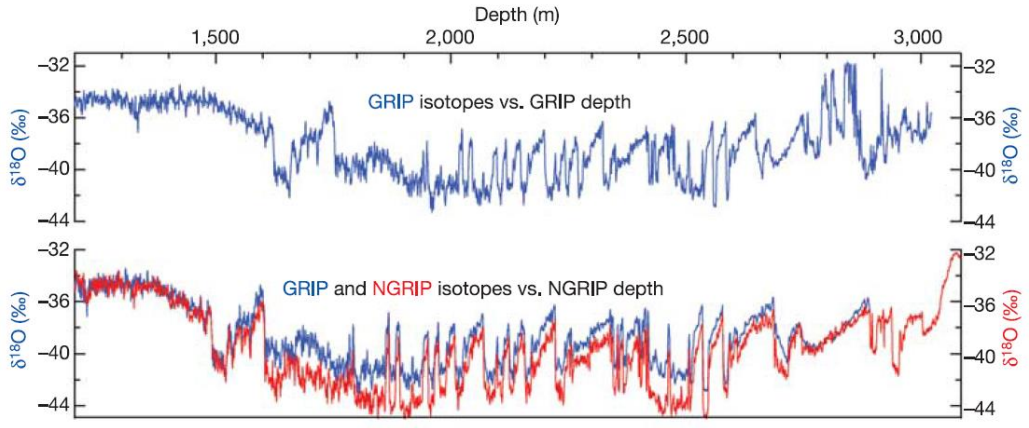

***Figure 21**: The NGRIP stable oxygen isotope record **(red)** compared to the GRIP record (blue). The GRIP record **(blue)** has been plotted on the NGRIP depth scale for the bottom plot. (Figure from NGRIP members, 2004).*

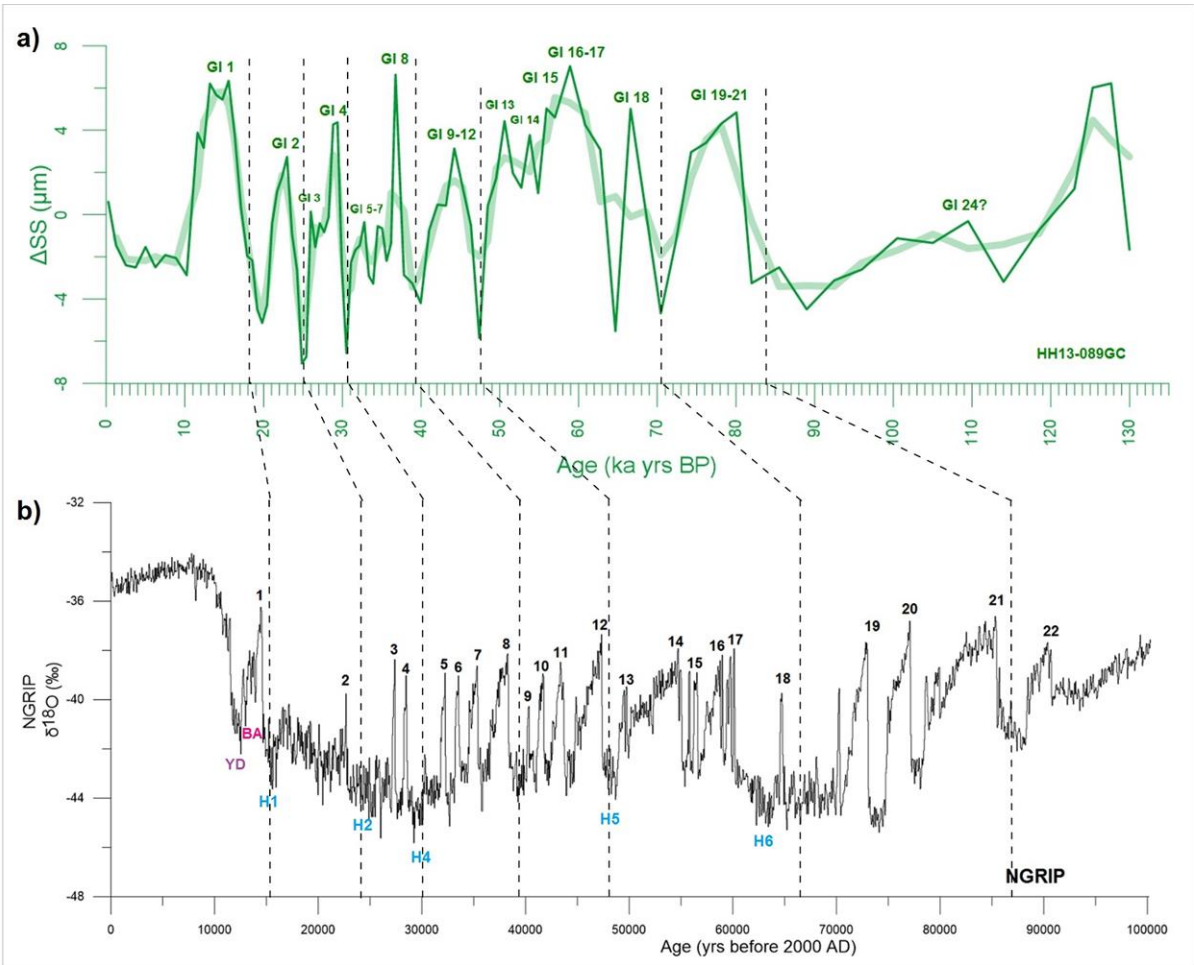

Figure 22: *Showing correlations between the **(a)** ΔSS record for core HH13-089GC (investigated in this thesis) plottet against age (ka yrs. BP) **(b)** δ18O record for the Greenland Ice Core NGRIP plotted against age (yrs. before 2000 AD) (data from NGRIP members, 2004; Andersen et al., 2006). The black and green numbers seen above each peak, represents the interstadials within the Dansgaard – Oeschger cycles, or Greenland Interstadials (GI) as they are also called. The blue letters show the identified Heinrich Events within the Greenland ice cores, YD = Younger Dryas, BA = Bølling – Allerød (Bond et al., 1993). The bold line within the ΔSS record represents a three-point-running-average for the record.*

6.2.2 Interpretation and implications

Each of the nine large oscillations seen within the ΔSS record for HH13-089GC, follow a pattern of abrupt increase, gradual decrease from a peak, followed by a distinct minimum, and ending with a new abrupt increase. This is similar to the pattern of the Dansgaard – Oeshger cycles and Bond cooling cycles. By using pattern matching (Figure 22) to correlate these results with the NGRIP ice core (NGRIP Members, 2004), it seems possible to identify 21 ΔSS peaks. These peaks correlate with the Dansgaard – Oeschger interstadials within the $\delta^{18}O$ (NGRIP) record. The interstadials will be referred to as Greenland Interstadials (GI) in this thesis.

All 21 peaks in the ΔSS record correlate with the 21 Greenland Interstadials (GI) seen on the NGRIP plot, whereas the distinct drops in the ΔSS record correlate with distinct drops in the NGRIP $\delta^{18}O$

record (Greenland Stadials) and Heinrich Events. Greenland Interstadial GI 1 for the ice core records include the warm Bølling – Allerød interstadials (BA), which is followed by a larger drop representing the Younger Dryas (YD) cold event (Bond et al., 1993). These smaller climatic events are however difficult to recognize within the ΔSS record of HH13-089GC.

Greenland Interstadials GI 1 – GI 8, GI 12, GI 13 – GI 18 were quite straight forward when correlating. Whereas GI 19 – GI 25 were more difficult. The very low sedimentation rates (< 3 cm/ka yrs.) in the bottom 100 cm of the core leading to low resolution, could be a reason for this. Considering that the ΔSS samples were taken every 5 cm, different features are relatively clear. The high sedimentation rates in the upper 400 cm, especially between 250 – 100 cm could have led to increased resolution within this part of the core.

The pattern-matching of the two records, suggests a relatively clear correlation between changes in bottom current activity (ΔSS) and the climatic oscillations recorded in terrestrial ice (NGRIP). The correlation, makes it possible to use the Greenland Interstadials (GI), Greenland Stadials (GS) and Heinrich Events as a base for the expanded interpretations and discussions of the results. It will be interesting to see if the additional results for core HH13-089GC can provide further information about these oscillations as the discussion continues.

6.3 Glacial history of the East Greenland margin

Several marine and terrestrial studies have taken place along the East Greenland margin. Fjord systems have been investigated in detail; The Scoresby Sund fjord system (e.g. Marienfeld, 1992; Dowdeswell et al., 1993, 1994; Cofaigh et al., 2001), the Kangerdlugssuaq Fjord (Syvitski et al., 1996; Andrews et al., 1994, 1996) and the Kejser Franz Joseph Fjord (e.g. Evans et al., 2002). The continental margin has also been studied (e.g Mienert et al., 1992; Dowdeswell et al., 1997; Nam et al., 1995; Stein et al., 1996). Correlations between these studies have provided detailed information about important climatic events, and the East Greenland glacial history (e.g. Funder et al., 1998; Funder et al., 2011).

In this subchapter, the glacial history of the East Greenland continental margin will be presented; The results regarding the lithology, magnetic susceptibility, grain sizes, IRD, stable isotopes and sortable silt will be interpreted, discussed and compared to other studies (Figure 24 and 25). Although there are several other paleoclimatic studies investigating IRD concentrations, stable isotopes and foraminiferal assemblages from the East Greenland continental margin (e.g. Marienfeld, 1992; Mienert et al., 1992; Stein et al., 1993; Williams et al., 1993; Jennings and Helgadottir, 1994; Nam et al., 1995; Stein et al.,

1996; Funder et al., 1998; Nam and Stein, 1999; Jennings et al., 2002; Jennings et al., 2011), many of them are restricted to post glacial times.

The studies by Stein et al. (1996), Nam et al. (1995) and Funder et al. (1998) however, covers both the late Pleistocene and the Holocene. Gravity cores collected during the R.V. Polarstern expedition ARK V/3 in 1988, will provide the basis for the local comparisons in this sub-chapter. The cores PS1726 and PS1730 were collected from the deep sea slope off Scoresby Sund, East Greenland and will be of particular interest (Figure 23). They have been collected from similar depths to that of HH13-089GC, one slightly shallower (PS1726), and one slightly deeper (PS1730). Similar investigations were made and their studies included stable isotope stratigraphy, sedimentation rates, grain size analysis and magnetic susceptibility, and others. The most dominant foraminiferal species were mentioned briefly by Nam et al. (1995), however a thorough faunal investigation was not preformed, nor was the sortable silt analysis. The characteristics of these two cores can be seen in figures 26 and 27.

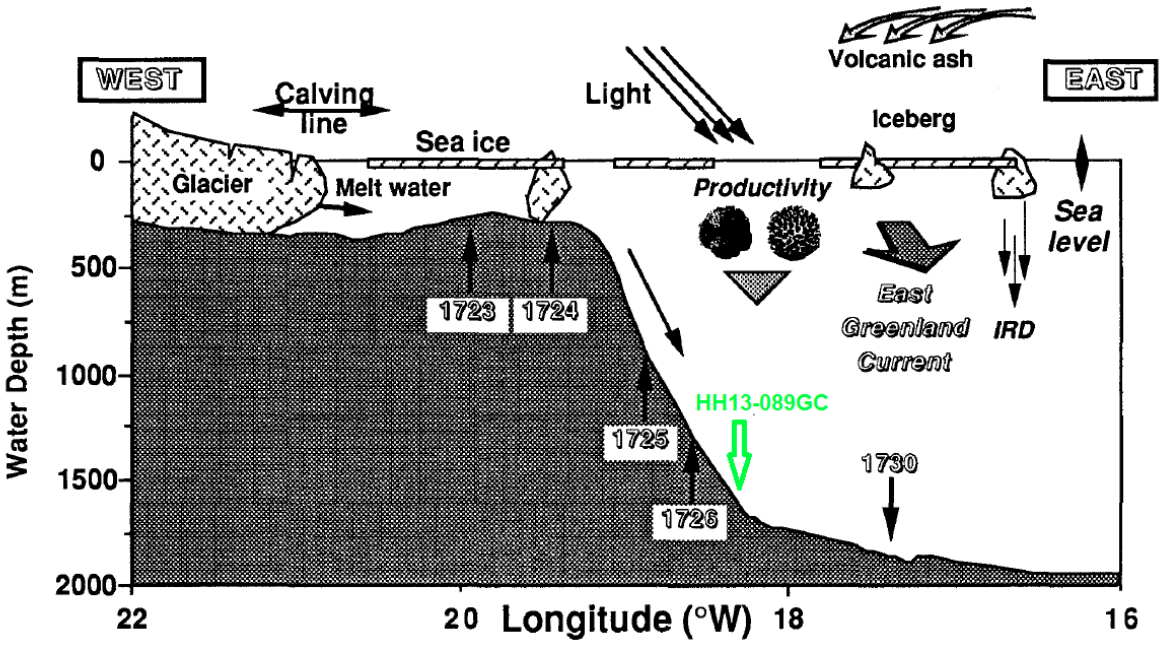

Figure 23: *Simplified scheme of the East Greenland continental margin, showing the major climatic and oceanographic factors and processes which control sedimentation in the area. These factors will be of great importance in the interpretation and discussion of the results. The approximate location for the investigated core is seen in green. Some of the cores investigated in Nam et al. (1995), Stein et al. (1996) and Funder et al. (1998). (Figure from Stein et al., 1993).*

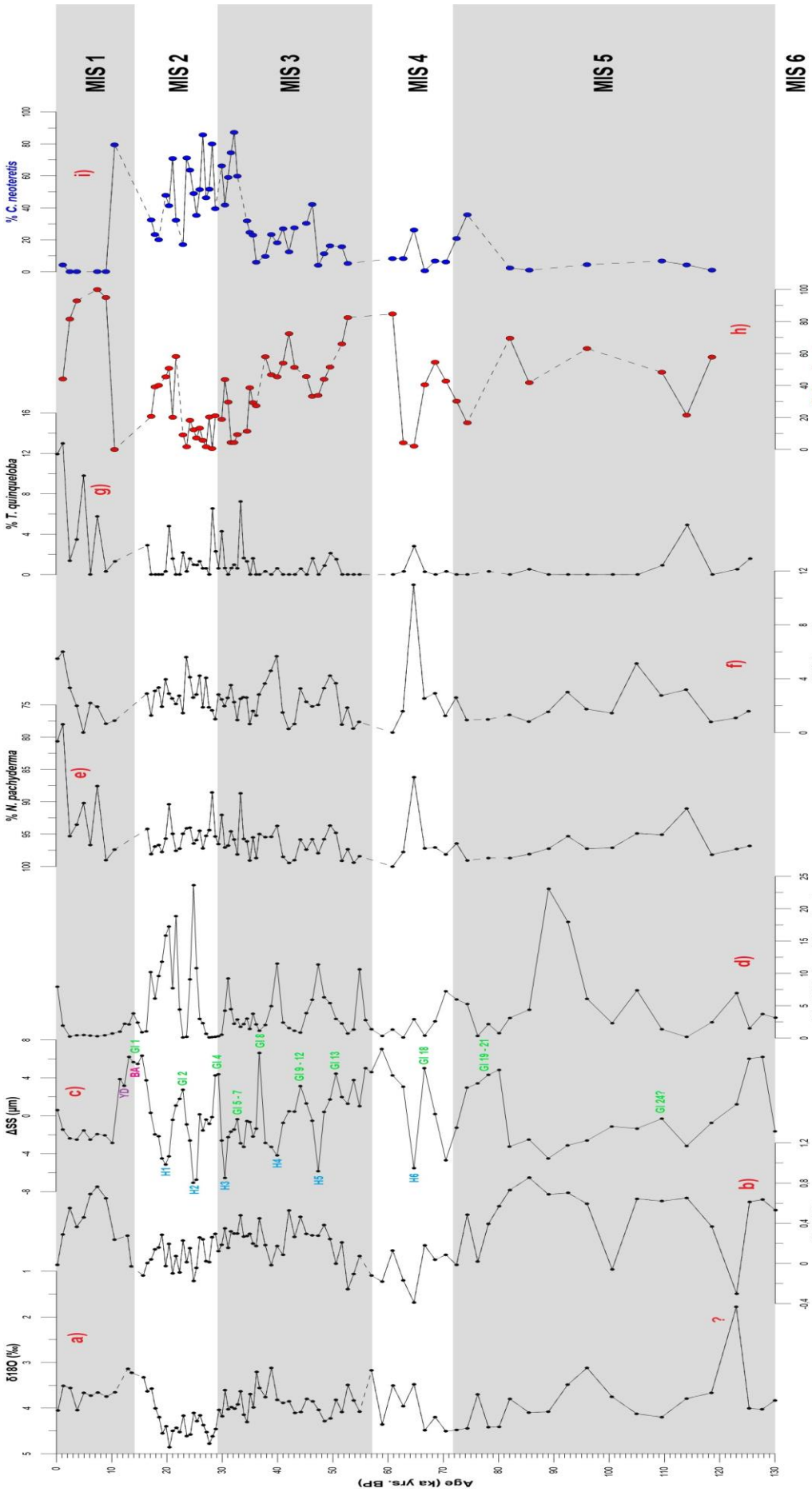

Figure 24: *Main results of the present investigation of core HH13-089GC plotted against age (ka yrs. BP).* ***(a)*** *Stable oxygen isotope record,* ***(b)*** *Stable carbon isotope record,* ***(c)*** *Sortable silt record,* ***(d)*** *Total IRD/g dry weight sediment,* ***(e)*** *Relative abundance of N. pachyderma,* ***(f)*** *Relative abundance of N. incompta,* ***(g)*** *Relative abundance of T. quinqueloba,* ***(h)*** *Relative abundance of O. umbonatus,* ***(i)*** *Relative abundance of C. neoteretis. Marine isotope stages are indicated on the record, in addition to Greenland Interstadials (**GI**), Heinrich Events (**H**), Younger Dryas (**YD**) and Bølling-Allerød (**BA**).*

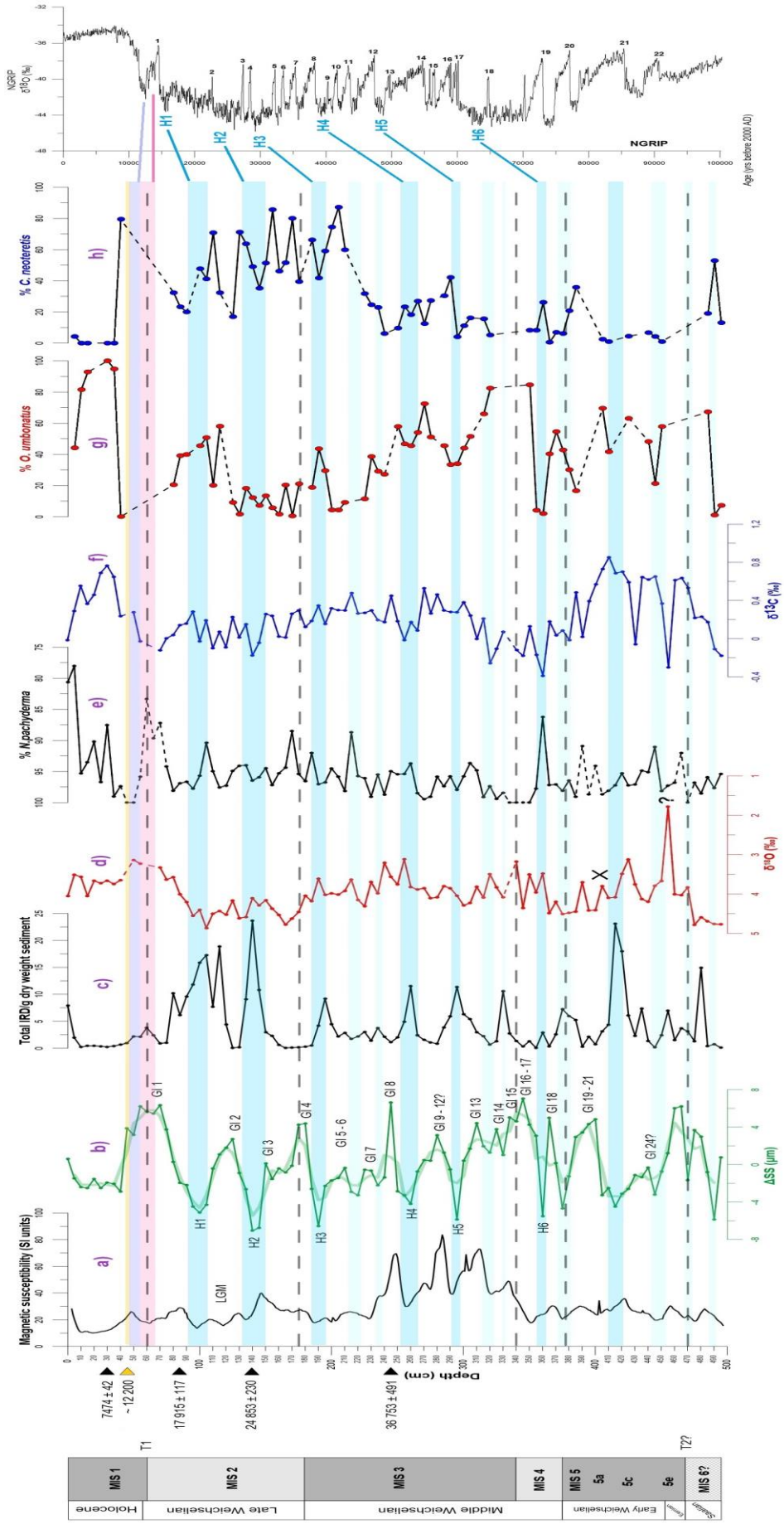

Figure 25: *Main results of the present investigation of core HH13-089GC, and interpreted chronology (**far left**). **(a)** Magnetic susceptibility record, **(b)** Sortable silt record (ΔSS), **(c)* Total IRD/g dry weight sediment, **(d)** Stable oxygen isotope record, (e) Relative abundance of N. pachyderma, **(f)** Stable carbon isotope record, **(g)** Relative abundance of O. umbonatus, **(h)** Relative abundance of C. neoteretis, **(i)** NGRIP oxygen isotope record. All records are plotted against depth, except for the NGRIP record which is plotted against age (yrs. before 2000 AD). Other features on the figure are: Radiocarbon dates, marine isotope stages (**horizontal stippled lines**), the Vedde Ash layer (**yellow**), Greenland Interstadials (**GI**), Greenland Stadials (**light blue**), Heinrich Events (**H**), Bølling-Allerød, Younger Dryas, The Last Glacial Maximum (**LGM**), The presence of P. bulloides (**X**) and intervals barren of foraminifera (**general stippled lines**).*

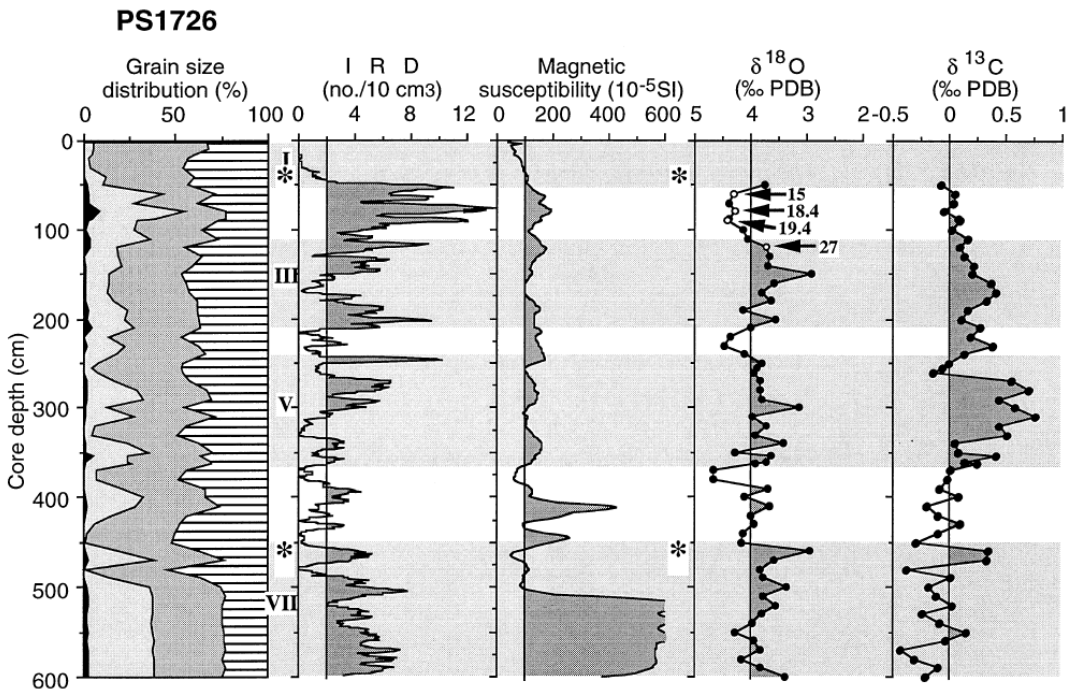

Figure 26: *Results of the local slope core PS1726 form the studies by Nam et al. (1995), Stein et al. (1996) and Funder et al. (1998). (Figure from Funder et al., 1998).*

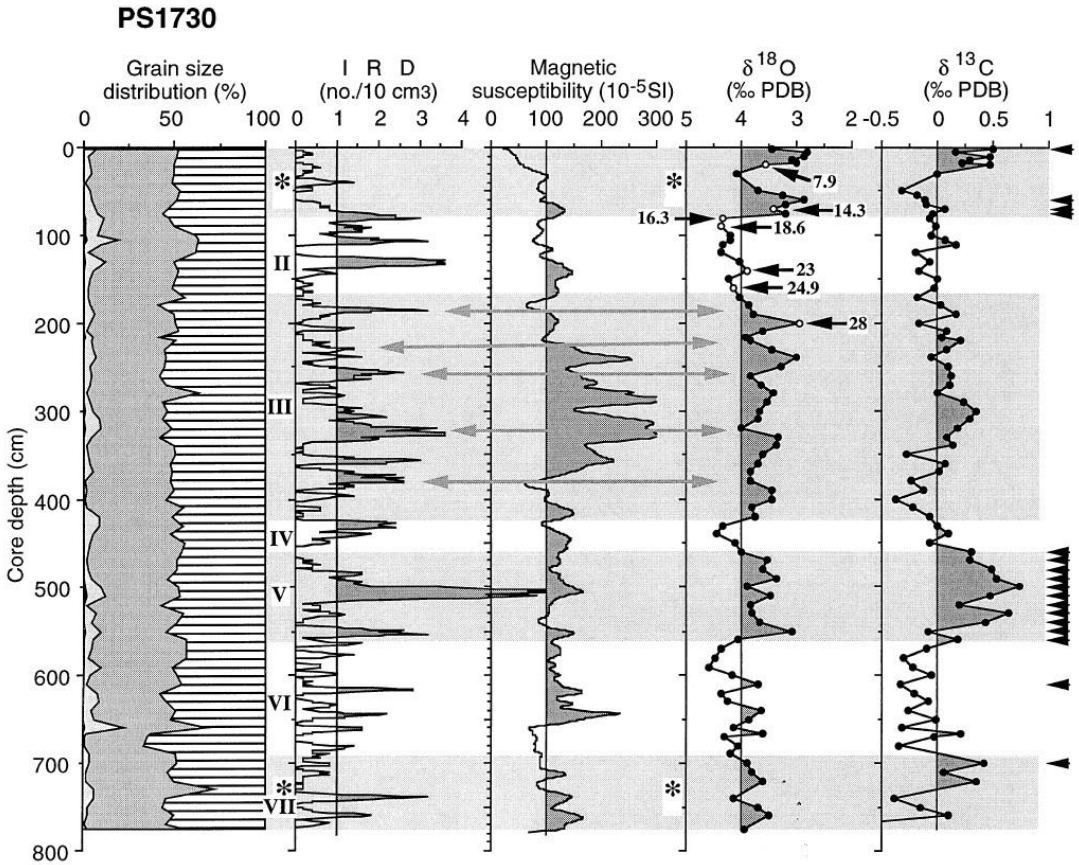

Figure 27: *Results of the local slope core PS1730 form the studies by Nam et al. (1995), Stein et al. (1996) and Funder et al. (1998). (Figure from Funder et al., 1998).*

6.3.1 The MIS 6/5 transition (core interval 497 – 470 cm)

Marine isotope stage 6 represents the Saalian glaciation, also known as the Scoresby Sund glaciation in several Greenland Studies. During this time, the ice sheet overrode the coastal mountains in the Jameson Land area (Figure 1), and maximum ice cover was achieved in East Greenland (Funder et al., 1998; Funder et al., 2011). Several studies have indicated that the deglaciation phase following the Saalian glaciation, was quite rapid in Greenland (e.g. Stoner et al., 1995; Fronval and Jansen, 1997).

Based on the oxygen isotope stratigraphy, it seems that only the transitional phase between MIS 6 and MIS 5 is present in the record, and it is this phase that will be given the most attention within this sub-chapter. The presence of the MIS 6/5 transition (~ 130 000 yrs. BP) has been determined by the very heavy but decreasing $\delta^{18}O$ values, showing a transition from glacial- to interglacial conditions, light $\delta^{13}C$ values, the presence of the benthic foraminifera *S. loeblichi*; a common species in foraminiferal faunas representing the late Saalian glaciation, MIS 6 (Knudsen, 1984), the presence of an IRD peak near the termination of MIS 6, and evidence of larger climatic oscillations within the ΔSS record.

Meltwater from terrestrial sources are generally depleted in ^{18}O, and the overall decreasing planktic $\delta^{18}O$ values between 495 – 470 cm could indicate the strong influence of cold and fresh meltwater at the surface (Spielhagen et al., 2004; Risebrobakken et al., 2006; Chauhan et al., 2014). A similar shift in the oxygen isotope record at the MIS 6/5 boundary was seen in the local studies by Nam et al. (1995), Stein et al. (1996) and Funder et al. (1998) from the continental slope off Scoresby Sund. This shift has also been identified and described for other areas in the North Atlantic by several studies (e.g. Martinson et al., 1987; Haake and Pflaumann, 1989; Fronval and Jansen, 1997; Spielhagen et al., 2004; Lisiecki and Raymo, 2005; Risebrobakken et al., 2006; Chauhan et al., 2014). Low, but increasing $\delta^{13}C$ values is seen right at the MIS 6/5 boundary for this study, which could indicate that surface ventilation is poor, but improving. Low $\delta^{13}C$ values at the MIS 6/5 transition was also seen in other regional studies as well (e.g. Haake and Pflaumann, 1989; Fronval and Jansen, 1997). In Fronval and Jansen (1997), the low $\delta^{13}C$ values was interpreted to reflect the dominance of perennially ice covered polar surface waters, which have been found to be ^{13}C depleted in relation to Arctic surface waters (Johannessen et al., 1994).

A peak in IRD record of HH13-089GC is seen near the interpreted MIS 6/5 boundary at ~ 470 cm (130 000 yrs. BP), which could indicate increased calving as a response to warming climatic conditions. Several regional studies have seen such a peak in IRD near the MIS 6/5 boundary, and described it to be a typical trait for the termination of the Saalian glaciation (T2) in the Arctic–, Nordic–, Barents– and Kara Seas (e.g. Fronval and Jansen, 1997; Spielhagen et al., 2004; Risebrobakken et al., 2006). Risebrobakken et al. (2006) saw a peak in IRD at 135 ka yrs, near the MIS 6/5 boundary in their study along a transect in the eastern Nordic Seas.

In sub-chapter 6.2, it was shown how the ΔSS record correlated with the larger climatic oscillations recorded in Greenland ice cores, however it was difficult to notice these oscillations in the $\delta^{18}O$ record for HH13-089GC. Since the $\delta^{18}O$ records for the present study represent the surface environment in an area that is highly influenced by icebergs and meltwater, it is possible that certain evidence for larger climatic changes has been overridden by local signals. Changes in the $\delta^{18}O$ values of the planktic species *N. pachyderma*, can relate to local temperature changes, salinity changes, freshwater input from meltwater and/or variations in global ice volume (Mix and Ruddiman, 1984; Maslin et al., 1995). The high latitude North Atlantic is generally highly affected by larger local meltwater input and temperature changes (Ruddiman and McIntyre, 1981), and such local changes may overshadow the global ice volume signal in the $\delta^{18}O$ record (Mix and Ruddiman, 1984).

During what is interpreted to represent the MIS 6/5 transition, several fluctuations in the ΔSS record is seen. They are rapid, occur over quite a short period of time, and are not clear in any other proxy records. As the ΔSS record has been found to correlate with the NGRIP climate oscillations, it is possible that these boundary fluctuations represent rapid climatic changes within the Saalian deglaciation. Such rapid climatic oscillations have been seen in the GRIP ice core record (e.g. Seidenkrantz et al., 1996), however, the parts of the Greenland ice core records which are older than the Eemian period, has since been found to be disturbed. Even so, there are several other studies that have also indicated a so called "two step" deglaciation phase, or a plateau/pause in the deglaciation near Termination 2 based on other records (e.g. Sarnthein and Tiedemann, 1990; Schweger and Matthews, 1991; Seidenkrantz et al., 1996; Shackleton et al., 2003; Gouzy et al., 2004; Bauch and Erlenkeuser, 2008; Bauch et al., 2011; Irvali et al., 2012). The results of Irvali et al. (2012) indicated that surface waters off southern Greenland reached temperatures ~3 – 5 °C higher than present during the MIS 5e, but that the warm interglacial climate was interrupted by a cooling event at ~ 126 000 yrs. BP. Bauch and Erlenkeuser (2008) on the other hand noticed a "step-like" deglaciation phase between ~ 135 000 – 124 500 yrs. BP, which could resemble the ΔSS signal below 470 cm (> 130 000 yrs. BP). Galaasen et al. (2014) found that the influence of North Atlantic Deep Water (NADW) was strong at the onset of MIS 5e, but that it was interrupted by several short, but prominent reductions where ice rafting was increased. As sortable silt has been found to be an indicator of bottom current activity, the identified ΔSS drops near the MIS 6/5 boundary could be related to the NADW reductions seen by Galaasen et al. (2014). I will come back to the possible connection between sortable silt, bottom current activity and NADW later.

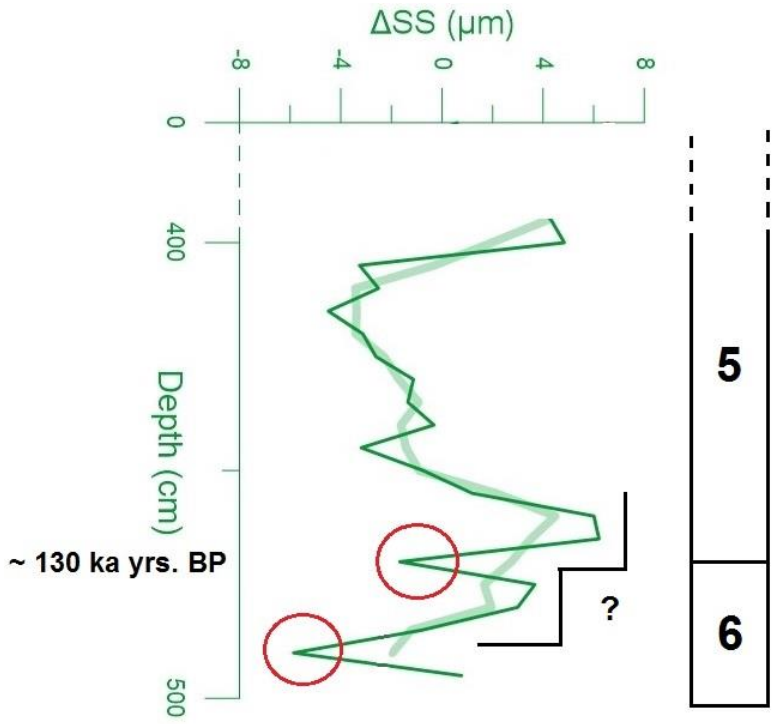

Figure 28: *The MIS 6/5 transition from the ΔSS record showing the rapid fluctuations (red circles) which could correlate with changing NADW (Galaasen et al., 2014), and the possible "step-like" deglaciation phase (black). Note that the ΔSS record is plotted against depth (cm) in order to see the features. The MIS 6/5 transition is set to ~ 130 000 yrs. BP.*

The age of the bottom 37 cm of HH13-089GC is only known to be > 130 000 yrs. BP, and so the ΔSS record in figure 28 is plotted against depth (cm) in order to see the features prior to 130 000 yrs. BP. The identification of a possible "two-step" deglaciation phase, provide additional evidence for the presence of the MIS 6/5 transitional zone within the core. The positioning of the boundary at ~ 470 cm seems accurate. Close to the MIS 6/5 transition, an interval barren of planktic foraminifera is seen. This could be a result of perennial sea ice coverage, causing limited foraminiferal growth (Chauhan et al., 2014), or reduced $CaCO_3$ production due to events of meltwater discharge. Large meltwater discharges could have led to a reduction in the vertical mixing between surface – and deep waters, leading to conditions which cause carbonate dissolution (Nam et al., 1995).

6.3.2 MIS 5: 130 ka – 75 ka yrs. BP (core interval 470 – 375 cm)

Marine isotope stage 5 represents the unusually warm Eemial interglacial (~ 130 000 – 115 000 yrs. BP), and the Early Weichselian glacial period (~ 115 000 – 71 000 yrs. BP). The Greenland ice sheet responded greatly to the warm temperatures and higher sea level of the Eemian, and models reconstructing the ice sheet's extent, have shown that it decreased to ~ 2/3 of its present size (Figure 29) (Letréguilly et al., 1991; Huybrechts, 2002; Funder et al., 2011). Funder et al. (2011) described the Scoresby Sund area to be the only investigated area in Greenland which has a detailed record of glaciation during the Early Weichselian. Lysså and Landvik, 1994 preformed detailed investigations of terrestrial sediments in Jameson Land, East Greenland (Figure 1), and found evidence for three Weichselian glacier advances in the area, two of which were restricted to MIS 5. These two were the Aucellaelv stadial (115 000 – 105 000 yrs. BP), MIS 5d, and the Jyllandselv stadial, MIS 5b.

Figure 29: *Modelled Eemian minimum ice sheet extent for Greenland (Letréguilly et al., 1991). Figure is from Funder et al., 2011, who noted that this reconstruction was based on certain erroneous assumptions. (Terminal moraines from the Saalian glaciation is also seen for south-western Greenland in blue, and arrows indicate ice sheet flow during MIS 6).*

MIS 5 was recognized in core HH13-089GC by the shift in the oxygen isotope record from high to generally low values. Even though the measurement which follows the MIS 6/5 boundary is uncertain, there still seems to be an overall lower trend in the $\delta^{18}O$ record, indicating a warmer climate and possibly increased influence of freshwater at the surface, which could be a result of increased iceberg calving (Rasmussen and Thomsen, 2008). Due to the evidence presented for the existence of the MIS 6/5 transition, the very low reading just above this boundary has under some doubt been interpreted to represent the Eemian interglacial, MIS 5e (~ 123 000 yrs. BP). A confirmation of the low $\delta^{18}O$ measurement could have been useful in order to validate or dismiss this claim. The benthic foraminifera *C. wuellerstorfi* has been found to be amongst the dominating benthic species during MIS 5 (Streeter et al., 1982). *Cibicides wuellerstorfi* in high numbers generally indicates interglacial conditions (e.g Haake and Pflaumann, 1989). This species dominates the benthic record during 5e in core HH13-089GC, which increases the credibility of the interpretation of this sub-stage. The local studies by Nam et al. (1995), Stein et al. (1996) and Funder et al. (1998) all identified MIS 5 within their continental slope cores (PS1726 and PS1730) based on the presence of *C. wuellerstorfi*. In other studies from the Nordic Seas, the species has been found to be amongst the most dominating during MIS 5 and MIS 1 (e.g. Streeter et al., 1982; Haake and Pflaumann, 1989; Rasmussen et al., 1996b). In the study by Streeter et al. (1982) from the central GIN-Seas, *C. wuellerstorfi* was also found to be amongst the dominating benthic species during MIS 4, and the middle of MIS 3 in addition to MIS 5e, 5c and the Holocene.

Marine isotope stage 5 is also defined by the very high $\delta^{13}C$ values (0.6 – > 0.8 ‰), which could indicate increased surface productivity or increased ventilation of the surface waters (Sarnthein et al., 1995; Voelker et al., 1998). Changes in productivity affects the amount of dissolved CO_2 in the water, and is together with temperature, depth and salinity one of the controlling factors for dissolution of carbonate (Steinsund and Hald, 1994). Increased productivity together with lower P:B ratios and decreased total abundance of foraminifera could be an indication of dissolution. The $\delta^{13}C$ values in MIS 5 were fluctuating quite drastically though, showing two major drops to – 0.3 and – 0.1 respectively. The largest drop seems to correlate with the interpreted MIS 5e. The local studies by Nam et al. (1995), Stein et al. (1996) and Funder et al. (1998) also saw high $\delta^{13}C$ values during MIS 5, however their values for the slope cores (PS1726 and PS1730) were far less fluctuating than those seen in HH13-089GC. Nam et al. (1995) found a generally higher abundance of especially planktic foraminiferal tests during MIS 5, and interpreted it to be an indication of greater preservation of carbonate as a result of the higher $\delta^{13}C$ values. The planktic foraminiferal abundance for HH13-089GC also reaches its highest levels during MIS 5 (Figure 9a). Several regional studies have found high $\delta^{13}C$ values to correlate with high abundance of foraminiferal tests, especially during MIS 5e. Fronval and Jansen (1997) found that the foraminiferal content in the Greenland and Iceland Seas was

5 – 10 times higher during 5e than any other parts of their investigated time interval. Such a correlation indicates increased surface productivity, possibly increased ventilation, resulting in increased carbonate preservation (Duplessy et al., 1988; Henrich, 1989; Nam et al., 1995), and reduced sea-ice cover (Kellogg, 1976, 1980). The finding of these regional studies do not correlate with the findings of HH13-089GC, where a drastic drop in the $\delta^{13}C$ record is seen during MIS 5e, indicating quite the contrary to the regional studies. As mentioned, the interpretation of 5e is uncertain due to the unusually low $\delta^{18}O$ measurement, and though low $\delta^{18}O$ values would be expected for the Eemian interglacial, which has been described to be very warm, it seems odd that it would correlate with such a drastic drop in the $\delta^{13}C$ record.

The very low sedimentation rates for this isotope stage seem to have resulted in reduced resolution. Because of this low resolution, it was not possible to recognize the remaining MIS 5 sub-stages by interpreting the isotope records alone. The benthic foraminiferal fauna did however provide some clues. One sample at 405 cm, included the stratigraphic biomarker for MIS 5a and 5e, *P. bulloides* (Haake and Pflaumnn, 1989), and correlated to a small peak in the $\delta^{18}O$ record. This is the only sample where *P. bulloides* is present, and its correlating $\delta^{18}O$ peak has been interpreted to represent MIS 5a due to its proximity to the MIS 5/4 boundary in the record. Lower sedimentation rates during MIS 5 was also seen by Nam et al. (1995) where it was interpreted to possibly be a result of decreased flow of terrigenous sediments into the Greenland Sea. The overall flux of coarser material, has been calculated for HH13-089GC, and is quite low for this time period (Figure 20).

The IRD record is fluctuating slightly within MIS 5. One major IRD peak at ~ 95 000 – 85 000 yrs. BP (425 – 410 cm) stands out as one of the highest peaks throughout the entire record. The peak correlates with higher $\delta^{18}O$ values, indicating colder climatic conditions, decreasing magnetic susceptibility values, the most prominent peak in the $\delta^{13}C$ record, and high relative abundance of the planktic foraminifera *N. pachyderma*, as well as a distinct low in the ΔSS record (Figure 24 and 25). As seen in the correlation with the NGRIP ice core in figure 22, this ΔSS drop correlates with a Greenland stadial, occurring just before GI 21. A large IRD peak was also seen during MIS 5 in core PS1730 from the local studies, where it was interpreted to possibly coincide with the MIS 5d, Aucellaelv stadial (Funder et al., 1998). It has in the present study however, been interpreted to represent MIS 5b, also known as the Jyllandselv stadial in Greenland studies. This interpretation is based on the approximate age of the IRD peak, and its proximity to the interpreted MIS 5a. The peak in IRD during this stadial, could indicate that glaciers in the area advanced as a response to the colder conditions and supplied the Greenland Sea with increased amounts of IRD (Funder et al., 1998). The lack of a high IRD signal for the Aucellaelv (5d) stadial was viewed as a problem in Funder et al. (1998). The Aucellaelv glacial advance has been described as a substantial advance in terrestrial studies form East Greenland, where the glacier probably extended over the Scoresby Sund fjord basin

(Lysså and Landvik, 1994). It is possible that the lack of such a peak in HH13-089GC is the result of lower resolution, and/or temperature drops, which inhibited IRD release.

The proxy records and comparison with other local and regional studies has allowed for a probable interpretation of sub-stages 5e, 5b and 5a. It is possible that MIS 5d and 5c is present in the $\delta^{18}O$ record as a small peak and drop respectively in between 5e and 5b (Fronval and Jansen, 1997), however due to the low resolution, it has not been possible to properly determine these sub-stages. The peak in ΔSS between ~ 82 000 – 71 000 yrs. BP has been seen to correlate with Greenland interstadials GI 21 – 19. The peak is sharp, whereas a more gradual decrease is seen towards the MIS 5/4 boundary, where the record drops to a low. (Figure 22 and 25)

The MIS 5/4 boundary at 375 cm was interpreted by a characteristic shift in the $\delta^{18}O$ and $\delta^{13}C$ records to higher and lower values respectively, and was found to have and age of ~ 70 500 yrs. BP. Just prior to the boundary is an interval barren of foraminifera. This interval occurs together with high $\delta^{13}C$ values and reduced total abundance of foraminifera, as well as a low P:B ratio. This could be an indication of dissolution.

6.3.3 MIS 4: 70.5 ka – 57 ka yrs. BP (core interval 375 – 340 cm)

Marine isotope stage 4 represents the Middle Weichselian glaciation, causing glacier advances in Greenland, however, evidence from this isotope stage is missing in terrestrial records from East Greenland (Funder et al., 1994; Stein et al., 1996). In southwest Greenland, some offshore results have indicated extensive glaciations during MIS 4 (Seidenkrantz et al., 2010; Funder et al., 2011). Based on the age model and the stable isotope stratigraphy for HH13-089GC, MIS 4 has been found to take place between ~ 70 500 – 57 000 yrs. BP (Figure 18).

MIS 4 was recognized by a significant drop in the $\delta^{13}C$ record, and slight increase in the $\delta^{18}O$ record, indicating a shift to colder climatic conditions. The oxygen isotope record was quite difficult to interpret for this interval, due to several fluctuations. The interpretation was therefore based on the minimum in the $\delta^{13}C$ record, which has been recognized as a well-known feature for MIS 4 in the northwest Atlantic (e.g. Haake and Pflaumann, 1989; Labeyrie and Duplessy, 1985).

Two ΔSS peaks are seen during this interval, which have been found to correspond to Greenland interstadials GI 18 and GI 17 – 16 respectively. The ΔSS drop in between these two peaks (~ 64 600 – 68 500 yrs. BP) could possibly be related to Heinrich Event 6 (H6) (Figure 22 and 25) (Heinrich, 1988; Bond et al., 1992; Bond et al., 1993), though the peak in the IRD record during this time is very small. The event correlates with a larger drop in the magnetic susceptibility record, a smaller drop in

the $\delta^{18}O$ record, a drop in the relative abundance of the planktic foraminifera *N. pachyderma*, and the major drop in $\delta^{13}C$. Cores from other studies in the GIN-Seas (Bond et al., 1993; Rasmussen et al., 1999; Rasmussen and Thomsen, 2014) have found very low $\delta^{18}O$ and $\delta^{13}C$ values to be typical for H6. The drop in the relative abundance of *N. pachyderma* seen in HH13-089GC at the same time, could be explained by decreased surface productivity, as indicated by the very low $\delta^{13}C$ values (Bond et al., 1992). These low vales could also indicate sea ice cover, which could be an explanation of the low flux of IRD during MIS 4. In the local study by Nam et al. (1995), a decreased influx of coarse grained terrigenous material was also seen during this isotope stage. An extensive sea ice cover which prevented iceberg drift was described as the possible explanation of the low influx. The dominance of the benthic foraminifera *O. umbonatus* within HH13-089GC, especially towards the end of MIS 4 and low sedimentation rates could also indicate the presence of sea ice.

Rasmussen et al. (1996a) found their interpreted Heinrich Events from the Faeroe margin to generally correlate with smaller increases in the presence of *N. pachyderma*, which contradicts the findings for at least H6 from HH13-089GC. The P:B ratio during this event drops, which could be an indication of increased dissolution. However, the total abundance of both benthic and planktic foraminifera is high during this event. The drop of *N. pachyderma*, together with an increase in the relative abundance of sub-polar species, could indicate subsurface warming beneath a layer of cold, fresh and sea-ice rich Polar Water.

The benthic foraminifera *C. wuellerstorfi* is present in HH13-089GC within this interval in smaller numbers, as was also recorded during MIS 4 in the study by Streeter et al. (1982) and Rasmussen et al. (1996b). *C. wuellerstorfi* was however absent during MIS 4 within all cores from the previously studied Scoresby Sund transect (Nam et al., 1995; Stein et al., 1996; Funder et al., 1998). They have also found the interval to correspond with higher $\delta^{13}C$ values than those found for HH13-089GC. Just prior to- and after Heinrich Event 6, there is a high relative abundance of the benthic foraminifera *S. loeblichi*. This species has been known to indicate higher productivity, and occurs together with increased $\delta^{13}C$ values. *S. loeblichi* was considered an important accessory species in MIS 4 in the study from the eastern North Sea by Knudsen (1984).

Approaching the MIS 4/3 boundary (~ 57 000 yrs. BP), an interval barren of foraminifera is seen. Poor preservation of the foraminiferal tests was also seen in some of the samples just prior to this interval. This could be a result of perennial sea ice coverage (Chauhan et al., 2014).

6.3.4 MIS 3: 57 ka – 28.8 ka yrs. BP (core interval 340 – 175 cm)

Marine isotope stage 3 also represents Middle Weichselian, and is known from Greenland studies as the beginning of the Flakkerhuk stadial (e.g. Lysså and Landvik, 1994; Funder et al., 1998; Elverhøi et al., 1998). Optically Stimulated Luminescence datings from terrestrial studies have indicated that glaciers in the Scoresby Sund area showed massive advances, and had come close to their last glacial maximum extent by ~ 60 000 yrs. BP (Hansen et al., 1999). The glacier occupying the Scoresby Sund fjord system and surrounding margin, seem to have been cold based (Funder et al., 1998). The oxygen isotope stratigraphy and the age model for HH13-089GC, suggests an approximate age span for MIS 3 between ~ 57 000 – 28 800 yrs.

The beginning of MIS 3 was recognized in core HH13-089GC by a small shift in the $\delta^{18}O$ records, lower $\delta^{13}C$ values, drastic increase in magnetic susceptibility, and increasing sedimentation rates. The sedimentation rates reach an absolute maximum within MIS 3, which has also been seen for MIS 3 in other studies from the GIN-Seas (e.g. Rasmussen et al., 1996b; Haake and Pflaumann, 1989; Nam et al., 1995). The high sedimentation rates provide higher resolution for this isotope stage. The very high increase in magnetic susceptibility indicates deposition form a source area high in ferromagnetic and/or paramagnetic minerals (Grousset et al., 1993). IRD rich deposits with volcanic components can also have high magnetic susceptibility, however, the peaks in IRD within MIS 3 do not correlate with peaks in magnetic susceptibility. Magnetic susceptibility has also been found to correlate with bottom current activity, which I will come back to later. The low $\delta^{13}C$ values in the beginning of this interval could indicate a period of increased sea ice cover in the area. The benthic foraminiferal fauna is dominated by *O. umbonatus* during the early- to mid MIS 3. The highest relative abundance of this species is seen to correlate with the low $\delta^{13}C$ values at the beginning of the interval, which could also indicate increased sea ice cover (Chapter 4.2.1). The occurrence of *C. wuellerstorfi* in small numbers only within MIS 3 could also be an indication of pack ice conditions (Haake and Pflaumann, 1989).

The whole of MIS 3 shows generally lower, but highly fluctuating $\delta^{18}O$ values, higher $\delta^{13}C$ values, which could indicate increased ventilation of the subsurface waters, repeated peaks in the IRD concentration, a slight overall decreasing trend in the relative abundance of the planktic foraminifera *N. pachyderma* and a highly fluctuating ΔSS and magnetic susceptibility record (Figure 24 and 25). The flux of foraminifera, IRD and other coarse grained fractions increase substantially within MIS 3 (Figure 20). The total abundance of planktic foraminifera (No. Planktic forams/g dry weight sediment) is lower than MIS 4 and 5 in general, with a decreasing trend throughout the interval. This was also seen in the early MIS 3 by Nørgaard-Pedersen (1997). The higher peaks in $\delta^{13}C$ in mid- to late MIS 3, could indicate that MIS 3 experienced several relatively ice-free periods, where the productivity increased.

Marine isotope stage 3 has been found to include Greenland Interstadials GI 15 – 4 (Figure 25), and three so called Bond cycles (Chapter 1.2.3.1), ending in Heinrich Events 5 – 3 respectively (Figure 24 and 25) (Heinrich, 1988; Bond et al., 1992). All Greenland Interstadials correlate with peaks in the ΔSS and magnetic susceptibility records, whereas the Heinrich Events correlate with drastic drops in ΔSS and magnetic susceptibility, small ^{18}O depletions, and peaks in the IRD concentration (Figure 24 and 25). Peaks in the IRD record during MIS 3, occur only in direct correlation with Heinrich Events, and is otherwise non-existent. Larger drop stones are also found to correlate with H4 and H3. Heinrich Events H5 (~ 48 400 – 46 300 yrs. BP), H4 (~ 41 000 – 37 800 yrs. BP) and H3 (~ 31 000 – 29 900 yrs. BP) occur between GI 13 and GI 12, between GI 9 and GI 8, and between GI 5 and GI 4 respectively. The small ^{18}O depletions indicate decreased salinities due to the input of freshwater during these events (e.g. Bond et al., 1992, 1993; Labeyrie et al., 1995; Vidal et al., 1997; Cortijo et al., 2000; Prins et al., 2002). The Heinrich Events identified within MIS 3 is well dated within the North Atlantic, and the ages proposed for these events by the presented age model, are very similar to those in previous studies (Bond et al., 1993; Bond and Lotti, 1995; Vidal et al., 1997; Vidal et al., 1999; Knies et al., 2001; Hemming, 2004; Rasmussen et al., 2014).

Nam et al. (1995), Stein et al. (1996) and Funder et al. (1998) also found low $\delta^{13}C$ values in the beginning of MIS 3 for the deep marine slope core PS1730. These values were interpreted to be the result of meltwater discharge which caused reduced CO_2 exchange between surface water and atmosphere (Sarnthein et al., 1995; Voelker et al., 1998; Funder et al., 1998). IRD concentrations were increased, as well as the magnetic susceptibility. The MS record for this core showed a striking resemblance to that of HH13-089GC, especially during MIS 3 (Figure 30). Since MIS 3 is very different from the other isotope stages for both core HH13-089GC and PS1730 when it comes to magnetic susceptibility, a change in the material source area and rock composition could be an explanation, although this would need to be investigated further.

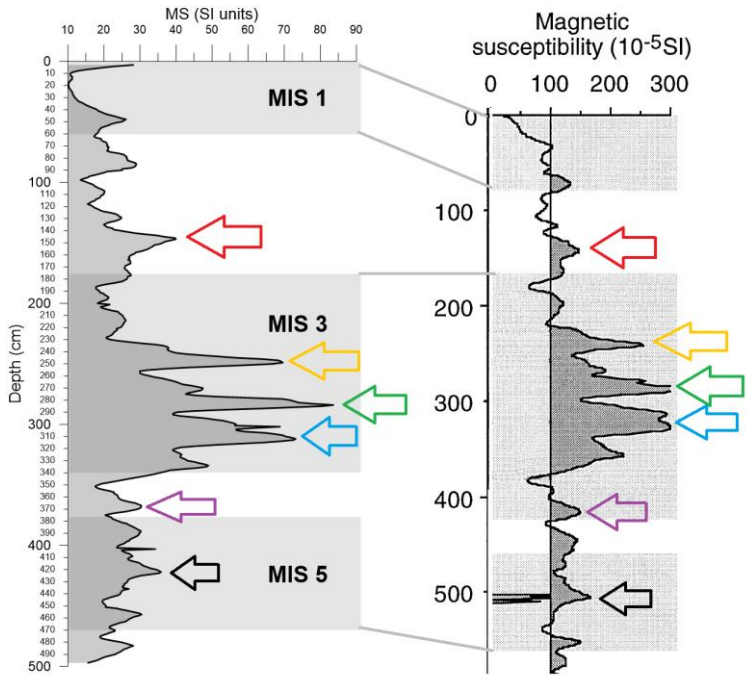

Figure 30: *Pattern matching between the magnetic susceptibility curves for cores HH13-089GC* ***(left)*** *and PS1730* ***(right)*** *(Right figure is from Funder et al., 1998, modified by author). Both cores are from the East Greenland continental slope and similar water depths. Marine isotope stage definitions are similar, except for MIS 4 which has been placed lower in PS1730. Coloured arrows show correlating peaks.*

The local studies found it difficult to determine if their IRD peaks correlated with the North Atlantic Heinrich Events. The increased IRD concentrations were found to either signify advancing glacier fronts, or the beginning of a period with reduced sea-ice cover (Funder et al., 1998). It is possible that difficulties with correlations would have been the case for the present study as well, if it was not for the sortable silt analysis, which provided the clearest corresponding signal with the Greenland ice cores.

Highly fluctuating values in the isotope records in the Nordic Seas is a typical trait for marine isotope stage 3 (Bond et al., 1993; Dokken and Hald, 1996, van Kreveld et al., 2000; Vogt et al., 2001; Rasmussen et al., 2014). Other studies from the North Atlantic and Arctic oceans have recorded higher IRD content and low presence of planktic foraminifera in the early parts of MIS 3, which has been interpreted to possibly represent increased presence of sea ice due to the retreat of the Eurasian Ice Sheet (Dokken and Hald, 1996; Nørgaard-Pedersen, 1997; Hebbeln, 2000; Chauhan et al.., 2014). Heinrich Events have been recorded throughout the North Atlantic, and the events of MIS 3 (H5, H4 and H3) has all been found to correlate with drops in the $\delta^{18}O$ record, as they do in the present study as well (Bond et al., 1992, 1993; Grousset et al., 1993).

6.3.5 MIS 2: 28.8 ka – 14.3 ka yrs BP (core interval 175 – 60 cm)

The Flakkerhuk stadial continues into marine isotope stage 2. The Last Glacial Maximum (~ 26 500 – 19 000 yrs. BP) occurs during this stage, as does the beginning of the last deglaciation (~ 19 000 yrs. BP). During the LGM, grounded glacial ice filled the entire Scoresby Sund fjord system, all the way out to the fjord mouth, which is probably represented by the Kap Brewster moraine ridge (Dowdeswell et al., 1994; Nam et al., 1995). Sea ice may have extended even farther out onto the shelf (Dowdeswell et al., 1994; Mangerud and Funder, 1994; Funder et al., 1998), though the complete extent of the ice sheet during this time has been debated. The Greenland Ice Sheet extent during the LGM has been modelled several times (e.g. Simpson et al., 2009; Lecavalier et al., 2014), and although uncertain, the figure below provides an image of the massive glacial advances which took place across Greenland during this time.

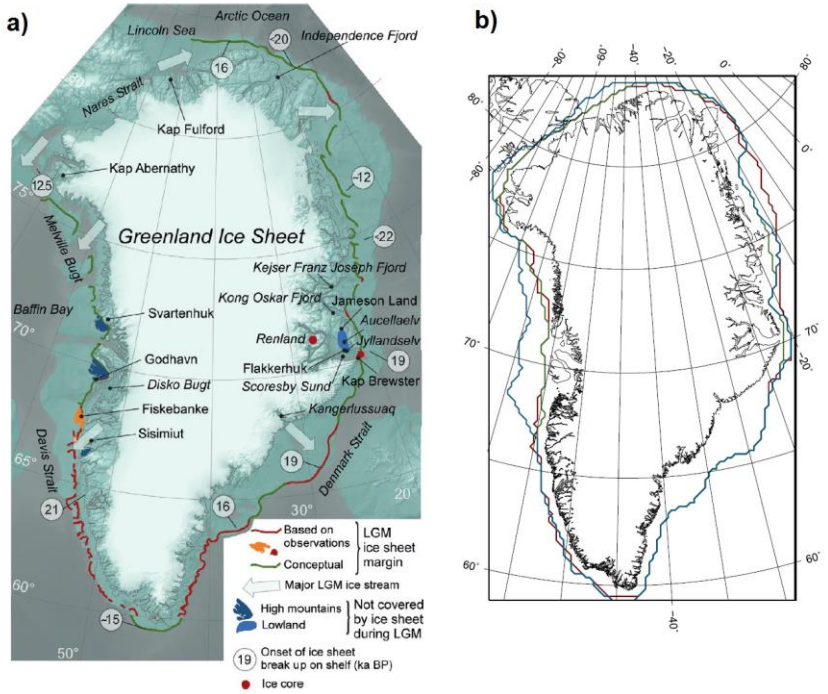

Figure 31: a) *Reconstructed LGM ice sheet margin, ice flow, dates for break-up of shelf bound ice (figure from Funder et al., 2011).* ***b)*** *Three LGM ice extents: Huy2 model (red) (Simpson et al., 2009), Funder et al. (2011) extent (green), and the revised Huy3 model (blue) (figure from Lecavalier et al., 2014).*

Marine isotope stage 2 has been identified in the HH13-089GC record by a clear shift in the stable oxygen isotope record from generally low values to high values (> 4 ‰). Only the very bottom of the core, representing the Saalian glaciation, shows higher $\delta^{18}O$ values than MIS 2 (Figure 24 and 25). The isotope stage was easily recognized in the isotope record, though the upper boundary (MIS 2/1) needed to be adjusted slightly after the results of the AMS-dating arrived, and the age model was completed (Figure 18). The MIS 3/2 boundary (~ 28 800 yrs. BP) is located just at the transition between Heinrich Event 3, and the Greenland Interstadial GI 4 at ~ 175 cm, whereas the upper

boundary (~ 14 300 yrs. BP) is located near the peak of GI 1 at ~ 60 cm (Figure 24 and 25). The samples near the MIS 2/1 boundary contain foraminifera of poor quality, or are barren.

In addition to the higher $\delta^{18}O$ values, the overall interval is represented by decreased magnetic susceptibility, in relation to MIS 3, a fluctuating ΔSS record, the two largest peaks in the IRD record, relatively low $\delta^{13}C$ values, high sedimentation rates, a highly fluctuating relative abundance record for the planktic foraminifera *N. pachyderma*, and a clear dominance of *C. neoteretis* in the benthic faunal records. *Cibicides wuellerstorfi* begins to reappear as a dominating benthic species towards the end of the isotope stage. The high sedimentation rates within MIS 2 provide high resolution within the ΔSS record, as seen by the very prominent GI 4 and GI 3 for example.

The total abundance of benthic foraminifera (No. Benthic forams/g dry weight sediment), in addition to the flux records for planktic foraminifera, benthic foraminifera, IRD and coarser sediment all reach a maximum within MIS 2. The benthic flux peaks at the beginning of the interval, whereas the planktic flux peaks just prior to the first drastic drop in the ΔSS record. This major drop (~ 140 cm) was dated to 24 853 cal. yrs. BP, and has based on this age, the correlation with the NGRIP ice core (Figure 22) and the other proxy records (Figure 24 and 25), been interpreted to represent Heinrich Event 2 (Bond et al., 1993). Another drop in the ΔSS record is seen at ~ 100 cm, and has been found to represent Heinrich Event 1, with an estimated age of ~ 20 400 – 18 500 yrs. BP. These events have been interpreted due to their obvious correlation with some of the largest Greenland Stadials, in addition to massive peaks in IRD concentration, indicating iceberg release, and small ^{18}O depletions, indicating an increased input of freshwater at the surface for core HH13-089GC. Larger drop stones are also found to correlate with H2. The events continue to be associated with decreasing or low magnetic susceptibility, which now seems to be a trend for all the interpreted Heinrich Events in the core. Heinrich Events H2 and H1 (Heinrich et al., 1988; Bond et al. 1992, 1993) also correlate with small peaks in the relative abundance of *N. pachyderma*, and small drops in the $\delta^{13}C$ record (Figure 24 and 25).

The Last Glacial Maximum is believed to occur in HH13-089GC between ~ 140 – 90 cm (~ 24 800 – 18 500 yrs. BP). The two Heinrich Events H2 and H1 occur before and after the LGM respectively. The increased flux of IRD and the coarser fractions, could be indications of LGM. Several studies describe the presence of massive land-based ice sheets in the northern hemisphere, and the extent of the sea ice margin reaching a maximum during the LGM (e.g. CLIMAP, 1981; Kellogg et al., 1978; Kellogg, 1980; Lambeck et al., 2002). Following what is interpreted to be the LGM, is H1. The IRD record decreases gradually, as the $\delta^{18}O$ record gradually shifts towards lighter values. This indicates increased presence of meltwater and warmer climatic conditions, and has been interpreted to represent the early deglaciation phase. The $\delta^{18}O$ shift occurs in HH13-089GC at about 90 cm, which has an

approximate age of ~18 500 yrs. BP. This is "spot on" in relation to the indicated beginning of the deglaciation in the Scoresby Sund area by previous studies (~ 19 000 yrs. BP) (e.g. Stein et al., 1996; Evans et al., 2002).

Distinct increases in IRD during MIS 2 has also been seen in the local studies from the area (Nam et al., 1995; Stein et al., 1996; Funder et al., 1998). The high input of IRD during this stage was interpreted to be a result of increased calving rates and iceberg drift from glaciers due to extensive glacial conditions on Greenland (Nam et al., 1995). Maximum fluxes of coarse-grained material in their cores, occurred in the interval interpreted to represent the LGM within HH13-089GC. Funder et al. (1998) described a maximum extension of the East Greenland glaciers, causing increased iceberg discharge into seasonally open coastal waters during this time. The distinct IRD peaks during MIS 2 in the local studies was not tied to any Heinrich Events, though two of these major peaks in core PS1730 correlate with the interpreted H2 and H1 in the present study.

In their comparison between the IRD record and magnetic susceptibility for core PS1726, it seems a correlation between the IRD peaks and high magnetic susceptibility was expected. They did however find, that this was not always the case, and mentioned changes in the IRD source area over time as a possible reason for it (Stein et al., 1996). Correlations between IRD peaks and low magnetic susceptibility is certainly the trend for the present study. Higher carbonate values were found for MIS 2 in all long cores investigates in the local studies (Nam et al., 1995).

In the study by Chauhan et al. (2014) from the Southern Yermak Plateau, near the Fram Strait, it was reported that open water conditions at the MIS 3/2 transition could have led to the growth of terrestrial ice sheets due to increased evaporation. Increased evaporation would have led to depletion of ^{16}O within the sea water, causing heavier $\delta^{18}O$ values within MIS 2. A similar signal is seen in the isotope record, and the high but decreasing $\delta^{13}C$ values at the MIS 3/2 transition indicates a shift from relatively ice free conditions to ice cover. The increased evaporation explanation could possibly be valid for the East Greenland as well. They also reported high fluxes of both planktic and benthic foraminifera, a dominance of the benthic species *C. netoretetis*, and a prominent IRD peak between 25 000 – 22 000 yrs. BP. This peak has been described to be the result of massive iceberg discharge of the Svalbard-Barents Sea Ice Sheet (SBIS) (e.g. Vogt et al., 2001). The massive IRD peak in HH13-089GC, representing H2 correlates with the IRD peak from the SBIS iceberg discharge. Studies from other areas in the North Atlantic such as the Labrador Sea, Norwegian Sea and the Faeroe margin, have found evidence for Heinrich Event H2 and H1 during the same time (e.g. Nave et al., 2007), indicating massive simultaneous discharge of iceberg from different sources within the North Atlantic.

6.3.6 MIS 1: 14.3 ka yrs. BP – present (core interval 60 – 0 cm)

The deglaciation continues into marine isotope stage 1, which represent the Holocene. The ice sheet receded from the its maximum position at different times for different Greenland areas, though southern Greenland and Scoresby Sund were amongst the first areas to become ice free (Funder et al., 2011). Ice free conditions on the continental shelf in the investigated area was probably reached around ~ 12 400 yrs. BP (Hall et al., 2008; Kelly et al., 2008). A marine transgression followed the retreat of the glaciers during the deglaciation (Funder et al., 1998).

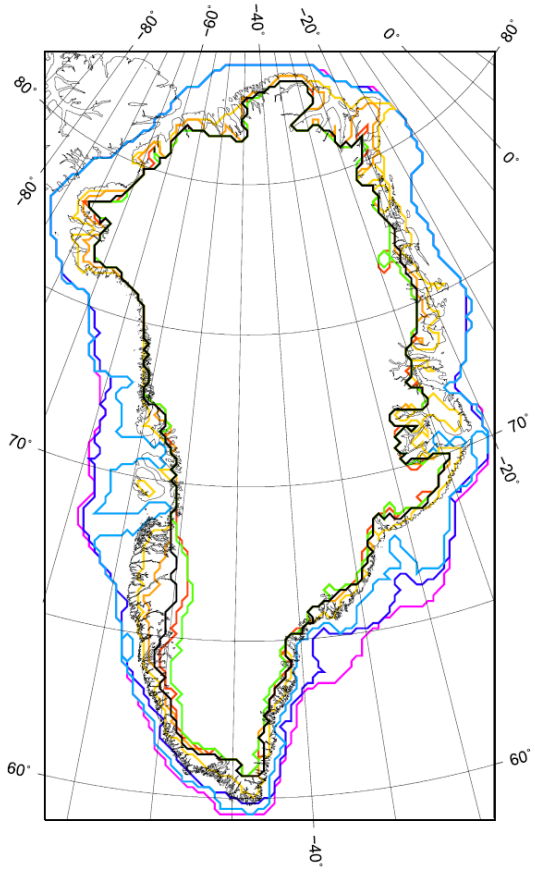

Figure 32: *Showing the chronology of lateral ice extent in Greenland from the Huy3 model (16 ka BP – **pink**; 14 ka BP – **dark blue**; 12 ka BP – **light blue**; 10 ka BP – **yellow**; 9 ka BP – **orange**; 6 ka BP – **red**; 4 ka BP – **green**; present-day – **black**). (Figure from Lecavalier et al., 2014)*

The MIS 2/1 boundary was identified based on the shift in the $\delta^{18}O$ record, the age model, and an ash layer which was interpreted to be the Vedde Ash. Lower values of $\delta^{18}O$ (< 4 ‰) just above the MIS 2/1 boundary indicates warmer conditions and are possibly related to large local meltwater flow during the deglaciation. The shift in $\delta^{18}O$ values is seen at approximately 90 cm (within MIS 2), but the age model suggests that the MIS 2/1 boundary is located at ~ 60 cm depth with an age of approximately 14 300 yrs. BP. This location is also marked by a drastic decrease in the amount of

IRD, which may be an indication of increased water temperatures, which could make IRD transportation to the slope difficult.

This upper core interval includes Greenland Interstadial GI 1, which is represented by the last major peak in ΔSS. This interstadial correlates with an interval that is completely barren of foraminifera, creating a gap in the isotope and foraminiferal records, and overall low magnetic susceptibility, which thereby separates it from the other interstadials in the record. Lower magnetic susceptibility was found for the Bølling-Allerød interstadials in the study by Rasmussen et al. (1996a), which has provided the basis for the interpretation of these interstadials within the HH13-089GC record at ~ 15 000 – 12 900 yrs. BP (65 – 50 cm) (Figure 24 and 25). This interstadial also correlates with a small peak in the IRD record, and possibly low $\delta^{18}O$ values (Grousset and Duplessy, 1983). Marienfeld et al. (1992), suggested that glacier ice filled the entire Scoresby Sund fjord system at the beginning of B-A, gradually retreating into the inner fjords (Figure 33a), though it has been questioned (e.g. Dowdeswell et al., 1994). The suggested age for the B-A interstadials is slightly older than the date of 13 400 yrs. BP by Karpuz and Jansen (1992), however it is similar to the age presented in Björck et al. (1998) of ~ 14 700 – 12 650 GRIP yrs. BP. Marienfeld et al. (1992) described the Allerød to be the first period of deglaciation, and that it ended about 11 000 yrs. BP in the Scoresby Sund region. This age is younger than the age for the interpreted B-A interval in HH13-089GC, and it is possible that the interpretation needs to be adjusted slightly. However, due to the gap in the $\delta^{18}O$- and $\delta^{13}C$ record and the foraminiferal records, the interpretation could only be made based on the ΔSS and magnetic susceptibility records.

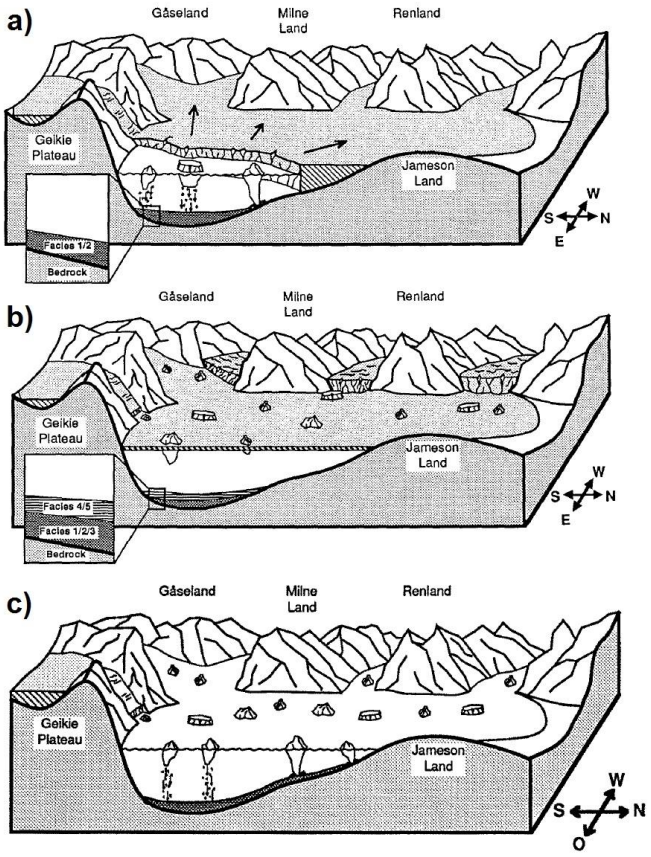

Figure 33: (a) *Depositional model for the Bølling-Allerød interstadials, where glacier ice filled the fjord system, gradually retreating towards the inner fjords. (note that the extent of glacier ice has been questioned).* ***(b)*** *Depositional model for the Younger Dryas cold event, where glaciers terminated near the mouths of the smaller fjords in the western fjord system, and a substantial sea ice cover was formed.* ***(c)*** *Near present day. (Figure a and b from Marienfeld et al., 1992, figure c from Stein et al., 1993).*

The small drop in the ΔSS record at ~ 12 900 yrs. BP (50 cm) which follows the B-A, correlates with a drastic decrease in IRD concentration, and could possibly represent the onset of the Younger Dryas cold event. Investigations from the Scoresby Sund fjord system has indicated that the climatic shift was abrupt, and that the glaciers in Scoresby Sund terminated near Milne Land, where several smaller fjords come together (Figure 33b) (Marienfeld et al., 1992). The formation of an increased sea ice covered, reduced iceberg drift, and the deposition of fine grained laminated sediment, barren of microfossils and IRD have been found to be the result of the ice cover (Marienfeld et al., 1992; Dowdeswell et al., 1994). This seem to correlate well with the HH13-089GC record, where a drastic decrease in coarse grained material is seen between 70 – 50 cm (~ 15 700 – 12 900 yrs. BP) together with gaps in the isotope and foraminiferal records. Dowdeswell et al. (1994) found that not all cores investigated were barren of foraminifera during this interval, and questioned whether the sea ice cover was completely closed. Following the YD, IRD > 1 mm is still very low, however there is an increase

in the fine-medium sand fraction, and IRD > 500 μm. Marienfeld et al. (1992) also reported increased presence of coarse grained materials following the YD.

The ΔSS record drops substantially after the YD, and this is the only part of the record where the ΔSS and the NGRIP isotope records do not correlate. It is possible that the upper parts of the Holocene are not reached within the HH13-089GC record, and that the larger drop in the ΔSS record, is the drop which corresponds with the Younger Dryas. This seems unlikely though due to the correlation between the core results, and results from other local studies for both B-A and the YD event (e.g. Marienfeld et al., 1992). Several pieces of evidence in the HH13-089GC record suggests that the initial interpretation is correct. The AMS-date at 30 cm, gave an age of 7474 yrs. BP, which is younger than the ages found for the Younger Dryas event in previous studies (~ 12 800 – 11 700 yrs. BP). The approximate age found for the interpreted YD event, and the Vedde Ash (~ 12 200 cal. yrs. BP) which has been described to represent a mid-Younger Dryas event (e.g. Nam et al., 1995), also falls within the interval from previous studies. Following the interpreted Younger Dryas, is a drastic increase in the $\delta^{13}C$ record, which indicate high surface productivity, and possibly ice free conditions. The shift occurs at ~ 12 200 yrs. BP (45 cm), and according to previous studies, ice free conditions in the area would have been reached by this time (Hall et al., 2008; Kelly et al., 2008). The benthic foraminifera *O. umbonatus* is the most dominant species during MIS 1. As this species is one of the most common benthic deep-sea species in the modern GIN-Seas, its dominance is most likely an indicator for climatic conditions that are similar to present day. The benthic species *C. wuellerstorfi* occurs in higher numbers within the uppermost parts of the core, also indicating ice free conditions. The relative abundance of *N. pachyderma* decreases quite drastically within the upper 35 cm, which may indicate warmer surface/near surface water temperatures. The presence of agglutinated foraminifera within the uppermost samples, could also indicate that the core top represents the present.

Following the Younger Dryas, the glaciers in the Scoresby Sund region retreated drastically by calving, causing increased ice rafting. It is possible that the low amounts of IRD recorded in the slope cores PS1726, PS1730 and HH13-089GC during this time reflects conditions where IRD was deposited in the fjord or on the shelf, never reaching the slope. The shelf cores investigated by Nam et al. (1995) and Stein et al. (1996) did not seem to have higher IRD content within MIS 1, and it is possible that most of the IRD was deposited within the fjord system, as described by Marienfeld et al. (1992). The decline in IRD during MIS 1 was believed by Nam et al. (1995) to be a response to either glacier retreat or permanent sea-ice cover. However, due to the increased surface water productivity observed during this time, the low IRD content was also found to be connected to glacial retreat (Nam et al., 1995).

In addition to a decrease in the amount of IRD, the nearby slope cores (PS1726 and PS1730) also saw low $\delta^{18}O$- and high $\delta^{13}C$ values during MIS 1. Even lower $\delta^{18}O$ values were seen in cores from the inner continental shelf, which indicated a higher influence of meltwater. Overall, they found that the $\delta^{18}O$ and $\delta^{13}C$ signals in most of their cores resembled the global deep sea pattern, which at the time was based on Martinson et al. (1987). The pattern for the slope cores however, was found to be deviating from the global signal in several places. These deviations were believed to indicate overprint by local signals such as meltwater events and diagenetic alteration of the isotope signal (Nam et al., 1995). Their magnetic susceptibility reading was the lowest throughout the cores, which is also the case for the interval between ~ 8800 – 2500 yrs. BP (35 – 10 cm) in HH13-089GC. The ash layer found within MIS 1, was also seen in the local cores at similar depths. It was also interpreted to correspond to the Vedde ash (Nam et al., 1995; Stein et al., 1996).

Samples barren of foraminifera within MIS 1 have been observed in other studies from the North Atlantic as well (e.g. Nørgaard-Pedersen, 1997; Chauhan et al., 2014), and was described to indicate poor carbonate preservation, or the result of re sedimentation. In their study from the southern Yermak Plateau, Chauhan et al. (2014) found barren samples and increased IRD content within the very top of their core. This is not the case for HH13-089GC, though there seems to be a slight increase in IRD in the uppermost sample, and the foraminiferal tests were poorly preserved and highly fragmented. In the study from the Faeroe Margin, Rasmussen et al. (1996a) did not find barren samples within the Holocene, however the preservation of the foraminiferal tests was only moderate.

6.4 Paleoceanographic implications

6.4.1 Foraminiferal record

The foraminiferal planktic and benthic faunal assemblages of core HH13-089GC vary over time, and the ecology of the different species present can be an indication for paleoceanographic changes in the past. Increased influence of warmer surface and subsurface waters, ice cover, surface productivity and nutrient supply, current activity, changes in the Polar- and Arctic Front are amongst the paleoceanographic characteristics which can be reflected in the foraminiferal fauna.

It is important to remember that the overall content of benthic foraminifera was quite low, and that the faunal composition presented here is only an approximate estimation. In order to get a clearer image of the faunal compositions, larger sample material would have been needed for quantification in certain intervals of foraminiferal concentration.

6.4.1.1 MIS 6: > 130 ka yrs. BP (core interval 497 – 470 cm)

The bottom interval of the core (497 – 470 cm) is dominated by the planktic species *N. pachyderma* (Figure 9). The presence of this species in the overall record represents cold surface or near surface water conditions of the EGC. As it has been found to live close to the transition between the cold surface Polar Water (PW) and the Atlantic Intermediate Water (AIW), changes in its relative abundance could be related to increased influence of AIW, or a response to other changes in the near-surface environment.

The benthic foraminiferal record (Figure 10 and 11) of MIS 6 is dominated by *S. loeblichi*, *C. reniforme* and *C. neoteretis*. *Melonis barleeanus* acts as an accessory species at the very bottom of the core. *Stainforthia loeblichi* is considered an opportunistic species that can be an indicator of high productivity at the sea surface (Chapter 4.2.6). The $\delta^{13}C$ values at this time however is very low, possibly indicating reduced productivity and surface ventilation. *C. reniforme* and *C. neoteretis* are under modern conditions common in areas that are under the slight influence subsurface Atlantic Water, distal to glaciers (Polyak et al., 2002). The bottom environment at the sampling site off East Greenland is under modern conditions influenced by cold and dense Greenland Sea Bottom Water, and the dominance of these species may therefore have a different explanation. In addition to thrive in temperate waters, both species are also found in areas affected by cooler water masses. *Cassidulina neoteretis* is found to be associated with sandy or muddy sediments on the continental shelves and slopes of the North Atlantic (Chapter 4.2.2), whereas *C. reniforme* is usually related to glaciomarine shelf and slope environments, and is often related to the Arctic benthic foraminiferal fauna (e.g. Mudie et al., 1984; Hald and Vorren, 1987; Seidenkrantz et al., 1995; Wollenburg et al., 2001). It thrives

within muddy, sediment loaded waters near calving glaciers, and under variable salinity conditions (Chapter 4.2.4). Due to the short core span of MIS 6, it is difficult to infer what their presence indicates at this time. *Melonis barleeanus* is often found in areas with buried organic material (e.g. Polyak et al., 2002), which could be indicated by the low $\delta^{13}C$ values, suggesting increased oxidation of organic matter.

Close to the MIS 6/5 transition, a shift in the faunal composition is seen, and *O. umbonatus* begins to dominate. The species has been found to be related to increased sea ice cover, and to be more adaptable to reductions in surface productivity (Chapters 4.2.1). The species peaks as climatic conditions are changing from cold to warmer, and surface productivity seems to increase. As the period still represents the end of the Saalian glaciation, it is possible that larger amounts of sea ice were present at the time.

6.4.1.2 MIS 5: 130 ka – 75 ka yrs. BP (core interval 470 – 375 cm)

The planktic foraminiferal record continues to be dominated by *N. pachyderma* (Figure 9). The percentage of *N. pachyderma* shows one drop within this interval at ~ 445 cm. This drop correlates with the first distinct low in ΔSS. As *N. pachyderma* drops, *N. incompta* and *T. quinqueloba* increases slightly. *Neogloboquadrina incompta* is often present in small numbers within the relatively cold surface waters. This species has been found in regions of extreme polar conditions such as the central Arctic Ocean as well, but it is not certain if they represent sporadic hydrographic change, or if there are other reasons for their existence under these conditions (Bauch et al., 2003). *Neogloboquadrina incompta* generally has a relative abundance below 3 %, which could make it difficult to imply any paleoceanographic changes based on the presence of this species. As *N. pachyderma* drops, the relative abundance of *N. incompta* could possibly represent an increased influence of subsurface AIW. *Globigerinita glutinata* and G*lobigerinita uvula* are present in small numbers, and *G. bulloides* is present at ~ 450 cm only. All of these planktic species are related to warmer water masses, and their increased presence could therefore indicate the increased presence of such water masses (Haake and Pflaumann, 1989). Increased influence of AIW to this area could be a result of change in the depth of the PW/AIW interface. A slight vertical migration of AIW could cause a drop in the *N. pachyderma* record and an increase in the presence of *N. incompta* and *T. quinqueloba*. It is also possible that the warm AW that is transported with the North Iceland Irminger Current (NIIC) through the Denmark Strait, ran slightly farther north, thereby influencing the investigated area. The $\delta^{18}O$ values within MIS 5 is generally lower, however the drop of *N. pachyderma* occurs together with an increase in $\delta^{18}O$, and high $\delta^{13}C$ values. The increase in $\delta^{18}O$ at this point seems quite large, however it occurs after the uncertain measurement which probably makes it seem larger than it is. The higher $\delta^{18}O$ value could indicate a period where surface water is not as influenced by ^{18}O depleted meltwater.

Through MIS 5, the benthic foraminiferal record (Figure 10 and 11) is dominated by *O. umbonatus* and *C. wuellerstorfi*. The two species alternate within the interval; when the percentage of *O. umbonatus* is high, *C. wuellerstorfi* is lower and vice versa. As previously described, *O. umbonatus* prefers high oxygen content in the sediment, can tolerate low food supply, is adaptable to reductions in surface productivity and dominate during periods of increased sea-ice cover. *C. wuellerstorfi* on the other hand has almost the exact opposite preferences (Chapter 4.2.5). Based on their different preferences, the alternation of the two species is expected, considering that they are both epifaunal, and therefore represent the same surroundings. *Cibicides wullerstorfi* prefers increased surface productivities, which is reflected in the overall high $\delta^{13}C$ values. The maximum occurrence of this species within MIS 5 does seem to correlate with times where the overall $\delta^{18}O$ values are higher, however some slight drops are seen. The higher $\delta^{18}O$ values indicate warmer conditions in relation to those in MIS 6. The small drops in the planktic $\delta^{18}O$ record could indicate decreased presence of meltwater at the surface, rather than colder surface temperatures. The ΔSS values of MIS 5 are low, and probably related to reduced bottom current activity, and maybe also reduced convection in the GIN-Seas, however I will come back to this in the last chapter of this discussion. *C. wuellerstorfi* is generally present during times of increased current activity, so the high productivity is probably the factor which controls its dominance during MIS 5. The presence of *C. neoteretis* and *C. reniforme* have been reduced drastically, and they now occur as accessory species together with *T. trihedra*. These species gradually increase towards the MIS 5/4 boundary, whereas *C. wuellerstorfi* decreases drastically. Other benthic species only occur sporadically within this interval.

6.4.1.3 MIS 4: 70.5 ka – 57 ka yrs. BP (core interval 375 – 340 cm)

Rasmussen et al. (1996a) found Heinrich Events to correlate with smaller increases in the presence of *N. pachyderma*. This is not the case for the interpreted H6 within the present core, where the relative abundance of *N. pachyderma* drops relatively drastically at the point of the event, and is accompanied by a large peak in the planktic species *N. incompta*, and a small peak in *T. quinqueloba*. The total relative abundance of planktic foraminifera increases during the event, so the lower presence of *N. pachyderma* is probably a result of warmer near-surface waters, as the surface waters would probably be quite cold and fresh as a result of the melting event; indicated by ^{18}O depletion in the $\delta^{18}O$ record. Following the event is a strong increase in the relative abundance of *N. pachyderma* at 355 – 340 cm together with relatively high $\delta^{18}O$ values (~ 3.75 ‰). This could suggest the presence of surface Polar Water (Chauhan et al., 2014), and reestablishment of colder surface and subsurface conditions. Accessory planktic species are generally absent during MIS 4.

At the MIS 5/4 boundary, the benthic foraminifers *C. neoteretis* and *C. reniforme* are quite high, showing a gradual decrease into MIS 4. Their relative abundances are still quite high during H6. *Oridorsalis umbonatus* shows a large drop during this event, but quickly recovers and reaches 80 % towards the MIS 4/3 boundary. The dominance of *O. umbonatus*, especially towards the end of MIS 4 could indicate the increased presence of sea ice in the area. At either side of the Heinrich Event, *S. loeblichi* accounts for ~ 35 % of the identified fraction. This indicates increased surface productivity, which is also inferred by the higher $\delta^{13}C$ values just before and after the event. *Triloculina trihedra, A. gallowayi* and *C. wuellerstorfi* acts as secondary species, whereas *E. excavatum, E. arctica, M. barleeanus* and *C. lobatulus* are accessory species. The presence of *A. gallowayi* together with *C. lobatulus* is often an indication of a high energy environment (Chapter 4.2.8), they occur during Greenland Interstadial 18 and GI 17 where sortable silt values are very high, but is absent during H6 where the ΔSS values are low. The occurrence of C. wuellerstorfi in small numbers could also indicate increased bottom current activity. Sortable silt is known to be a proxy for paleocurrent activity, and its peaks indicate a high energy environment. *Epistominella arctica* is a species which takes advantage of short, local pulses of increased productivity. The presence of this species in MIS 4 could therefore be an indicator for sea-ice cover, which breaks up now and then to give abrupt blooms of phytoplankton (chapter 4.2.9).

6.4.1.4 MIS 3: 57 ka – 28.8 ka yrs. BP (core interval 340 – 175 cm)

The relative abundance record for *N. pachyderma* is high and fluctuating during MIS 3, but there seems to be an overall decreasing trend in the interval, whereas the relative abundance of *N. incompta* increases. The percentage of *T. quinqueloba* is low in the beginning of the interval, but begins to peak above 250 cm where *N. pachyderma* percentages are relatively low. The relative abundance of the accessory planktic species increases above 250 cm, especially *G. bulloides*. This faunal composition has been described from the South-eastern Greenland shelf, and could be related to a nearby presence of the Polar Front (Andersen et al., 2012).

The benthic fauna is dominated by *O. umbonatus*, which gradually decreases into MIS 3. *Oridorsalis umbonatus* seems to decrease drastically when sedimentation rates reach a maximum. This is similar to the findings of Haake and Pflaumann (1989). The trend is opposite for *C. neoteretis* which gradually increases in relative abundance towards the MIS 3/2 boundary. The species reaches its maximum relative abundance at 205 cm (32 200 yrs. BP), just prior to Heinrich Event H3. In relation to the glacial history of East Greenland, *C. neoteretis* reached its maximum relative abundance during the great glacier advances which occurred during MIS 3. *Cassidulina reniforme* and *T. trihedra* are generally quite high throughout MIS 3, peaking during Greenland Interstadials. *C. reniforme* shows an overall increase towards MIS 3/2, which indicates that the species prefers colder climatic condition in

the area, increasing as climate cools. *Triloculina trihedra* has its maximum relative abundance (~ 50 %) at 295 cm (~ 47 400 yrs. BP) and 225 cm (~ 34 500 yrs. BP), the former representing Heinrich Event H5 and the latter representing the upper boundary of GI 7. This species is considered to be part of the Arctic cold-water fauna (Chapter 4.2.3).

Several secondary and accessory species have their maximum relative abundance during MIS 3. *Ioanella tumidula* peaks early in the interval. Due to the timing of its presence, it probably represents seasonally open surface waters. Its peaks occur just before and after H5 and H4. *Epistominella arctica* peaks in the middle of MIS 3, during H4. *Astrononion gallowayi* has a low relative abundance through most of MIS 3, but reaches its absolute core maximum of 50 % at 245 cm (36 753 cal. yrs. BP). This part of the core is represented by a large peak in the sortable silt record (GI 8), indicating increased current activity in the area. *Cibicides lobatulus* is also present during MIS 3, however not together with *A. gallowayi*.

6.4.1.5 MIS 2: 28.8 ka – 14.3 ka yrs BP (core interval 175 – 60 cm)

The continuous dominance of *N. pachyderma* suggests that the near-surface water temperatures in the area have remained relatively low. Its relative abundance decreases slightly though, whereas the relative abundance of *T. quinqueloba* increases. The increasing presence of *T. quinqueloba* and presence of *G. uvula*, *G. glutinata* and *G. bulloides* could indicate influence of warmer waters at the surface. Some other studies from the North Atlantic and Nordic Seas have found this faunal composition to be an indication of AW influence (e.g. Johannessen et al., 1994; Jennings et al., 2004). It could also be related to a nearby presence of the Polar Front (Andersen et al., 2012).

There is a slight increase in the total abundance of especially benthic foraminifera during MIS 2, which could be an indication of increased preservation of $CaCO_3$. Reduced productivity due to the increased sea ice cover, could lead to decreased dissolution of CO_2 in the sea water, thereby increasing the preservation potential of foraminiferal tests (e.g. Steinsund and Hald, 1994).

The presence of *C. neoteretis* remains high throughout MIS 2 and the Last Glacial Maximum, though there are several barren samples near the LGM. The presence of *C. reniforme* is also quite high in the beginning of MIS 2 and during the LGM. Following this maximum, there is a gradual decrease towards the barren interval at the MIS 2/1 boundary. *Triloculina trihedra* follows a similar pattern, but is absent during the LGM. *Elphidium excavatum* reaches its maximum relative abundance of < 30 % during the beginning of the LGM at 125 cm (~ 23 000 yrs. BP). Its presence indicates colder water temperatures (<1^{O}C) (Steinsund et al., 1994), low salinities and the presence of an ice margin

(Wollenburg et al., 2001). It could indicate local meltwater events (Andersen et al., 2012), as it occurs in smaller numbers during H2 just prior to LGM.

Oridosalis umbonatus follows an opposite trend to *C. reniforme*, where its relative abundance increases following the LGM towards the barren interval. There is also an increase in the relative abundance of *C. wuellerstorfi* following the LGM, which could be an indication of warmer conditions at the beginning of the deglaciation.

The increased presence of *A. gallowayi* in the beginning of MIS 2 indicates coarser sediments (Chapter 4.2.8). This is also indicated by the grain size record. *C. lobatulus* is also present in small numbers during this time, and together they indicate a bottom environment of higher energy (Chapter 4.2.8). The two species are only present together when the ΔSS record peaks, also indicating stronger bottom currents. *Melonis barleeanus* could indicate increased presence of buried organic material within the sediments (e.g. Polyak et al., 2002).

6.4.1.6 MIS 1: 14.3 ka yrs. BP – present (core interval 60 – 0 cm)

Following Heinrich Event H1, the foraminiferal record is barren until the end of the interpreted Younger Dryas cold event. From this point onwards, there is a drastic decrease in the relative abundance of *N. pachyderma*. The presence of *N. incompta* and *T. quinqueloba* in great numbers is related to warmer waters and high surface productivity. Warmer climatic conditions are shown by the low $\delta^{18}O$ values, and the very high $\delta^{13}C$ values indicate increased productivity. There is quite a drastic increase in these subpolar species as the deglaciation continues and modern oceanographic conditions are reached. It is possible that their increase could indicate increased influence of AW at the sub-surface or surface (Chapter 4.1.4). *Neogloboquadrina pachyderma* is the dominating species throughout the record, reaching a minimum at 5 cm. Several other studies have found that changes in the position of the Arctic Front can be related to shifts in the planktic fauna. The dominance of *T. quinqueloba* versus *N. pachyderma* in the sediment has been found to indicate the proximity of the Arctic Front in other studies (e.g. Johannessen et al., 1994; John et al., 2004). It is possible that the faunal shift near the top of the core relates to movement of this front. Northward retreat of the Polar Front has been seen slightly south of the investigated are, East Greenland. This retreat occurs following the Younger Dryas (Jennings et al., 2011).

Oridorsalis umbonatus is one of the most common benthic deep-sea species in the modern GIN-Seas, and the dominance of this species during MIS 1, probably indicates that conditions are similar to the modern conditions. The increased presence of *C. wuellerstorfi* and *T. quinqueloba* together with high

$\delta^{13}C$ values however indicate ice-free conditions and increased productivity. Other benthic species are only accessory during MIS 1.

6.4.1.7 Summary and discussion

In the study by Wollenburg et al. (2001) from the Arctic Ocean, the foraminiferal assemblage which was dominated by *C. reniforme* was found to characterize stadial sediments of MIS 6, MIS 4 and MIS 3. The highest presence of *C. reniforme* within core HH13-089GC is related to periods moderate $\delta^{13}C$ values, higher $\delta^{18}O$ values, and extended sea ice cover (MIS 6, MIS 4, the end of MIS 3, and MIS 2). Its highest presence is related to the times where the Greenland Ice Sheet was at its maximum position (the Saalian glaciation, MIS 6), or was advancing towards its LGM maximum position (The Flakkerhuk stadial, MIS 3 and MIS 2). Wollenburg et al. (2001) also found *C. reniforme* to be amongst the dominant species during times of maximum glacial ice sheet extension in the Arctic Ocean, and during times of moderate productivity. Sejrup and Guilbault (1980) concluded that *C. reniforme* prefers an Arctic environment.

In this investigation, *C. neoteretis* has a somewhat similar pattern to *C. reniforme*, in that it has its highest relative abundance as the ice sheet reaches its last maximum position (MIS 3 and MIS 2), and during late MIS 6. Wollenburg et al. (2001) found the species *Cassidulina teretis* (Tappan, 1951) to be related to glacial intervals, just like the identified *C. neoteretis* in HH3-089GC. These two species are very similar morphologically, and Lazar et al. (2016) described it as very difficult, if not impossible to distinguish between the two under a regular light microscope, which is what was used during the present investigation. The use of *C. neoteretis* in Pleistocene stratigraphy has not been universal since it was first described by Seidenkrantz et al (1995), and many researchers continue to use *C. teretis*. Due to the difficulties of differentiating between the two, it is probable that the *C. neoteretis* found to be related to glacial conditions in HH13-089GC is the same species as the *C. teretis* identified during similar conditions in the Arctic Ocean by Wollenburg et al. (2001). They found that the presence of this species during glacial stadials indicated relatively high seasonal productivity, despite of glacial conditions.

In their study from the Vøring Plateau, Norwegian Sea, Haake and Pflaumann (1989) described *O. umbonatus* to be one of the most relevant species for stratigraphy of the GIN-Seas together with *C. wuellerstorfi* and *P. bulloides*. They found that *O. umbonatus* was present during both interglacial and glacial times, which was also the case for HH13-089GC. Its presence seems to follow the general trend of the planktic $\delta^{13}C$ record, however there seemed to be an overall higher relative abundance during the relatively warmer MIS 5, early to mid- MIS 3 and MIS 1 within HH13-089GC. Haake and Pflaumann (1989) indicated that *O. umbonatus* was only suppressed by ice rafting. In core HH13-

089GC however, only minor drops are seen during high IRD concentrations with the exception of H6. It seems that *O. umbonatus* and *C. neoteretis* has an inverse relationship. It appears *C. neoteretis* may be able to make the most of periods where surface productivity is moderate to low, and thereby outperforms *O. umbonatus*. During warmer periods of high- to moderate surface productivity and reduced sea ice cover, it appears to be *O. umbonatus* which outperforms *C. neoteretis*. *Oridorsalis umbonatus* is amongst the dominating benthic species throughout the record, which indicates that it is very tolerant to changing climatic conditions (Haake and Pflaumann, 1989).

6.4.1.8 Influence of Atlantic Water

As described in chapter 2.1.2, the East Greenland Current is made up of several water masses of different properties. One of these water masses is the warmer Atlantic Intermediate Water (AIW), which is found in between the cold, ice-bearing surface Polar Water and the cold and dense Greenland Sea Deep Water. The source of the AIW to the East Greenland Current is believed to be the Return Atlantic Current (RAC), which in turn has its source in the even warmer Atlantic Water (AW) (Bourke et al., 1987). The Return Atlantic Current represents the part of the West Spitsbergen Current that turns southward and joins the ECG in the Fram Strait. Atlantic Water is also brought into the Greenland-Iceland Seas through the Denmark Strait, however this branch is believed to follow the Icelandic continental shelf as the North Icelandic Irminger Current (NIIC) (Figure 3).

Even though warmer Atlantic Intermediate Water is present within the water masses of the East Greenland Current, the benthic foraminiferal fauna generally represents the bottom or near bottom environment, which in this area is generally affected by the cold Greenland Sea Deep Water. Increased abundances of *C. neoteretis* and *C. reniforme* have been found to be an indication of increased AW influence in the modern GIN-Seas, however, their increased presence in the investigated area has not been interpreted to be related to such influence due to the depth of the core site, and the overall presence of these species during glacial conditions. It is therefore believed that the presence of *C. reniforme* and *C. neoteretis* in core HH13-089GC is not an indication of influence of warm AW, but rather a representation of an Arctic environment (Sejrup and Huilbault, 2012).

It is however possible, that the planktic foraminiferal fauna could have been influenced by increased flow of subsurface AIW. The planktic foraminifera *N. pachyderma* and *N. incompta* can be relatively deep dwellers, and have been found to live near the PW/AIW interface. It is possible that increased influence of AIW, or slightly vertical movement of the AIW interface could be able to influence the sub-surface and surface faunas enough to see a slight change in the planktic faunal composition.

Samples which are highly influenced by the WSC in the Fram Strait has been found to be dominated by *T. quinqueloba*, and have an increased presence of *N. incompta* (e.g. Carstens et al., 1997). It is possible that an increased RAC could influence the near-surface and surface environment of the investigated East Greenland area enough for subpolar species to increase, as seen during the Holocene.

6.4.2 Sortable silt record in relation to magnetic susceptibility and bottom current activity

Background

In chapter 2.1.3, the processes for Deep Water formation in the GIN-Seas was presented, and its importance explained. Several studies have proposed a connection between changes in the operation of the thermohaline circulation in the North Atlantic Ocean, and the climatic oscillations recorded in Greenland ice cores (e.g. Broecker et al., 1985; Broecker and Denton, 1989; Broecker et al., 1990; Birchfield and Broecker, 1990, Broecker, 1990). Most of the land areas surrounding the North Atlantic today are ice free, and the thermohaline circulation system relatively stable. Since the Younger Dryas, the ice records are also relatively stable, at least if compared to the last glacial (Broecker et al, 1990). Broecker et al. (1990) described how the millennial scale climatic oscillations from the last glacial period, could be related to shifts, or so called "conveyor-on" and "conveyor-off" phases in the global oceanic circulation system. When the circulation is in an operative mode ("conveyor-on"), Deep Water is continuously formed through convection in the GIN-Sea gyres, carrying some of the densest waters in the world southwards across the Greenland – Scotland Ridge, to become part of the NADW. The latent heat released to the atmosphere during Deep Water formation, could have caused melting of the surrounding ice covers. Meltwater release causes a freshening of the surface waters. Such freshening, combined with salt exportation by the Deep Water, would cause a gradual decrease in water density. This could eventually have reduced Deep Water production drastically and lead the conveyor into a "conveyor-off" mode where it is reduced to a minimum. Such a minimum would cause a colder climate in the North Atlantic, as the supply of ocean heat from southern latitudes is abruptly cut off. This cooling of the climate is reflected by the D-O oscillations in the Greenland ice records. When the thermohaline circulation system has reached this minimum, the ice melting is decreased, as is the salt exportation. Surface evaporation causes a gradual build-up of salt in the waters of the GIN-Seas and North Atlantic. At some point, the salt content will have increased the density of the waters enough for Deep Water production to be restored. The thermohaline circulation has reached its "conveyor-on" mode, and a new cycle has been started (Broeckeret al., 1990). Theories which try to explain the mechanisms of abrupt millennial-scale climate oscillations usually brings out changes in the global thermohaline circulation. Whether these changes are triggering climatic change or are a result of climatic change, will not be discussed in this thesis.

Correlation between the HH13-089GC sortable silt record and regional magnetic susceptibility records

The cooling phases of the Dansgaard-Oeschger climatic oscillations recorded in Greenland ice cores, have been described to be related to reduced production of NADW (Oppo and Lehman, 1995). In their investigation of core ENAM93-21 from the Faeroe Margin, Rasmussen et al. (1996a) found the D-O cooling events to generally correlate with increased IRD content, ^{18}O depletions in the isotope record, higher relative abundance of *N. pachyderma*, and low magnetic susceptibility values. The positive correlation between the D-O oscillations and the magnetic susceptibility record, thereby indicates a correlation between magnetic susceptibility and changes in bottom current activity. Several other studies in addition to Rasmussen et al. (1996a) from the Nordic Seas and North Atlantic, have also found positive correlations between the climatic oscillations and magnetic susceptibility (Moros et al., 1997; Kissel et al., 1999; Ballini et al., 2006; Jessen and Rasmussen, 2015). Kissel et al. (1999) inferred that the changes in the amount of magnetic material within their investigated cores, was a result of changes in the efficiency of the transport of these particles by deep ocean currents. The cores from these studies combined, cover a large area in the Nordic Seas and North Atlantic, providing a regional signal for the correlation between bottom current activity and magnetic susceptibility. The study by Jessen and Rasmussen (2015) also provides a positive correlation between the climatic oscillations, magnetic susceptibility and sortable silt.

The sortable silt (ΔSS) record from the East Greenland slope core HH13-089GC has already been found to have a positive correlation with the Dansgaard – Oeschger climatic cycles displayed within the Greenland ice core records, thereby indicating a correlation with changes in deep current activity. In chapter 6.2 and 6.3 of the discussion, it was established that major drops in the ΔSS record correlate with Greenland Stadials, larger peaks in IRD and low magnetic susceptibility values. A general correlation with slight ^{18}O depletion was also seen. This is similar to the findings of Rasmussen et al. (1996a), which also provided a basis for the interpretation of Heinrich Events in the present study. In figure 34 below, is a correlation between the HH13-089GC sortable silt record and the ENAM93-21 magnetic susceptibility record. This was done to see the clear regional correlation.

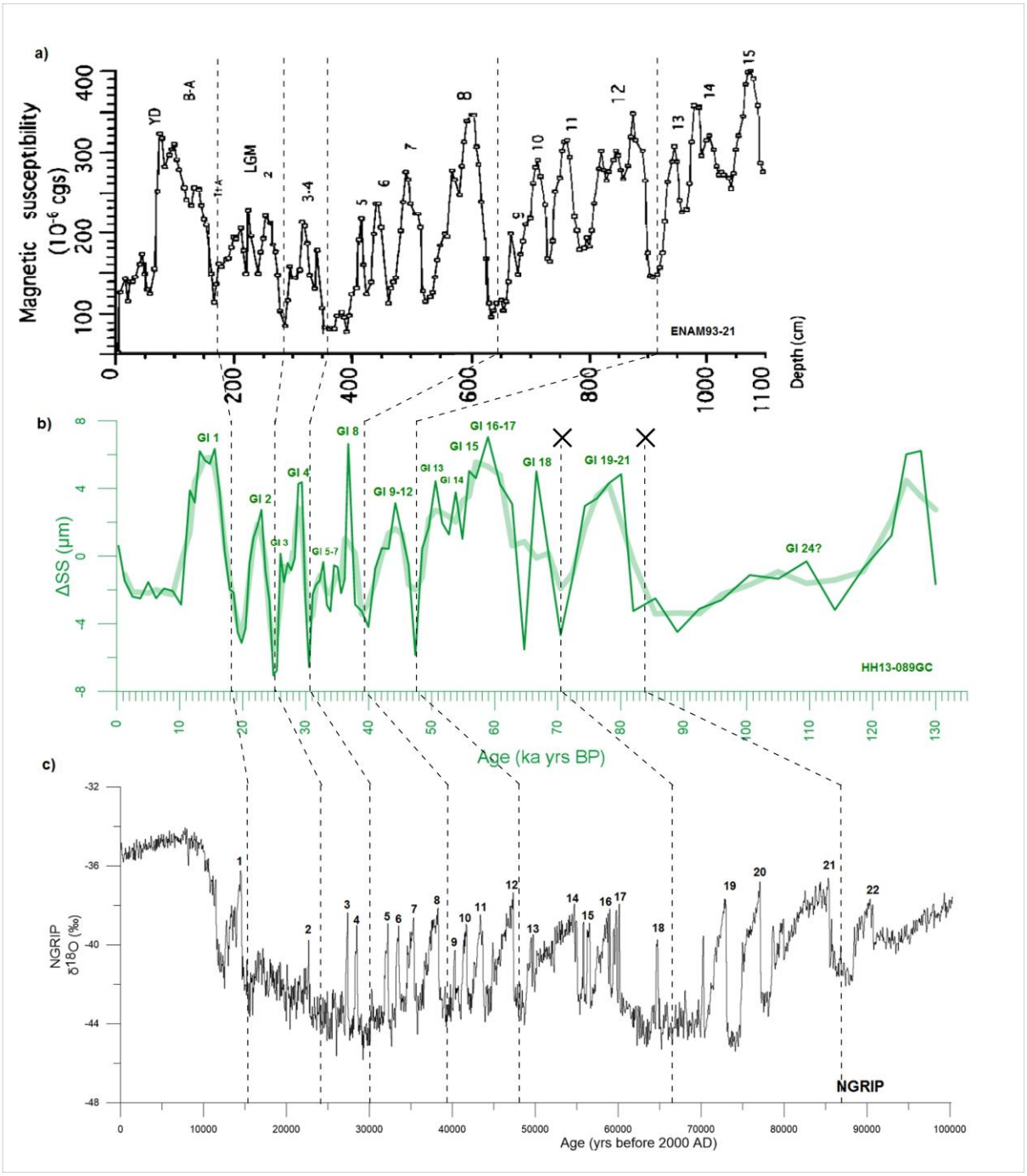

Figure 34: *Correlation between **(a)** The magnetic susceptibility record from the Faeroe Margin core ENAM93-21 (Rasmussen et al., 1996a) **(b)** sortable silt (ΔSS) record for core HH13-089GC and **(c)** NGRIP stable oxygen isotope record (NGRIP members, 2004; Andersen et al., 2006). There seems to be a correlation between the first 15 oscillations recorded in all three records. **X** symbols mark the end of certain correlations.*

Interpretation and discussion

As seen in the figure, the sortable silt record for HH13-089GC also shows a positive correlation with the magnetic susceptibility curve for ENAM93-21. This means that the HH13-089GC sortable silt record is also in phase with the magnetic susceptibility records of several different cores in the Nordic Seas and the North Atlantic (Moros et al., 1997; Kissel et al., 1999; Jessen and Rasmussen, 2015).

Core HH13-089GC is located in an area that is affected by the input of volcanic material from several zones associated with volcanism (Jan Mayen, Iceland and Faeroe Islands) (e.g. Mangerud et al., 1984) This is also the case for ENAM93-21. Materials from such zones can be transported with oceanic currents, and will give a high magnetic susceptibility signal in the record, if the current strength has been high enough to transport the material. The positive correlation between the sortable silt record and other magnetic susceptibility records, suggests that magnetic susceptibility from deep marine cores can be an indicator for variations in bottom current activity. This is similar to the findings of previous studies (e.g. Rasmussen et al., 1996a; Moros et al., 1997; Kissel et al., 1999).

Sortable silt is, as mentioned several times, considered to be the most suitable parameter for paleocurrent speed reconstruction (McCave et al., 1995a, 1995b; Bianchi and McCave, 1999; Hass, 2002). The IRD correction which was applied to the HH13-089GC ΔSS record in chapter 5.6 made sure that data clearly affected by IRD was filtered out. The result of this correction is a record, reflecting changes in bottom current activity, which may or may not be affected by vertical current migration. To determine the possible influence of such migration, additional studies of this proxy are needed for East Greenland. For the time being however, the sortable silt record has been interpreted to reflect changes in current strength and possibly variation in Deep Water production based on its correlation with other studies.

The results of the sortable silt analysis show that current speed possibly follows two different patterns. First, a slight reduction in current activity is seen during every Greenland Stadial identified in the record (Figure 25). This indicates a possible relationship between current activity and Dansgaard-Oeschger cycles. Secondly, a much larger reduction in current activity is found to correlate with the interpreted Heinrich Events. This correlation could indicate a possible connection between the long term cooling trend of the so called Bond cycled (bundling of progressively colder D-O events) and gradually reduced bottom current activity, ending in a Heinrich Event or a “conveyor-off mode” (Broecker et al., 1990). Reduced bottom current activity during Greenland Stadials could indicate a weakening of the Deep Water formation process in the GIN-Seas, and thereby a weakening in NADW (Kellogg, 1980; Rasmussen and Thomsen, 2004; Jessen and Rasmussen, 2015). Other studies from the North Atlantic have also indicated a relationship between current changes, D-O cycles and surging ice

sheets (e.g. Broecker, 1994; Maslin et al., 1995; Vidal et al., 1997; van Kreveld et al., 2000), however there are many theories on the mechanisms behind changes in current activity during these cycles.

Vidal et al. (1997) investigated Heinrich Events in the lower latitude North Atlantic, especially H4, and their possible effects on the thermohaline circulation. They found that deep circulation patterns during H4, H1 and the LGM where different, and related to changes in convection sites. They indicated that the thermohaline circulation was highly sensitive to fresh water forcing related to Heinrich Events. Broecker (1994) also investigated the cyclic pattern of Heinrich Events and Bond cycles, and their possible connection to the D-O cycles. He however found the relationship between especially Bond cycles and D-O cycles to remain a mystery.

Dokken and Jansen (1999) suggested that the formation of deep water in the GIN-Seas was always present during both interstadials (GI) and stadials (GS). Their theory was that the formation of brines during stadials (GS) maintained the deep-water formation, eventually restarting the open ocean convection that we see at present. This convection is what was believed to drive deep-water formation during interstadials (GI). The sortable silt record from HH13-089GC, suggests that the current activity during Greenland Stadials periods was very reduced to practically non-existent. The overall foraminiferal preservation is also quite good during stadials, especially during MIS 4 and MIS 5, as represented by high P:B ratios. Since brines are generally cold and dense water masses, rich in CO_2, one would expect the foraminiferal preservation to be lower if such waters were present during the stadials (e.g. Steinsund and Hald, 1994).

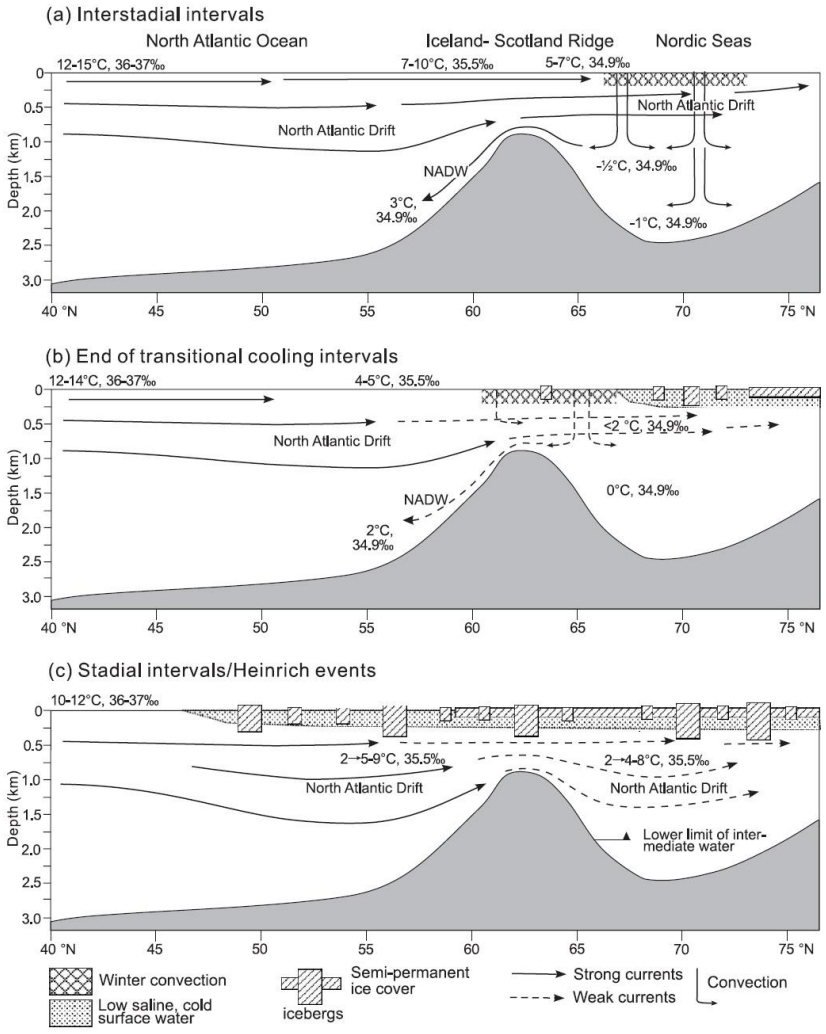

Figure 35: *Describes the hypothesis of Rasmussen and Thomsen (2004) on causes for D-O events.* ***(a)*** *Interstadial intervals with open ocean convection in the GIN-Seas and NADW production.* ***(b)*** *Transitional cooling intervals with limited convection and NADW formation.* ***(c)*** *Stadial intervals where the NAC/North Atlantic Drift flowed beneath the fresh surface waters, warming the deep waters, and eventually breaking through to the surface, releasing large amounts of energy to the atmosphere. (Figure from Rasmussen and Thomsen (2004).*

Rasmussen et al. (1996a) suggested that the interstadials were connected to inflow of warmer surface waters and NADW formation. During the transitional cooling phases, surface waters cooled, and the formation of NADW was reduced. During the stadials, which included Heinrich Events, the convection had been highly reduced to the point where deep-water outflow from the Nordic Seas was very limited. Rasmussen and Thomsen (2004) expanded this interpretation. Their theory was that the deep-water outflow from the Nordic Seas during stadials was non-existent. However, the warm NAC continued to flow towards the Nordic Seas underneath the cold, and low saline surface waters, which was highly affected by meltwater. This continuous inflow of warmer water would warm the deep water masses and decrease their density. Eventually this would cause the warm water masses to break through the stratified waters above, releasing large amounts of heat to the atmosphere. The warmer climate would cause the open ocean convection, and hence NADW formation to be restarted. Increased freshening of the surface during cooling intervals, would cause decreased production of

NADW. This theory may be more in tune with the sortable silt results of HH13-089GC, showing limited bottom current activity during stadials and high activity during interstadials.

To summarize; The HH13-089GC sortable silt record has been shown to be in phase with local and regional magnetic susceptibility records, and marine (HH13-089GC and ENAM93-21) and terrestrial (NGRIP ice core) $\delta^{18}O$ records. These positive correlations indicate that the sortable silt record reflects variations in the flow of the Greenland Sea Deep Water, which will eventually join the NADW. Reduced Deep Water activity suggest reduced, and possibly shallower thermohaline convection in the Greenland Sea gyre, and thereby weaker deep ocean ventilation and NADW. Greenland Stadials are shown as periods of highly reduced bottom current activity, especially those that correlate with Heinrich Events.

It is important to remember that this thesis is based on the data from one core in the North Atlantic Ocean only, and any connections on the level of the "great conveyor" would need to be investigated further. Perhaps a benthic $\delta^{18}O$ and $\delta^{13}C$ record, and SST/SSS reconstructions from the area could provide additional information about deep ocean ventilation during times of current change. Nonetheless, it seems clear that there is a connection between the sortable silt record, magnetic susceptibility, bottom current activity and climatic oscillations during the last glacial, and that is where I will leave this discussion.

7 Summary and conclusions

Sediment core HH13-089GC from the continental slope off central east Greenland has been analysed in order to reconstruct the paleoclimatic- and paleoceanographic history through the late Pleistocene and Holocene in the area, and to investigate these changes in relation to deep current variations. The main findings and conclusions of this study are:

- The sediment core provides important information about the East Greenland continental margin during the last ~ 130 000 years. The overall planktic oxygen isotope record resembles the global isotope record of Lisiecki and Raymo (2005). Local signals however, seem to have overridden the global signal, making it slightly more difficult to interpret. It is possible that a stable isotope record based on benthic foraminifera would have shown a clearer signal.
- The stable isotope records indicated the presence of marine isotope stages 1 – 5, as well as the upper parts of MIS 6. The benthic foraminifera *P. bulloides* provided the identification of MIS 5a. The possible presence of short-term climatic oscillations and/or changes in deep water activity at the MIS 6/5 boundary is similar to previous findings in the North Atlantic.
- The IRD record indicated several large ice rafting events, where the supply of coarse grained material by icebergs and sea ice increased. These ice rafting events where tied to pulsing glacial activity. The maximum flux of coarse grained material to the slope was seen between ~ 26 000 – 16 400 yrs. BP, which also includes the Last Glacial Maximum.
- The beginning of the last deglaciation was found to be ~ 18 500 yrs. BP, which is similar to previous findings for the central East Greenland. The Bølling-Allerød interstadials and the Younger Dryas cold event is also believed to have been found within the records.
- The sortable silt record (a new proxy for the area) revealed an interesting pattern which needed to be investigated further. The record was found to have a positive correlation with the NGRIP stable isotope record, and the ENAM93-21 magnetic susceptibility record, which revealed a correlation to other North Atlantic records as well. The sortable silt correlations indicate a relationship between large atmospheric climate variations and bottom current activity. A possible connection between the sortable silt record and changes in North Atlantic Deep Water activity, and thermohaline circulation has also been indicated. Additional studies from the area are needed to validate this claim and to investigate possible influence from vertical current migration. The sortable silt record has been found to be an important tool for increased stratigraphic control in future paleoceanographic and paleoclimatic investigations in the area.
- The comparison between all proxy records for HH13-089GC showed that the large ice rafting events correlated with the largest drops in the NGRIP- and sortable silt records, as well as with drops in the magnetic susceptibility- and stable oxygen isotope records. Similar findings

have been recorded elsewhere in the North Atlantic, and the IRD events where interpreted to represent Heinrich Events 1 – 6. The approximate ages for these events were provided by the age model; H6 ~ 64 600 – 68 500 yrs. BP, H5 ~ 48 400 – 46 300 yrs. BP, H4 ~ 41 000 – 37 800 yrs. BP, H3 ~ 31 000 – 29 900 yrs. BP, H2 24 853 cal. yrs. BP and H1 ~ 20 400 – 18 500 yrs. BP.

- The planktic foraminiferal fauna is highly influenced by the cold EGC, as seen in the dominance of *N. pachyderma*, however small amounts of subpolar species provide information about possible changes in water temperatures, and possible movement in the Polar- and Arctic Fronts.
- The benthic foraminifera *O. umbonatus* dominates through both glacial and interglacial times. *C. neoteretis* and *C. renifome* are found to dominate the faunal composition during colder climatic conditions with increased presence of sea ice cover, and is believed to indicate an Arctic environment.
- The sortable silt-, oxygen- and carbon isotope-, and foraminiferal records provide important paleoceanographic information, such as variations in surface productivity, surface ventilation, events of surface freshening, influence of warmer surface waters, sea ice coverage, nutrient supply, and energy changes in the bottom environment.

References

Aagaard, K., & Coachman, L. K. (1968a). The East Greenland Current north of Denmark Strait: part I. *Arctic*, 181-200.

Aagaard, K., & Coachman, L. (1968b). The East Greenland Current north of Denmark Strait: Part II. *Arctic*, 267-290.

Aagaard, K., Swift, J., & Carmack, E. (1985). Thermohaline circulation in the Arctic Mediterranean seas. *Journal of Geophysical Research, 90*(C3), 4833-4846.

Aagaard, K., Foldvik, A., & Hillman, S. (1987). The West Spitsbergen Current: disposition and water mass transformation. *Journal of Geophysical Research: Oceans, 92*(C4), 3778-3784.

Alley, R., Meese, D., Shuman, C., Gow, A., Taylor, K., Grootes, P., White, J, W, C., Ram, M., Waddington, E, D., & Mayewski, P. (1993). Abrupt increase in Greenland snow accumulation at the end of the Younger Dryas event. *Nature, 362*, 527-528.

Andersen, K. K., Svensson, A., Johnsen, S. J., Rasmussen, S. O., Bigler, M., Röthlisberger, R., Ruth, U., Siggaard-Andersen, M. L., Steffensen, J. P., Dahl-Jensen, D., Vinther, B. O., & Clausen, H. B. (2006). The Greenland Ice Core Chronology 2005, 15–42 ka. Part 1: constructing the time scale. *Quaternary Science Reviews, 25*(23–24), 3246-3257.

Andresen, C., Hansen, M., Seidenkrantz, M.-S., Jennings, A., Knudsen, M., Nørgaard-Pedersen, N., Larsen, N. K., Kuijpers, A., & Pearce, C. (2012). Mid-to late-Holocene oceanographic variability on the Southeast Greenland shelf. *The Holocene, 23*(2), 167-178.

Andrews, J., Milliman, J., Jennings, A., Rynes, N., & Dwyer, J. (1994). Sediment thicknesses and Holocene glacial marine sedimentation rates in three East Greenland fjords (ca. 68 N). *The Journal of Geology, 102*(6), 669-683.

Andrews, J., Jennings, A. E., Cooper, T., Williams, K. M., & Mienert, J. (1996). Late Quaternary sedimentation along a fjord to shelf (trough) transect, East Greenland (c. 68 N). *Geological Society, London, Special Publications, 111*(1), 153-166.

Armstrong, H. A., & Brasier, M. D. (2005). *Microfossils* (2 ed.): Blackwell Publishing.

Ballini, M., Kissel, C., Colin, C., & Richter, T. (2006). Deep-water mass source and dynamic associated with rapid climatic variations during the last glacial stage in the North Atlantic: A multiproxy investigation of the detrital fraction of deep-sea sediments. *Geochemistry, Geophysics, Geosystems, 7*(2).

Bamber, J. L., Layberry, R. L., & Gogineni, S. P. (2001). A new ice thickness and bed data set for the Greenland ice sheet: 1. Measurement, data reduction, and errors. *Journal of Geophysical Research: Atmospheres (1984–2012), 106*(D24), 33773-33780.

Bauch, D., Darling, K., Simstich, J., Bauch, H. A., Erlenkeuser, H., & Kroon, D. (2003). Palaeoceanographic implications of genetic variation in living North Atlantic *Neogloboquadrina pachyderma*. *Nature, 424*(6946), 299-302.

Bauch, H. A., & Erlenkeuser, H. (2008). A “critical” climatic evaluation of last interglacial (MIS 5e) records from the Norwegian Sea. *Polar research, 27*(2), 135-151.

Bauch, H. A., Kandiano, E. S., Helmke, J., Andersen, N., Rosell-Mele, A., & Erlenkeuser, H. (2011). Climatic bisection of the last interglacial warm period in the Polar North Atlantic. *Quaternary Science Reviews, 30*(15–16), 1813-1818.

Bé, A. W. H., & Tolderlund, D. S. (1971). Distribution and ecology of living planktonic foraminifera in surface waters of the Atlantic and Indian Oceans. In B. M. Funnel & W. R. Riedel (Eds.), *The Micropalaeontology of Oceans.* (pp. 105-149). Cambridge: Cambridge University Press.

Bé, A. W. H., & Hutson, W. H. (1977). Ecology of Planktonic Foraminifera and Biogeographic Patterns of Life and Fossil Assemblages in the Indian Ocean. *Micropaleontology, 23*(4), 369-414.

Bennike, O., & Björck, S. (2002). Chronology of the last recession of the Greenland Ice Sheet. *Journal of Quaternary Science, 17*(3), 211-219

Bennike, O., Björck, S., & Lambeck, K. (2002). Estimates of South Greenland late-glacial ice limits from a new relative sea level curve. *Earth and Planetary Science Letters, 197*(3–4), 171-186.

Bennike, O., & Weidick, A. (2001). Late Quaternary history around Nioghalvfjerdsfjorden and Jøkelbugten, North-East Greenland. *Boreas, 30*(3), 205-227.

Bergsten, H. (1994). Recent benthic foraminifera of a transect from the North Pole to the Yermak Plateau, eastern central Arctic Ocean. *Marine geology, 119*(3-4), 251-267.

Bianchi, G. G., & McCave, I. N. (1999). Holocene periodicity in North Atlantic climate and deep-ocean flow south of Iceland. Nature, 397(6719), 515-517. *Nature, 397*(6719), 515-517.

Bianchi, G., Vautravers, M., & Shackleton, N. (2001). Deep flow variability under apparently stable North Atlantic Deep Water production during the last interglacial of the. *Paleoceanography, 16*(3), 306-316.

Birchfield, G. E., & Broecker, W. S. (1990). A salt oscillator in the glacial Atlantic? 2. A “scale analysis” model. *Paleoceanography, 5*(6), 835-843.

Birks, H. H., Gulliksen, S., Haflidason, H., Mangerud, J., & Possnert, G. (1996). New radiocarbon dates for the Vedde Ash and the Saksunarvatn Ash from western Norway. *Quaternary Research, 45*(2), 119-127.

Björck, S., Walker, M. J., Cwynar, L. C., Johnsen, S., Knudsen, K. L., Lowe, J. J., & Wohlfarth, B. (1998). An event stratigraphy for the Last Termination in the North Atlantic region based on the Greenland ice-core record: a proposal by the INTIMATE group. *Journal of Quaternary Science, 13*(4), 283-292.

Blake, W. (1999). Glaciated landscapes along Smith Sound, Ellesmere Island, Canada and Greenland. *Annals of Glaciology, 28*(1), 40-46.

Blindheim, J., & Østerhus, S. (2005). The Nordic Seas, main oceanographic features. *The Nordic seas: an integrated perspective*, 11-37.

Bond, G., Heinrich, H., Broecker, W., Labeyrie, L., McManus, J., Andrews, J., Huon, S., Jantschik, R., Clasen, S., & Simet, C. (1992). Evidence for massive discharges of icebergs into the North Atlantic Ocean during the last glacial period. *Nature 360*, 245 – 249.

Bond, G., Broecker, W., Johnsen, S., McManus, J., Labeyrie, L., Jouzel, J., & Bonani, G. (1993). Correlations between climate records from North Atlantic sediments and Greenland ice. *Nature, 365*(6442), 143-147.

Bond, G. C., & Lotti, R. (1995). Iceberg discharges into the North Atlantic on millennial time scales during the last glaciation. *Science, 267*(5200), 1005.

Bond, G. C., Showers, W., Elliot, M., Evans, M., Lotti, R., Hajdas, I., Bonani, G., & Johnson, S. (1999). The North Atlantic's 1-2 Kyr Climate Rhythm: Relation to Heinrich Events, Dansgaard/Oeschger Cycles and the Little Ice Age. *Mechanisms of global climate change at millennial time scales*, 35-58.

Bourke, R. H., Newton, J. L., Paquette, R. G., & Tunnicliffe, M. D. (1987). Circulation and water masses of the East Greenland Shelf. *Journal of Geophysical Research: Oceans, 92*(C7), 6729-6740.

Bowman, S. (1990). *Radiocarbon Dating*: University of California Press/British Museum.

Bradley, R. S. (2014). *Paleoclimatology - Reconstructing Climate of the Quaternary* (3 ed.): Elsevier Inc.

Broecker, W. S., Peteet, D. M., & Rind, D. (1985). Does the ocean-atmosphere system have more than one stable mode of operation? *Nature, 315*(6014), 21-26.

Broecker, W. S., & Denton, G. H. (1989). The role of ocean-atmosphere reorganizations in glacial cycles. *Geochimica et Cosmochimica Acta, 53*(10), 2465-2501.

Broecker, W. S., Bond, G., Klas, M., Bonani, G., & Wolfli, W. (1990). A salt oscillator in the glacial Atlantic? 1. The concept. *Paleoceanography, 5*(4), 469-477.

Broecker, W. S. (1990). Salinity history of the northern Atlantic during the last deglaciation. *Paleoceanography, 5*(4), 459-467.

Broecker, W. S. (1991). The great ocean conveyor. *AIP Conference Proceedings 247*, 129.

Broecker, W., Bond, G., Klas, M., Clark, E., & McManus, J. (1992). Origin of the northern Atlantic's Heinrich events. *Climate Dynamics, 6*(3-4), 265-273.

Broecker, W. S. (1994). Massive iceberg discharges as triggers for global climate change. *Nature, 372*(6505), 421.

Carstens, J., Hebbeln, D., & Wefer, G. (1997). Distribution of planktic foraminifera at the ice margin in the Arctic (Fram Strait). *Marine Micropaleontology, 29*(3-4), 257-269.

Chauhan, T., Rasmussen, T., Noormets, R., Jakobsson, M., & Hogan, K. (2014). Glacial history and paleoceanography of the southern Yermak Plateau since 132 ka BP. *Quaternary Science Reviews, 92*, 155-169.

Chi, J., & Mienert, J. (1996). Linking physical property records of Quaternary sediments to Heinrich events. *Marine geology, 131*(1), 57-73.

Clark, P. U., Dyke, A. S., Shakun, J. D., Carlson, A. E., Clark, J., Wohlfarth, B., Mitrovica, J. X., Hostetler, S. W., & McCabe, A. M. (2009). The Last Glacial Maximum. *Science, 325*(5941), 710.

CLIMAP, P. (1981). Seasonal Reconstruction of the Earth's Surface at the Last Glacial Maximum. *Geological Society of America*.

Cofaigh, C. O., Dowdeswell, J. A., & Grobe, H. (2001). Holocene glacimarine sedimentation, inner Scoresby Sund, East Greenland: the influence of fast-flowing ice-sheet outlet glaciers. *Marine geology, 175*(1), 103-129.

Corliss, B. H. (1985). Microhabitats of benthic foraminifera within deep-sea sediments. *Nature, 314*, 435-438.

Cortijo, E., Labeyrie, L., Elliot, M., Balbon, E., & Tisnerat, N. (2000). Rapid climatic variability of the North Atlantic Ocean and global climate: a focus of the IMAGES program. *Quaternary Science Reviews, 19*(1–5), 227-241.

Cronin, T. M. (1999). *Principles of Paleoclimatology*: Columbia University Press.

Cuffey, K. M., & Marshall, S. J. (2000). Substantial contribution to sea-level rise during the last interglacial from the Greenland ice sheet. *Nature, 404*(6778), 591-594.

Dansgaard, W., Clausen, H., Gundestrup, N., Hammer, C., Johnsen, S., Kristinsdottir, P., & Reeh, N. (1982). A new Greenland deep ice core. *Science, 218*(4579), 1273-1277.

Dansgaard, W., Johnsen, S., Clausen, H., Hvidberg, C., & Steffensen, J. (1993). Evidence for general instability of past climate from a 250-kyr. *Nature, 364*, 15.

Darling, K. F., Kucera, M., Pudsey, C. J., & Wade, C. M. (2004). Molecular evidence links cryptic diversification in polar planktonic protists to Quaternary climate dynamics. *Proceedings of the National Academy of Sciences of the United States of America, 101*(20), 7657-7662.

Darling, K. F., Kucera, M., Kroon, D., & Wade, C. M. (2006). A resolution for the coiling direction paradox in *Neogloboquadrina pachyderma*. *Paleoceanography, 21*(2).

Denbigh, P. N. (1989). Swath bathymetry: Principles of Operation and an Analysis of Errors. *IEEE Journal of Oceanic Engineering, 14*(4), 289-298.

Dokken, T. M., & Hald, M. (1996). Rapid climatic shifts during isotope stages 2–4 in the Polar North Atlantic. *Geology, 24*(7), 599-602.

Dokken, T. M., & Jansen, E. (1999). Rapid changes in the mechanism of ocean convection during the last glacial period. *Nature, 401*(6752), 458-461.

Dowdeswell, J. A., Villinger, H., Whittington, R. J., & Marienfeld, P. (1993). Iceberg scouring in Scoresby Sund and on the East Greenland continental shelf. *Marine geology, 111*(1-2), 37-53.

Dowdeswell, J. A., Uenzelmann-Neben, G., Whittington, R. J., & Marienfeld, P. (1994). The Late Quaternary sedimentary record in Scoresby Sund, East Greenland. *Boreas, 23*(4), 294-310.

Dowdeswell, J., Kenyon, N., & Laberg, J. (1997). The glacier-influenced Scoresby Sund Fan, East Greenland continental margin: evidence from GLORIA and 3.5 kHz records. *Marine geology, 143*(1-4), 207-221.

Duplessy, J., Shackleton, N., Fairbanks, R., Labeyrie, L., Oppo, D., & Kallel, N. (1988). Deepwater source variations during the last climatic cycle and their impact on the global deepwater circulation. *Paleoceanography, 3*(3), 343-360.

Duplessy, J.-C., Labeyrie, L., Arnold, M., Paterne, M., Duprat, J., & van Weering, T. C. (1992). Changes in surface salinity of the North Atlantic Ocean during the last deglaciation. *Nature, 358*(6386), 485-488.

Elverhøi, A., & Bomstad, K. (1980). Late Weichselian glacial and glaciomarine sedimentation in the western, central Barents Sea. *Norsk Polarinstitutt*, Oslo, Norway.

Elverhøi, A., Dowdeswell, J. A., Funder, S., Mangerud, J. A. N., & Stein, R. (1998). Glacial And Oceanic History Of The Polar North Atlantic Margins: An Overview. *Quaternary Science Reviews, 17*(1), 1-10.

England, J. (1999). Coalescent Greenland and Innuitian ice during the Last Glacial Maximum: revising the Quaternary of the Canadian High Arctic. *Quaternary Science Reviews, 18*(3), 421-456.

Evans, J., Dowdeswell, J. A., Grobe, H., Niessen, F., Stein, R., Hubberten, H.-W., & Whittington, R. (2002). Late Quaternary sedimentation in Kejser Franz Joseph Fjord and the continental margin of East Greenland. *Geological Society, London, Special Publications, 203*(1), 149-179.

Ezat, M. M., Rasmussen, T. L., & Groeneveld, J. (2014). Persistent intermediate water warming during cold stadials in the southeastern Nordic seas during the past 65 ky. *Geology, 42*(8), 663-666.

Fronval, T., Jansen, E., Bloemendal, J., & Johnsen, S. (1995). Oceanic evidence for coherent fluctuations in Fennoscandian and Laurentide ice sheets on millennium timescales. *Nature, 374*(6521), 443.

Fronval, T., & Jansen, E. (1997). Eemian and early Weichselian (140–60 ka) paleoceanography and paleoclimate in the Nordic Seas with comparisons to Holocene conditions. *Paleoceanography, 12*(3), 443-462.

Funder, S., Hjort, C., & Landvik, J. Y. (1994). The last glacial cycles in East Greenland, an overview. *Boreas, 23*(4), 283-293.

Funder, S., & Hansen, L. (1996). The Greenland ice sheet—a model for its culmination and decay during and after the last glacial maximum. *Bulletin of the Geological Society of Denmark, 42*(2), 137-152.

Funder, S., Hjort, C., Landvik, J. Y., Nam, S.-I., Reeh, N., & Stein, R. (1998). History Of A Stable Ice Margin - East Greenland During The Middle And Upper Pleistocene. *Quaternary Science Reviews, 17*(1), 77-123.

Funder, S., Jennings, A., & Kelly, M. (2004). Middle and late quaternary glacial limits in Greenland. *Developments in Quaternary Sciences, 2*(B), 425-430.

Funder, S., Kjeldsen, K. K., Kjær, K. H., & Cofaigh, C. (2011). The Greenland Ice Sheet during the past 300,000 years: A review *Developments in Quaternary Science* (Vol. 15, pp. 699-713): Elsevier.

Galaasen, E. V., Ninnemann, U. S., Irvalı, N., Kleiven, H. K. F., Rosenthal, Y., Kissel, C., & Hodell, D. A. (2014). Rapid reductions in North Atlantic deep water during the peak of the last interglacial period. *Science, 343*(6175), 1129-1132.

GEOTEK. MSCL-XCT. Retrieved from http://www.geotek.co.uk/products/mscl-xct

GEOTEK. (2014). Multi-Sensor Core Logger, Manual.

Gouzy, A., Malaizé, B., Pujol, C., & Charlier, K. (2004). Climatic "pause" during Termination II identified in shallow and intermediate waters off the Iberian margin. *Quaternary Science Reviews, 23*(14–15), 1523-1528.

Green, K. E. (1960). Ecology of some Arctic foraminifera. *Micropaleontology*, 57-78.

Greve, R. (2005). Relation of measured basal temperatures and the spatial distribution of the geothermal heat flux for the Greenland ice sheet. *Annals of Glaciology, 42*(1), 424-432.

Grousset, F., & Duplessy, J. C. (1983). Early deglaciation of the Greenland Sea during the last glacial to interglacial transition. *Marine geology, 52*(1), M11-M17.

Grousset, F., Labeyrie, L., Sinko, J., Cremer, M., Bond, G., Duprat, J., Cortijo, E., & Huon, S. (1993). Patterns of ice-rafted detritus in the glacial North Atlantic (40–55 N). *Paleoceanography, 8*(2), 175-192.

Haake, F. W., & Pflaumann, U. (1989). Late Pleistocene foraminiferal stratigraphy on the Vøring Plateau, Norwegian Sea. *Boreas, 18*(4), 343-356.

Hald, M., & Vorren, T. O. (1987). Foraminiferal stratigraphy and environment of Late Weichselian deposits on the continental shelf off Troms, Northern Norway. *Marine Micropaleontology, 12*, 129-160.

Hald, M., & Steinsund, P. I. (1992). Distribution of surface sediment benthic foraminifera in the southwestern Barents Sea. *Journal of Foraminiferal Research, 22*(4), 347-362.

Hald, M., & Korsun, S. (1997). Distribution of modern benthic foraminifera from fjords of Svalhard, European Arctic. *Journal of Foraminiferal Research, 27*, 101-122.

Hall, B., Baroni, C., Denton, G., Kelly, M. A., & Lowell, T. (2008). Relative sea-level change, Kjove Land, Scoresby Sund, East Greenland: Implications for seasonality in Younger Dryas time. *Quaternary Science Reviews, 27*(25–26), 2283-2291.

Hansen, A., & Knudsen, K. L. (1995). Recent foraminiferal distribution in Freemansundet and Early Holocene stratigraphy on Edgeøya, Svalbard. *Polar research, 14*(2), 215-238.

Hansen, B., & Østerhus, S. (2000). North atlantic–nordic seas exchanges. *Progress in oceanography, 45*(2), 109-208.

Hansen, B., Østerhus, S., Turrell, W. R., Jónsson, S., Valdimarsson, H., Hátún, H., & Olsen, S. M. (2008). The inflow of Atlantic water, heat, and salt to the nordic seas across the Greenland–Scotland ridge *Arctic–Subarctic Ocean Fluxes* (pp. 15-43): Springer.

Hansen, L., Funder, S., Murray, A. S., & Mejdahl, V. (1999). Luminescence dating of the last Weichselian Glacier advance in East Greenland. *Quaternary Science Reviews, 18*(2), 179-190.

Hass, H. C. (2002). A method to reduce the influence of ice-rafted debris on a grain size record from northern Fram Strait, Arctic Ocean. *Polar research, 21*(2), 299-306.

Hebbeln, D. (2000). Flux of ice-rafted detritus from sea ice in the Fram Strait. *Deep Sea Research Part II: Topical Studies in Oceanography, 47*(9–11), 1773-1790.

Heinrich, H. (1988). Origin and consequences of cyclic ice rafting in the northeast Atlantic Ocean during the past 130,000 years. *Quaternary Research, 29*(2), 142-152.

Hemleben, C., Spindler, M., & Anderson, O. R. (1989). *Modern planktonic foraminifera*: Springer New York.

Hemming, S. R. (2004). Heinrich events: Massive late Pleistocene detritus layers of the North Atlantic and their global climate imprint. *Reviews of Geophysics, 42*(1).

Henrich, R., Kassens, H., Vogelsang, E., & Thiede, J. (1989). Sedimentary facies of glacial-interglacial cycles in the Norwegian Sea during the last 350 ka. *Marine geology, 86*(4), 283-319.

Hjort, C. (1973). A sea correction for East Greenland. *Geologiska Föreningen i Stockholm Förhandlingar, 95*(1), 132-134. doi:10.1080/11035897309455434

Hopkins, T. S. (1991). The GIN Sea—A synthesis of its physical oceanography and literature review 1972–1985. *Earth-Science Reviews, 30*(3), 175-318.

Huddart, D., & Peacock, J. (1990). Early Holocene morainal bank sedimentology and marine ecology, Skjoldungebrae gorge, North Scoresby Land, East Greenland. *Geological Society, London, Special Publications, 53*(1), 289-305.

Hughen, K. A., Baillie, M. G., Bard, E., Beck, J. W., Bertrand, C. J., Blackwell, P. G., Buck, C. E., Burr, G, S., Cutler, K, B., & Damon, P. E. (2004). Marine04 marine radiocarbon age calibration, 0–26 cal kyr BP. *Radiocarbon, 46*(03), 1059-1086.

Husum, K., & Hald, M. (2012). Arctic planktic foraminiferal assemblages: Implications for subsurface temperature reconstructions. *Marine Micropaleontology, 96–97*, 38-47.

Huybrechts, P. (2002). Sea-level changes at the LGM from ice-dynamic reconstructions of the Greenland and Antarctic ice sheets during the glacial cycles. *Quaternary Science Reviews, 21*(1), 203-231.

Håkansson, L., Briner, J., Alexanderson, H., Aldahan, A., & Possnert, G. (2007). 10Be ages from central east Greenland constrain the extent of the Greenland ice sheet during the Last Glacial Maximum. *Quaternary Science Reviews, 26*(19–21), 2316-2321.

Ingólfsson, Ó., Frich, P., Funder, S., & Humlum, O. L. E. (1990). Paleoclimatic implications of an early Holocene glacier advance on Disko Island, West Greenland. *Boreas, 19*(4), 297-311.

Irvalı, N., Ninnemann, U. S., Galaasen, E. V., Rosenthal, Y., Kroon, D., Oppo, D. W., Kleiven, H. F., Darling, K. F., & Kissel, C. (2012). Rapid switches in subpolar North Atlantic hydrography and climate during the Last Interglacial (MIS 5e). *Paleoceanography, 27*(2).

Jansen, E., Sejrup, H. P., Fjæran, T., Hald, M., Holtedahl, H., & Skarbø, O. (1983). Late Weichselian paleoceanography of the southeastern Norwegian Sea. *Norsk geologisk tidsskrift* (2-3).

Jansen, E. (1989). The use of stable oxygen and carbon isotope stratigraphy as a dating tool. *Quaternary International, 1*, 151-166.

Jennings, A. E., & Helgadottir, G. (1994). Foraminiferal assemblages from the fjords and shelf of eastern Greenland. *Journal of Foraminiferal Research, 24*(2), 123-144.

Jennings, A. E., Knudsen, K. L., Hald, M., Hansen, C. V., & Andrews, J. T. (2002). A mid-Holocene shift in Arctic sea-ice variability on the East Greenland Shelf. *The Holocene, 12*(1), 49-58.

Jennings, A. E., Weiner, N. J., Helgadottir, G., & Andrews, J. T. (2004). Modern foraminiferal faunas of the southwestern to northern Iceland shelf: oceanographic and environmental controls. *Journal of Foraminiferal Research, 34*(3), 180-207.

Jennings, A., Hald, M., Smith, M., & Andrews, J. (2006). Freshwater forcing from the Greenland Ice Sheet during the Younger Dryas: evidence from southeastern Greenland shelf cores. *Quaternary Science Reviews, 25*(3), 282-298.

Jennings, A., Andrews, J., & Wilson, L. (2011). Holocene environmental evolution of the SE Greenland Shelf North and South of the Denmark Strait: Irminger and East Greenland current interactions. *Quaternary Science Reviews, 30*(7–8), 980-998.

Jessen, S. P., & Rasmussen, T. L. (2015). Sortable silt cycles in Svalbard slope sediments 74–0 ka. *Journal of Quaternary Science, 30*(8), 743-753.

Johannessen, T., Jansen, E., Flatøy, A., & Ravelo, A. C. (1994). The Relationship between Surface Water Masses, Oceanographic Fronts and Paleoclimatic Proxies in Surface Sediments of the Greenland, Iceland, Norwegian Seas. In Zahn, R., Pedersen, T, F., Kaminski, M, A., Labeyrie, L (eds) *Carbon Cycling in the Glacial Ocean: Constraints on the Ocean's Role in Global Change.* NATO ASI Series (Series 1: Global Environmental Change), vol 17. Springer, Berlin, Heidelberg.

John, K. S., Flower, B. P., & Krissek, L. (2004). Evolution of iceberg melting, biological productivity, and the record of Icelandic volcanism in the Irminger basin since 630 ka. *Marine geology, 212*(1), 133-152.

Johnsen, S., Clausen, H., Dansgaard, W., Fuhrert, K., Gundestrup, N., Hammer, C., Iversen, P., Jouzel, I., & Stauffer, B. (1992). Irregular glacial interstadials, recorded in a new Greenland. *Nature, 3*, 24.

Jones, R. W. (2011). *Applications of Palaeontology: Techniques and Case Studies*: Cambridge University Press.

Jones, R. W. (2014). *Foraminifera and their Applications*: Cambridge University Press.

Karpuz, N. K., & Jansen, E. (1992). A high-resolution diatom record of the last deglaciation from the SE Norwegian Sea: Documentation of rapid climatic changes. *Paleoceanography, 7*(4), 499-520.

Kellogg, T. B. (1976). Late Quaternary climatic changes: evidence from deep-sea cores of Norwegian and Greenland Seas. *Geological Society of America Memoirs, 145*, 77-110.

Kellogg, T. B., Duplessy, J. C., & Shackleton, N. J. (1978). Planktonic foraminiferal and oxygen isotopic stratigraphy and paleoclimatology of Norwegian Sea deep-sea cores. *Boreas, 7*(1), 61-73.

Kellogg, T. B. (1980). Paleoclimatology and paleo-oceanography of the Norwegian and Greenland seas: glacial-interglacial contrasts. *Boreas, 9*(2), 115-137.

Kelly, M., & Bennike, O. (1992). The Quaternary geology of central North Greenland. *Rapport Grønlands Geologiske Undersøgelse, 153*, 34-34.

Kelly, M. A., Lowell, T. V., Hall, B. L., Schaefer, J. M., Finkel, R. C., Goehring, B. M., Alley, R. B., & Denton, G. H. (2008). A 10Be chronology of late glacial and Holocene mountain glaciation in the Scoresby Sund region, east Greenland: implications for seasonality during late glacial time. *Quaternary Science Reviews, 27*(25–26), 2273-2282.

Kissel, C., Laj, C., Labeyrie, L., Dokken, T., Voelker, A., & Blamart, D. (1999). Rapid climatic variations during marine isotopic stage 3: magnetic analysis of sediments from Nordic Seas and North Atlantic. *Earth and Planetary Science Letters, 171*(3), 489-502.

Klitgaard-Kristensen, D., Rasmussen, T., Sejrup, H., Haflidason, H., & van Weering, T. C. (1998). Rapid changes in the oceanic fronts in the Norwegian Sea during the last deglaciation: implications for the Younger Dryas cooling event. *Marine geology, 152*(1), 177-188.

Knies, J., Kleiber, H. P., Matthiessen, J., Miller, C., & Nowaczyk, N. (2001). Marine ice-rafted debris records constrain maximum extent of Saalian and Weichselian ice-sheets along the northern Eurasian margin. *Global and Planetary Change 31,* 45 – 64.

Knudsen, K. L. (1984). Foraminiferal stratigraphy in a marine Eemian-Weichselian sequence at Apholm, North Jutland. *Bulletin of the Geological Society of Denmark, 32*(3-4), 169-180.

Kohfeld, K. E., Fairbanks, R. G., Smith, S. L., & Walsh, I. D. (1996). *Neogloboquadrina pachyderma* (sinistral coiling) as paleoceanographic tracers in polar oceans: Evidence from Northeast Water Polynya plankton tows, sediment traps, and surface sediments. *Paleoceanography, 11*(6), 679-699.

Kreveld, S. V., Sarnthein, M., Erlenkeuser, H., Grootes, P., Jung, S., Nadeau, M. J., Pflaumann, U., & Voelker, A. (2000). Potential links between surging ice sheets, circulation changes, and the Dansgaard-Oeschger Cycles in the Irminger Sea, 60–18 Kyr. *Paleoceanography, 15*(4), 425-442.

Labeyrie, L. D., & Duplessy, J. C. (1985). Changes in the oceanic 13C12C ratio during the last 140 000 years: High-latitude surface water records. *Palaeogeography, Palaeoclimatology, Palaeoecology, 50*(2-3), 217-240.

Labeyrie, L., Vidal, L., Cortijo, E., Paterne, M., Arnold, M., Duplessy, J. C., Vautravers, M., Labracherie, M., Duprat, J., Turon, J, L., Grousset, F., & Weering, T. V. (1995). Surface and Deep Hydrology of the Northern Atlantic Ocean during the past 150 000 Years. *Philosophical Transactions of the Royal Society of London. Series B: Biological Sciences, 348*(1324), 255.

Lagoe, M. B. (1977). *Recent benthic foraminifera from the central Arctic Ocean*. (Master's thesis), University of Wisconsin, Madison.

Lagoe, M. B. (1979). Recent Arctic foraminifera: an overview.

Lambeck, K., Yokoyama, Y., & Purcell, T. (2002). Into and out of the Last Glacial Maximum: sea-level change during Oxygen Isotope Stages 3 and 2. *Quaternary Science Reviews, 21*(1–3), 343-360.

Landvik, J. Y. (1994). The last glaciation of Germania Land and adjacent areas, northeast Greenland. *Journal of Quaternary Science, 9*(1), 81-92.

Lane, T. P., Roberts, D. H., Rea, B. R., Cofaigh, C. Ó., Vieli, A., & Rodés, A. (2013). Controls upon the Last Glacial maximum deglaciation of the northern Uummannaq ice stream system, West Greenland. *Quaternary Science Reviews, 92*, 324-344.

Larsen, H. C., Saunders, A. D., Clift, P. D., Beget, J., Wei, W., Spezzaferri, S., Ali, J., Cambray, H., Demant, A., Fitton, G., Fram, M, S., Faukuma, K., Gieskes, J., Holmes, M, A., Hunt, J., Lacasse, C., Larsen, L, M., Lykke-Andersen, H., Meltser, A., Morrison, M, L., Nemoto, N., Okay, N., Saito, S., Slnto, C., Stax, R., Vallier, T, L., Vandamme, D., & Werner, R. (1994).

Seven Million Years of Glaciation in Greenland. *Papers in the Earth and Atmospheric Sciences* (55).

Larsen, N. K., Kjær, K. H., Funder, S., Möller, P., van der Meer, J. J. M., Schomacker, A., Linge, H., & Darby, D. A. (2010). Late Quaternary glaciation history of northernmost Greenland – Evidence of shelf-based ice. *Quaternary Science Reviews, 29*(25–26), 3399-3414.

Larsen, N. K., Kjær, K. H., Olsen, J., Funder, S., Kjeldsen, K. K., & Nørgaard-Pedersen, N. (2011). Restricted impact of Holocene climate variations on the southern Greenland Ice Sheet. *Quaternary Science Reviews, 30*(21–22), 3171-3180.

Lazar, K. B., Polyak, L., & Dipre, G. R. (2016). Re-Examination of the use of Cassidulina neoteretis as a Pleistocene Biostratigrephic Marker in the Arctic Ocean. *The Journal of Foraminiferal Research, 46*(2), 115.

Lecavalier, B. S., Milne, G. A., Simpson, M. J. R., Wake, L., Huybrechts, P., Tarasov, L., . . . Larsen, N. K. (2014). A model of Greenland ice sheet deglaciation constrained by observations of relative sea level and ice extent. *Quaternary Science Reviews, 102*, 54-84.

Lemke, P., Ren, J., Alley, R. B., Allison, I., Carrasco, J., Flato, G., Fujii, Y., Kaser, G., Mote, P., Thomas, R. H., & Zhang, T. (2007). Observations: Changes in Snow, Ice and Frozen Ground. In S. Solomon, D. Qin, M. Manning, Z. Chen, M. Marquis, K. B. Averyt, M. Tignor, & H. L. Miller (Eds.), *Climate Change 2007: The Pysical Science Basis. Contribution of Working Group I to the Fourth Assessment Report of the Intergovernmental Panel on Climate Change* (pp. 337-383). Cambridge, UK: Cambridge University Press.

Letréguilly, A., Reeh, N., & Huybrechts, P. (1991). The Greenland ice sheet through the last glacial-interglacial cycle. *Palaeogeography, Palaeoclimatology, Palaeoecology, 90*(4), 385-394.

Lisiecki, L. LR04 - Marine Isotope Stage boundaries. Retrieved from http://www.lorraine-lisiecki.com/LR04_MISboundaries.txt

Lisiecki, L. E., & Raymo, M. E. (2005). A Pliocene-Pleistocene stack of 57 globally distributed benthic δ18O records. *Paleoceanography, 20*(1).

Lloyd, J. M., Park, L. A., Kuijpers, A., & Moros, M. (2005). Early Holocene palaeoceanography and deglacial chronology of Disko Bugt, West Greenland. *Quaternary Science Reviews, 24*(14–15), 1741-1755.

Lofi, J., & Weber, O. (2001). SCOPIX-digital processing of X-ray images for the enhancement of sedimentary structures in undisturbed core slabs. *Geo-Marine Letters, 20*(3), 182-186.

Lyså, A., & Landvik, J. Y. (1994). The lower Jyllandselv succession: evidence for three Weichselian glacier advances over coastal Jameson Land, East Greenland. *Boreas, 23*(4), 432-446.

Mackensen, A., Sejrup, H., & Jansen, E. (1985). The distribution of living benthic foraminifera on the continental slope and rise off southwest Norway. *Marine Micropaleontology, 9*(4), 275-306.

Mackensen, A., & Hald, M. (1988). *Cassidulina teretis* Tappan and *C. laevigata* d'Orbigny; their modern and late Quaternary distribution in northern seas. *Journal of Foraminiferal Research, 18*(1), 16-24.

Mangerud, J., Lie, S. E., Furnes, H., Kristiansen, I. L., & Lømo, L. (1984). A Younger Dryas ash bed in western Norway, and its possible correlations with tephra in cores from the Norwegian Sea and the North Atlantic. *Quaternary Research, 21*(1), 85-104.

Mangerud, J., & Funder, S. (1994). The interglacial-glacial record at the mouth of Scoresby Sund, East Greenland. *Boreas, 23*, 349-358.

Mangerud, J., Bondevik, S., Gulliksen, S., Hufthammer, A. K., & Høisæter, T. (2006). Marine 14 C reservoir ages for 19th century whales and molluscs from the North Atlantic. *Quaternary Science Reviews, 25*(23), 3228-3245.

Marienfeld, P. (1992). Postglacial Sedimentary History of Scoresby Sund, East Greenland. *Polarforschung, 60*(3), 181-195.

Martinson, D. G., Pisias, N. G., Hays, J. D., Imbrie, J., Moore, T. C., & Shackleton, N. J. (1987). Age dating and the orbital theory of the ice ages: development of a high-resolution 0 to 300,000-year chronostratigraphy. *Quaternary Research, 27*(1), 1-29.

Maslin, M. A., Shackleton, N. J., & Pflaumann, U. (1995). Surface water temperature, salinity, and density changes in the northeast Atlantic during the last 45,000 years: Heinrich events, deep water formation, and climatic rebounds. *Paleoceanography, 10*(3), 527-544.

Maslin, M. A., & Swann, G. E. A. (2006). Isotopes In Marine Sediments. In M. J. Leng (Ed.), *Isotopes in palaeoenvironmental research* (Vol. 10): Springer.

McCabe, A. M., Haynes, J. R., & Macmillan, N. F. (1986). Late-Pleistocene tidewater glaciers and glaciomarine sequences from north County Mayo, Republic of Ireland. *Journal of Quaternary Science, 1*(1), 73-84.

McCave, I., Manighetti, B., & Beveridge, N. (1995a). Circulation in the glacial North Atlantic inferred from grain-size measurements. *Nature, 374*(6518), 149.

McCave, I., Manighetti, B., & Robinson, S. (1995b). Sortable silt and fine sediment size/composition slicing: parameters for palaeocurrent speed and palaeoceanography. *Paleoceanography, 10*(3), 593-610.

McCave, I., & Hall, I. R. (2006). Size sorting in marine muds: Processes, pitfalls, and prospects for paleoflow-speed proxies. *Geochemistry, Geophysics, Geosystems, 7*(10).

McManus, J. F., Oppo, D. W., & Cullen, J. L. (1999). A 0.5-million-year record of millennial-scale climate variability in the North Atlantic. *Science, 283*(5404), 971-975.

Mienert, J., Andrews, J. T., & Milliman, J. D. (1992). The East Greenland continental margin (65°N) since the last deglaciation: Changes in seafloor properties and ocean circulation. *Marine geology, 106*(3), 217-238.

Miller, A. A., Scott, D. B., & Medioli, F. S. (1982). *Elphidium excavatum* (Terquem); ecophenotypic versus subspecific variation. *Journal of Foraminiferal Research, 12*(2), 116-144.

Mix, A. C., & Ruddiman, W. F. (1984). Oxygen-isotope analyses and Pleistocene ice volumes. *Quaternary Research, 21*(1), 1-20.

Mokeddem, Z., & McManus, J. F. (2016). Persistent climatic and oceanographic oscillations in the subpolar North Atlantic during the MIS 6 glaciation and MIS 5 interglacial. *Paleoceanography, 31*(6), 758-778.

Moros, M., Endler, R., Lackschewitz, K., Wallrabe-Adams, H., Mienerr, J., & Lemke, W. (1997). Physical properties of Reykjanes Ridge sediments and their linkage to high-resolution Greenland Ice Sheet Project 2. *Paleoceanography, 12*(5), 687-695.

Mortensen, K. (2016, 11.11). MSCL with spectrophotometer - Multi sensor core logger. Retrieved from https://uit.no/om/enhet/artikkel?p_document_id=390245&p_dimension_id=88137&men=28927

Mudie, P., Keen, C., Hardy, I., & Vilks, G. (1984). Multivariate analysis and quantitative paleoecology of benthic foraminifera in surface and Late Quaternary shelf sediments, northern Canada. *Marine Micropaleontology, 8*(4), 283-313.

Munsell, R. (1973). Soil color charts. *Macbeth Division of Kollmorgen Corporation, New York*, 19.

Murray, J. W. (1991). *Ecology and Palaeoecology of Benthic Foraminifera*: Longman Scientific & Technical.

Nam, S.-I., Stein, R., Grobe, H., & Hubberten, H. (1995). Late Quaternary glacial-interglacial changes in sediment composition at the East Greenland continental margin and their paleoceanographic implications. *Marine geology, 122*(3), 243-262.

Nam, S.-I., & Stein, R. (1999). Late Quaternay variations in sediment accumulation rates and their paleoenvironmental implications: A case study from the East Greenland Continental Margin, On the determination of sediment accumulation rates (P Bruns, HC Hass, eds) *GeoResearch Forum 5*, Trans Tech Publications, 223 – 240.

Nave, S., Labeyrie, L., Gherardi, J., Caillon, N., Cortijo, E., Kissel, C., & Abrantes, F. (2007). Primary productivity response to Heinrich events in the North Atlantic Ocean and Norwegian Sea. *Paleoceanography, 22*(3).

NGRIP Members. (2004). High-resolution record of Northern Hemisphere climate extending into the last interglacial period. *Nature, 431*, 147-151.

Nørgaard-Pedersen, N. (1997). *Late quaternary Arctic Ocean sediment records: surface ocean conditions and provenance of ice rafted debris* (Doctoral dissertation), Christian Albrechts University, Kiel.

Oppo, D. W., & Lehman, S. J. (1995). Suborbital timescale variability of North Atlantic Deep Water during the past 200,000 years. *Paleoceanography, 10*(5), 901-910.

Oppo, D., McManus, J., & Cullen, J. (1998). Abrupt climate events 500,000 to 340,000 years ago: Evidence from subpolar North Atlantic sediments. *Science, 279*(5355), 1335-1338.

Phleger, F. B. (1960). *Ecology and Distribution of Recent Foraminifera*. Baltimore: John Hopkins Press.

Polyak, L., Korsun, S., Febo, L. A., Stanovoy, V., Khusid, T., Hald, M., Paulsen, B. E., & Lubinski, D. J. (2002). Benthic foraminiferal assemblages from the southern Kara Sea, a river-influenced Arctic marine environment. *Journal of Foraminiferal Research, 32*(3), 252-273.

Polyak, L., & Solheim, A. (1994). Late-and postglacial environments in the northern Barents Sea west of Franz Josef Land. *Polar research, 13*(2), 197-207.

Prins, M., Bouwer, L., Beetw, C., Troelstra, S., Weltha, G., Kruk, R., Kuijpers, A., & Vroon, P. (2002). Ocean circulation and iceberg discharge in the glacial North Atlantic: Inferences from unmixing of sediment size distributions. *Geology, 30*(6), 555-558.

Quadfasel, D., Gascard, J.-C., & Koltermann, K.-P. (1987). Large-scale oceanography in Fram Strait during the 1984 Marginal Ice Zone Experiment. *Journal of Geophysical Research: Oceans, 92*(C7), 6719-6728.

Quinn, R., Bull, J. M., & Dix, J. K. (1998). Optimal Processing of Marine High-Resolution Seismic Reflection (Chirp) Data. *Marine Geophysical Researches, 20*(1), 13-20.

Rasmussen, T. L., Thomsen, E., Weering, T. C., & Labeyrie, L. (1996a). Rapid changes in surface and deep water conditions at the Faeroe Margin during the last 58,000 years. *Paleoceanography, 11*(6), 757-771.

Rasmussen, T. L., Van Weering, T. C., & Labeyrie, L. (1996b). High resolution stratigraphy of the Faeroe-Shetland Channel and its relation to North Atlantic paleoceanography: the last 87 kyr. *Marine geology, 131*(1-2), 75-88.

Rasmussen, T. L., Thomsen, E., Labeyrie, L., & van Weering, T. C. (1996c). Circulation changes in the Faeroe-Shetland Channel correlating with cold events during the last glacial period (58–10 ka). *Geology, 24*(10), 937-940.

Rasmussen, T. L., Balbon, E., Thomsen, E., Labeyrie, L., & Van Weering, T. C. (1999). Climate records and changes in deep outflow from the Norwegian Sea~ 150–55 ka. *Terra Nova, 11*(2-3), 61-66.

Rasmussen, T. L., & Thomsen, E. (2004). The role of the North Atlantic Drift in the millennial timescale glacial climate fluctuations. *Palaeogeography, Palaeoclimatology, Palaeoecology, 210*(1), 101-116.

Rasmussen, T. L., & Thomsen, E. (2008). Warm Atlantic surface water inflow to the Nordic seas 34–10 calibrated ka BP. *Paleoceanography, 23*(1).

Rasmussen, T. L., & Thomsen, E. (2014). Brine formation in relation to climate changes and ice retreat during the last 15,000 years in Storfjorden, Svalbard, 76–78°N. *Paleoceanography, 29*(10), 911-929.

Rasmussen, T. L., Thomsen, E., & Nielsen, T. (2014). Water mass exchange between the Nordic seas and the Arctic Ocean on millennial timescale during MIS 4–MIS 2. *Geochemistry, Geophysics, Geosystems, 15*(3), 530-544.

Reimer, P. J., Bard, E., Bayliss, A., Beck, J. W., Blackwell, P. G., Ramsey, C. B., Buck, C. E., Cheng, H., Edwards, R. L., & Friedrich, M. (2013). IntCal13 and Marine13 radiocarbon age calibration curves 0–50,000 years cal BP. *Radiocarbon, 55*(4), 1869-1887.

Risebrobakken, B., Balbon, E., Dokken, T., Jansen, E., Kissel, C., Labeyrie, L., Richter, T., & Senneset, L. (2006). The penultimate deglaciation: high-resolution paleoceanographic evidence from a north–south transect along the eastern Nordic seas. *Earth and Planetary Science Letters, 241*(3), 505-516.

Risebrobakken, B., Moros, M., Ivanova, E. V., Chistyakova, N., & Rosenberg, R. (2010). Climate and oceanographic variability in the SW Barents Sea during the Holocene. *The Holocene, 20*(4), 609-621.

Roberts, D. H., Long, A. J., Schnabel, C., Davies, B. J., Xu, S., Simpson, M. J. R., & Huybrechts, P. (2009). Ice sheet extent and early deglacial history of the southwestern sector of the Greenland Ice Sheet. *Quaternary Science Reviews, 28*(25–26), 2760-2773.

Robinson, S. G., Maslin, M. A., & McCave, I. N. (1995). Magnetic susceptibility variations in Upper Pleistocene deep-sea sediments of the NE Atlantic: Implications for ice rafting and paleocirculation at the last glacial maximum. *Paleoceanography, 10*(2), 221-250.

Ruddiman, W. F. (2013). *Earth's Climate: Past and Future.* W.H.Freeman & Co Ltd.

Ruddiman, W. F., & McIntyre, A. (1981). The North Atlantic Ocean during the last deglaciation. *Palaeogeography, Palaeoclimatology, Palaeoecology, 35*, 145-214.

Rudels, B. (1989). The formation of Polar Surface Water, the ice export and the exchanges through the Fram Strait. *Progress in Oceanography, 22*(3), 205-248.

Rudels, B., Björk, G., Nilsson, J., Winsor, P., Lake, I., & Nohr, C. (2005). The interaction between waters from the Arctic Ocean and the Nordic Seas north of Fram Strait and along the East Greenland Current: results from the Arctic Ocean-02 Oden expedition. *Journal of Marine Systems, 55*(1), 1-30.

Rytter, F., Knudsen, K. L., Seidenkrantz, M.-S., & Eiríksson, J. (2002). Modern distribution of benthic foraminifera on the North Icelandic shelf and slope. *Journal of Foraminiferal Research, 32*(3), 217-244.

Sarnthein, M., Jansen, E., Weinelt, M., Arnold, M., Duplessy, J. C., Erlenkeuser, H., Flatøy, A., Johannessen, G., Johannessen, T., & Jung, S. (1995). Variations in Atlantic surface ocean paleoceanography, 50°-80° N: A time-slice record of the last 30,000 years. *Paleoceanography, 10*(6), 1063-1094.

Sarnthein, M., & Tiedemann, R. (1990). Younger Dryas-Style Cooling Events at Glacial Terminations I-VI at ODP Site 658: Associated benthic δ13C anomalies constrain meltwater hypothesis. *Paleoceanography, 5*(6), 1041-1055.

Schiebel, R., & Hemleben, C. (2016). *Planktic Foraminifers in the Modern Ocean: Ecology, Biogeochemistry, and Application*: Springer Berlin Heidelberg.

Schnitker, D. (1994). Deep-sea benthic foraminifers: food and bottom water masses *Carbon Cycling in the glacial ocean: constraints on the ocean's role in Global Change* (pp. 539-554): Springer.

Schröder, J. (2014). *The Late Quaternary glacial history (MIS 1 - 5b/c) northeast of Scoresby Sund (East Greenland) seen in core HH12-092GC.* (Geology Project - GEO-3222), University of Tromsø, The Arctic University of Norway.

Schröder-Adams, C., Mudie, P., Cole, F., & Medioli, F. (1990). Late Holocene benthic formainifera beneath perennial sea ice on an Arctic continental shelf. *Marine geology, 93*, 225-242.

Schweger, C. E., & Matthews, J. V. (1991). The last (Koy-Yukon) interglaciation in the Yukon: comparisons with Holocene and interstadial pollen records. *Quaternary International, 10*, 85-94.

Seidenkrantz, M.-S. (1995). Cassidulina teretis Tappan and Cassidulina neoteretis new species (Foraminifera): stratigraphic markers for deep sea and outer shelf areas. *Journal of Micropalaeontology, 14*(2), 145-157.

Seidenkrantz, M.-S., Bornmalm, L., Johnsen, S. J., Knudsen, K. L., Kuijpers, A., Lauritzen, S.-E., Leroy, S. A. G., Mergeal, I., Schweger, C., & Van Vliet-Lanoë, B. (1996). Two-step deglaciation at the oxygen isotope stage 6/5e transition: the Zeifen-Kattegat climate oscillation. *Quaternary Science Reviews, 15*(1), 63-75.

Seidenkrantz, M.-S., Kuijpers, A., Aagaard-Sørensen, S., Andersson, S., Lindgreen, H., Ploug, J., Przybylo, P., Snowball, I., & Ivanov, M. (2010). Glacial ocean circulation and shelf edge glaciation offshore SW Greenland during the past 75.000 years. *Paper presented at the EGU General Assembly Conference Abstracts 12*, 4721.

Sejrup, H., Birks, H., Kristensen, D. K., & Madsen, H. (2004). Benthonic foraminiferal distributions and quantitative transfer functions for the northwest European continental margin. *Marine Micropaleontology, 53*(1), 197-226.

Sejrup, H. P., & Guilbault, J. P. (1980). *Cassidulina reniforme* and *C. obtusa* (Foraminifera), taxonomy, distribution, and ecology. *Sarsia, 65*(2), 79-85.

Shackleton, N. J., & Opdyke, N. D. (1973). Oxygen isotope and palaeomagnetic stratigraphy of Equatorial Pacific core V28-238: Oxygen isotope temperatures and ice volumes on a 105 year and 106 year scale. *Quaternary Research, 3*(1), 39-55.

Shackleton, N. J., & Pisias, N. (1985). Atmospheric carbon dioxide, orbital forcing, and climate. *The Carbon Cycle and Atmospheric CO: Natural Variations Archean to Present*, 303-317.

Shackleton, N. J., Sánchez-Goñi, M. F., Pailler, D., & Lancelot, Y. (2003). Marine Isotope Substage 5e and the Eemian Interglacial. *Global and Planetary Change, 36*(3), 151-155.

Simpson, M. J. R., Milne, G. A., Huybrechts, P., & Long, A. J. (2009). Calibrating a glaciological model of the Greenland ice sheet from the Last Glacial Maximum to present-day using field observations of relative sea level and ice extent. *Quaternary Science Reviews, 28*(17–18), 1631-1657.

Simstich, J., Sarnthein, M., & Erlenkeuser, H. (2003). Paired δ 18 O signals of *Neogloboquadrina pachyderma* (s) and *Turborotalita quinqueloba* show thermal stratification structure in Nordic Seas. *Marine Micropaleontology, 48*(1), 107-125.

Solheim, A., Faleide, J. I., Andersen, E. S., Elverhøi, A., Forsberg, C. F., Vanneste, K., Uenzelmann-Neben, G., & Channell, J. E. T. (1998). Late Cenozoic Seismic Stratigraphy and Glacial Geological Development of the East Greenland and Svalbard-Barents Sea Continental Margins. *Quaternary Science Reviews, 17*(1), 155-184.

Sparrenbom, C. J., Bennike, O., Björck, S., & Lambeck, K. (2006). Relative sea-level changes since 15 000 cal. yr BP in the Nanortalik area, southern Greenland. *Journal of Quaternary Science, 21*(1), 29-48.

Spielhagen, R. F., Baumann, K.-H., Erlenkeuser, H., Nowaczyk, N. R., Nørgaard-Pedersen, N., Vogt, C., & Weiel, D. (2004). Arctic Ocean deep-sea record of northern Eurasian ice sheet history. *Quaternary Science Reviews, 23*(11), 1455-1483.

Stein, R., Grobe, H., Hubberten, H., Marienfeld, P., & Nam, S. (1993). Latest Pleistocene to Holocene changes in glaciomarine sedimentation in Scoresby Sund and along the adjacent East Greenland Continental Margin: Preliminary results. *Geo-Marine Letters, 13*(1), 9-16.

Stein, R., Nam, S.-i., Grobe, H., & Hubberten, H. (1996). Late Quaternary glacial history and short-term ice-rafted debris fluctuations along the East Greenland continental margin. *Geological Society, London, Special Publications, 111*(1), 135-151.

Steinsund, P. I., & Hald, M. (1994). Recent calcium carbonate dissolution in the Barents Sea: paleoceanographic applications. *Marine geology, 117*(1-4), 303-316.

Stoner, J. S., Channell, J. E., & Hillaire-Marcel, C. (1995). Magnetic properties of deep-sea sediments off southwest Greenland: Evidence for major differences between the last two deglaciations. *Geology, 23*(3), 241-244.

Streeter, S. S., Belanger, P. E., Kellogg, T. B., & Duplessy, J. C. (1982). Late Pleistocene paleo-oceanography of the Norwegian-Greenland Sea: benthic foraminiferal evidence. *Quaternary Research, 18*(1), 72-90.

Stuiver, M., & Reimer, P. J. (1993). Extended 14 C data base and revised CALIB 3.0 14 C age calibration program. *Radiocarbon, 35*(01), 215-230.

Survey, U. S. G. WHSC Bathymetry systems. Retrieved from https://woodshole.er.usgs.gov/operations/sfmapping/swath.htm

Swift, J. H. (1984). The circulation of the Denmark Strait and Iceland-Scotland overflow waters in the North Atlantic. *Deep Sea Research Part A. Oceanographic Research Papers, 31*(11), 1339-1355.

Swift, J. H., & Aagaard, K. (1981). Seasonal transitions and water mass formation in the Iceland and Greenland seas. *Deep Sea Research Part A. Oceanographic Research Papers, 28*(10), 1107-1129.

Syvitski, J., Andrews, J., & Dowdeswell, J. (1996). Sediment deposition in an iceberg-dominated glacimarine environment, East Greenland: basin fill implications. *Global and Planetary Change, 12*(1-4), 251-270.

Tappan, H., & Loeblich, A. R. (1988). Foraminiferal evolution, diversification, and extinction. *Journal of Paleontology, 62*(05), 695-714.

Tarasov, L., & Peltier, W. R. (2003). Greenland glacial history, borehole constraints, and Eemian extent. *Journal of Geophysical Research: Solid Earth, 108*(B3).

Thomas, R., Csatho, B., Davis, C., Kim, C., Krabill, W., Manizade, S., McConnell, J., & Sonntag, J. (2001). Mass balance of higher-elevation parts of the Greenland ice sheet. *Journal of Geophysical Research: Atmospheres, 106*(D24), 33707-33716.

Thornalley, D. J., Barker, S., Becker, J., Hall, I. R., & Knorr, G. (2013). Abrupt changes in deep Atlantic circulation during the transition to full glacial conditions. *Paleoceanography, 28*(2), 253-262.

Tripati, A. K., Eagle, R. A., Morton, A., Dowdeswell, J. A., Atkinson, K. L., Bahé, Y., Dawber, C. F., Khadun, E., Shaw, R. M. H., Shorttle, O., & Thanabalasundaram, L. (2008). Evidence for glaciation in the Northern Hemisphere back to 44 Ma from ice-rafted debris in the Greenland Sea. *Earth and Planetary Science Letters, 265*(1–2), 112-122.

Urey, H. C. (1948). Oxygen isotopes in nature and in the laboratory. *Science, 108*(2810), 489-496.

Vidal, L., Labeyrie, L., Cortijo, E., Arnold, M., Duplessy, J. C., Michel, E., Becqué, S., & van Weering, T. C. E. (1997). Evidence for changes in the North Atlantic Deep Water linked to meltwater surges during the Heinrich events. *Earth and Planetary Science Letters, 146*(1), 13-27.

Vidal, L., Schneider, R., Marchal, O., Bickert, T., Stocker, T., & Wefer, G. (1999). Link between the North and South Atlantic during the Heinrich events of the last glacial period. *Climate Dynamics, 15*(12), 909-919.

Voelker, A. H., Sarnthein, M., Grootes, P. M., Erlenkeuser, H., Laj, C., Mazaud, A., Nadeau, M. J., & Schleicher, M. (1998). Correlation of marine 14 C ages from the Nordic Seas with the GISP2 isotope record: Implications for 14 C calibration beyond 25 ka BP. *Radiocarbon, 40*(01), 517-534.

Vogt, C., Knies, J., Spielhagen, R. F., & Stein, R. (2001). Detailed mineralogical evidence for two nearly identical glacial/deglacial cycles and Atlantic water advection to the Arctic Ocean during the last 90,000 years. *Global and Planetary Change, 31*(1–4), 23-44.

Volkmann, R. (2000). Planktic foraminifer ecology and stable isotope geochemistry in the Arctic Ocean: implications from water column and sediment surface studies for quantitative

reconstructions of oceanic parameters. *Berichte zur Polarforschung (Reports on Polar Research), 361*.

Wastegård, S., Björck, S., Possnert, G., & Wohlfarth, B. (1998). Evidence for the occurrence of Vedde Ash in Sweden: radiocarbon and calendar age estimates. *Journal of Quaternary Science, 13*(3), 271-274.

Wastegård, S., & Rasmussen, T. L. (2001). New tephra horizons from Oxygen Isotope Stage 5 in the North Atlantic: correlation potential for terrestrial, marine and ice-core archives. *Quaternary Science Reviews, 20*(15), 1587-1593.

Weltje, G. J., & Prins, M. A. (2003). Muddled or mixed? Inferring palaeoclimate from size distributions of deep-sea clastics. *Sedimentary Geology, 162*(1), 39-62.

Williams, K. M. (1993). Ice Sheet and Ocean Interactions, Margin of the East Greenland Ice Sheet (14 Ka to Present): Diatom Evidence. *Paleoceanography, 8*(1), 69-83.

Wolf, T. C., & Thiede, J. (1991). History of terrigenous sedimentation during the past 10 my in the North Atlantic (ODP Legs 104 and 105 and DSDP Leg 81). *Marine geology, 101*(1-4), 83-102.

Wollenburg, J., & Kuhnt, W. (2000). The response of benthic foraminifers to carbon flux and primary production in the Arctic Ocean. *Marine Micropaleontology, 40*(3), 189-231.

Wollenburg, J. E., Kuhnt, W., & Mackensen, A. (2001). Changes in Arctic Ocean paleoproductivity and hydrography during the last 145 kyr: The benthic foraminiferal record. *Paleoceanography, 16*(1), 65-77.

Wollenburg, J. E., & Mackensen, A. (1998). Living benthic foraminifers from the central Arctic Ocean: faunal composition, standing stock and diversity. *Marine Micropaleontology, 34*(3), 153-185.

Woodroffe, S. A., Long, A. J., Lecavalier, B. S., Milne, G. A., & Bryant, C. L. (2014). Using relative sea-level data to constrain the deglacial and Holocene history of southern Greenland. *Quaternary Science Reviews, 92*, 345-356.

Zreda, M., England, J., Phillips, F., Elmore, D., & Sharma, P. (1999). Unblocking of the Nares Strait by Greenland and Ellesmere ice-sheet retreat 10,000 years ago. *Nature, 398*(6723), 139-142.

Appendix A: Benthic species list and distribution

Species (*Genus only)	Total number identified in samples
***Oridorsalis umbonatus* (Reuss, 1851)**	2292
***Cassidulina neoteretis* (Seidenkrantz, 1995)**	2318
***Triloculina trihedra* (Loeblich & Tappan, 1953)**	649
***Cassidulina reniforme* (Nørvang, 1945)**	615
***Cibicides wuellerstorfi* (Schwager, 1866)**	559
***Stainforthia loeblichi* (Feyling-Hanssen, 1954)**	345
***Astrononion gallowayi* (Loeblich & Tappan, 1953)**	206
***Epistominella arctica* (Green, 1959)**	194
***Elphidium excavatum* (Terquem, 1875)**	125
****Lagena spp.* (Walker & Boys, 1798)**	90
***Nonionella iridea* (Heron-Allen & Earland, 1932)**	89
****Miliolinella spp.* (Wiesner, 1931)**	78
***Melonis barleeanus* (Williamson, 1858)**	70
***Cibicides lobatulus* (Walker & Jacob, 1798)**	33
***Ioanella tumidula* (Brady, 1884)**	25

***Quinqueloculina spp.* (d'Orbigny, 1826)**	23
***Fissurina spp.* (Reuss, 1850)**	23
***Pyrgo spp.* (Defrance, 1824)**	15
***Parafissurina spp.* (Parr, 1947)**	7
***Parafissurina tectulostoma* (Loeblich & Tappan, 1953)**	7
***Siphotextularia rolshauseni* (Phleger & Parker, 1951)**	4
***Hyalinea balthica* (Schroeter, 1783)**	4
***Fissurina orbignyana* (Seguenza, 1862)**	3
***Nodosaria spp.* (Lamarck, 1816)**	3
***Pullenia bulloides* (d'Orbigny, 1846)**	3
***Cornuspira involvens* (Reuss, 1850)**	3
***Oolina spp.* (d'Orbigny, 1839)**	3
***Oolina hexagona* (Williamson, 1848)**	2
***Nonionellina labradorica* (Dawson, 1860)**	2
***Lenticulina spp.* (Lamarck, 1804)**	1